PFC/JA-91-33

Papers Presented at the IEEE 14th Symposium on Fusion Engineering by the Alcator C-MOD Engineering Staff, Oct. 1991

S. Fairfax and the Alcator Group, William Beck, H. Becker, P. Titus*, J. Bosco, W.M. Burke, Jr., J. Daigle, K. Sueker†, T.P. Fuller, C.L. Fiore, B. LaBombard, B. Lipschultz, S. Kochan, J.S. Paranay, W. Parkin, Y. Takase, S. Golovato, M. Porkolab, K. Bajwa, D. Caldwell

Plasma Fusion Center
Massachusetts Institute of Technology
Cambridge, MA 02139

October, 1991

* Stone & Webster Engineering Corp.
† Robicon Corp., Pittsburg, PA.

To be published in Proceedings of IEEE 14th Symposium on Fusion Engingeering.

This work was supported by the U. S. Department of Energy Contract No. DE-AC02-78ET51013.

PAPERS PRESENTED AT THE IEEE
14TH SYMPOSIUM ON FUSION ENGINEERING
BY THE ALCATOR C-MOD ENGINEERING STAFF
OCTOBER 1991

ALCATOR C-MOD
S. Fairfax and the Alcator Group
pp. 1-6

ALCATOR C-MOD TOROIDAL FIELD MAGNET ASSEMBLY
William Beck
pp. 7-9

PROPOSED STANDARDS FOR MAGNETC STRUCTURAL DESIGN
H. Becker, P. Titus
pp. 10-14

THE ALCATOR C-MOD CONTROL SYSTEM
J. Bosco, S. Fairfax
pp. 15-18

TEMPERATURE CONTROL AND MAGNET INSTRUMENTATION IN ALCATOR C-MOD
William M. Burke, Jr.
pp. 19-22

FABRICATION OF ALCATOR C-MOD OHMIC HEATING COIL AND COAXIAL BUS
J. Daigle
pp. 23-26

THYRISTOR DC CIRCUIT BREAKERS FOR ALCATOR C-MOD
S. Fairfax, K. Sueker
pp. 27-30

DESIGN AND CONSTRUCTION OF THYRISTOR DC CIRCUIT BREAKDERS FOR ALCATOR C-MOD
Keith H. Sueker, Stephen A. Fairfax
pp. 31-35

ALCATOR C-MOD ENVIRONMENTAL HEALTH AND RADIATION PROGRAM DEVELOPMENT
T. Fuller, C.L. Fiore
pp. 36-39

DESIGN OF LIMITER/DIVERTOR FIRST-WALL COMPONENTS FOR ALCATOR C-MOD
B. LaBombard, B. Lipschultz, S. Kochan
pp. 40-45

POWER SUPPLIES FOR POLOIDAL MAGNETS IN THE ALCATOR C-MOD TOKAMAK
J.S. Paranay, S. Fairfax
pp. 46-49

SIGNAL CONDITIONING ELECTRONICS AND PACKAGING FOR THE ALCATOR C-MOD TOKAMAK
W. Parkin
pp. 50-53

ENGINEERING DESIGN AND ANALYSIS OF THE ALCATOR C-MOD TWO-STRAP ICRF ANTENNA
Y. Takase, S. Golovato, M. Porkolab, K. Bajwa, H. Becker, D. Caldwell
pp. 54-57

Plasma Fusion Center
Massachusetts Institute of Technology
Cambridge, MA 02139

October 1991

A cross-sectional view of the device is shown in Figure 2, with design parameters in Table 1. The choice of parameters is intended to provide maximum performance and relevance to future experiments consistent with today's limited budgets. Ohmic performance is expected to provide values of $n\tau$ up to $10^{20}m^{-3}$ at temperatures up to 3 keV. The addition of the present 4 MW ICRF heating will raise electron and ion temperatures to $\approx$ 6 keV and provide important information for next generation experiments.[1]

Table 1: Alcator C-MOD Parameters

Major Radius	R	=	0.666 m.
Minor Radius	a	=	0.21 m.
Toroidal Field	B_T	=	9 T.
Plasma Current	I_p	=	3 MA.
Elongation	κ	=	1.8 (typical)
Triangularity	δ	=	0.4 (typical)
Flat-top Duration			1 s(@ 9T)
			7 s(@ 5T)
Inductive Volt-seconds			7.5 Wb.
Required Energy			500 MJ.

Toroidal Field Magnet

The rectangular TF magnet consists of a circular cylindrical central core, radial arms top and bottom, and vertical legs. The magnet turns are fabricated from copper C-10700 with a 250 MPa yield strength. They are precooled by liquid nitrogen before each current pulse to enhance conductivity.

Each of the 120 turns has sliding joints at all four corners. The joints utilize a material called feltmetal [2,3] to pass currents up to 260 kA while moving vertically and radially as much as 3 mm. A spring preloads each feltmetal pad in a joint at 3 MPa pressure to pass the current effectively. Joint resistivity is less than 0.5 $n\Omega - m^2$ with peak current densities approaching 5 kA/cm^2. Figure 1 is a photograph of the tokamak prior to placement of the outer cylinder and upper cover. The outer sections of the TF magnet turns are visible, as are the drawbars, the lower cover, and the vacuum chamber. Figure 3 shows the TF magnet with an enlarged view of a sliding joint.

The presence of the sliding joints requires a superstructure to react the Lorentz arms. They consist of vertical and out-of plane loads on the radial arms, and outward and out-of-plane loads on the vertical loads. The core resists the radial inward Lorentz loads and 1/4 of the total vertical separating load. Each core conductor plate is reinforced by a thin sheet of 216 steel. This prevents the copper from flowing under face pressure that exceeds the copper yield near the bore region of the core. The steel sheets protrude into the bore to assist in cooling the plates with liquid nitrogen.

The superstructure was forged and machined from a modified 316LN stainless steel. The 30 ton covers were among the largest one-piece forgings ever made from that material. The success in forging such large pieces may provide valuable experience and data for ITER.

Each of the two covers is 0.66 m thick. They deflect 3 mm under the 110 MN vertical forces. The one-piece outer cylinder reacts the cover separating forces, the 2.8 MN-m torque, and the radial outward load on each vertical leg.

The vertical Lorentz load on the covers is transmitted to the cylinder by 96 alloy 718 drawbars with a yield strength of 1 GPa. The drawbars are pretensioned to 2.2 MN, which is the maximum possible because of the 300 MPa yield strength of the cylinder, to which they are pinned. During cooldown, the drawbars shrink 20 percent less than the steel. As a result, 20 percent of the preload is lost. That results in maintenance of contact between the cover and cylinder up to 8 tesla, with no load change in a drawbar. From 8 to 9 tesla, the covers and cylinder are no longer in contact, and the draw bar load increases from 1.8 MN to 2.2 MN. That cycle range controls the drawbar life, which exceeds 200,000 maximum performance pulses for a comfortable margin of safety over the 50,000 required.[4] All lifetime calculations include known defects or twice the minimum detectable defect size, whichever is larger.

The TF magnet is instrumented with 60 thermocouples and 360 voltage monitoring points. These will aid in assessing the performance of the cooling system and sliding joints.

Vacuum Chamber

The vacuum chamber provides structural support for all PF magnets, first wall hardware, ICRF antennae, and many diagnostic elements. The vessel consists of welded sections of 304L stainless steel with many sections over 20 mm thick. There is no electrical break. Significant eddy currents are generated during plasma initiation and disruptions, creating loads that add to those from the PF coils, the vacuum, and hardware mounted on the vessel. The exterior of the chamber is covered with an array of 366 foil heaters. Each heater has redundant elements

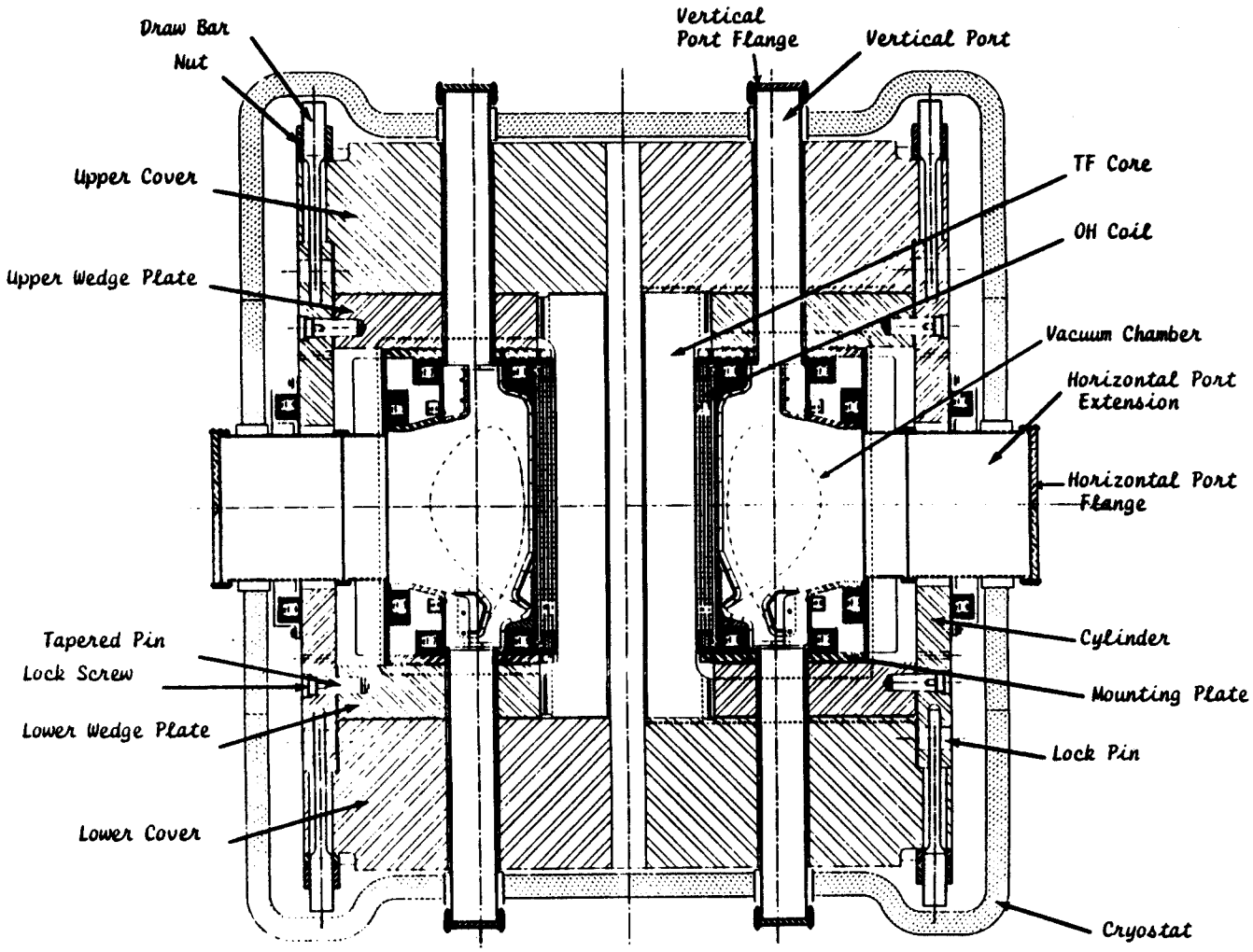

Figure 2: Cross-Sectional View of Alcator C-MOD

and 2 thermocouples. A computer controls power to each foil element and monitors the thermocouple.[5] The chamber may be baked at 150°C or maintained at any desired temperature from –60°C to 0°C when the magnets are under full cooling with liquid nitrogen.

There are 10 radial ports and 20 vertical ports. The radial ports are 200 mm wide and allow human access to the interior. All ports have long extensions to penetrate the steel superstructure, the foam cryostat, and the neutron-adsorbing igloo surrounding the machine.

Vacuum pumping on the 4000-liter chamber is provided by a single 1000 l/s turbomolecular pump. Base pressures in the low 10^{-8} torr range are obtained. All materials used inside the vacuum chamber are screened for outgassing properties. Components are vacuum baked before installation. Metal seals are used on all ports. The interior walls of the chamber are covered with an array of metal studs used to mount first wall and diagnostic hardware.

Poloidal Field Magnets

There are 5 pairs of strip-wound ring coils in addition to 3 coils in the central solenoid. Most magnets control more than one parameter. The OH2 magnets, for example, influence plasma current, elongation, vertical position, and the diverter.

The central solenoid was wound from copper C-10700 bar stock. The production of the OH1 conductor length required brazing sections together prior to final drawing. The full 250 MPa yield strength was regained after drawing. The solenoid consists of 4 layers, wound on the TF core but free to move with respect to it. Disruption forces approaching 3 MN can displace the magnet 3 mm from its normal operating position. The terminals were soft- soldered to the hard conductor to preserve conductor strength. A special joint was designed for this purpose and proof-tested to over 200,000 cycles at both liquid nitrogen and room temperature. Coaxial bus is utilized to carry the PF currents across the toroidal field.[6] The central solenoid is pre-cooled by liquid

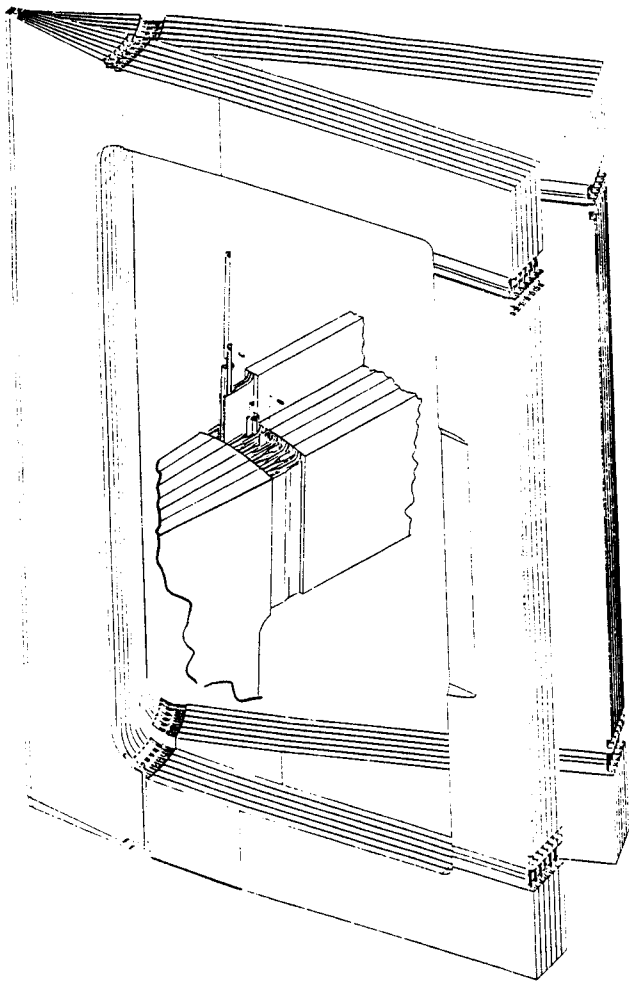

Figure 3: TF Magnet and Sliding Joint

nitrogen on both its inner and outer surfaces.

The 10 PF ring coils provide shaping and positioning control in addition to significant Ohmic drive. Each coil is pre-cooled along one or both edges with liquid nitrogen and instrumented with thermocouples. The EF4 coil set is mounted outside the steel superstructure and is the only PF coil not supported by the vacuum chamber.

First Wall

The first wall is composed of nearly 7000 molybdenum tiles in 120 separate shapes. Tiles are mounted on modules of sixteen to one hundred tiles, which are in turn mounted to the vacuum vessel walls. The first wall is designed to withstand disruption loads resulting from a 3MA/3msec current termination at 9 Tesla toroidal field. The first wall instrumentation include thermocouples, IR cameras, and integral electrostatic probe assemblies.[7] The magnetic sensor array consists of 3 Rogowski coils, 104 B_p coils, 29 flux loops, 16 Mirnov coils, 2 diamagnetic loops, and 4 saddle coils.[8] Leads, coils, and gas puffing tubes are positioned in tunnels built into the backs of the first wall modules. The inner belt limiter is interrupted by an optical viewing dump for the Thomson scattering diagnostic.

The first wall design provides a cylindrical limiter on the central cylinder, a shaped diverter on the bottom of the chamber and a flat-plate divertor on the top. The shaped divertor includes provisions for measuring current flow into the outer sections, or biasing these assemblies. All first wall surfaces are aligned to within 1 mm, using the machined central cylinder as a reference. First wall heat fluxes are conservatively estimated to be 6 MW/m^2 for the limiter and shaped divertor tiles and up to 40 MW/m^2 on the flat plates. [7] Total heat loads of 6 MW are anticipated. The outer shaped divertor tiles are cooled primarily by radiation in order to avoid heating the nearby PF coils. The estimated operating temperature is 500°C. The strike point will be swept to avoid melting the tiles.

Power System

Primary power and energy storage for the experiment is provided by the same alternator used with Alcator C. The energy storage is being upgraded from 500 to 2000 MJ by the addition of a 75-ton flywheel.[9] The forging of this piece proved to be quite challenging.[10] A maximum performance pulse requires over 500 MJ, slowing the alternator/flywheel from 1800 to 1500 RPM in three seconds. Peak demand can approach 400 MVA. The alternator/flywheel is accelerated by a 2000 HP wound-rotor induction motor with an electronic drive system. Acceleration time after a maximum performance pulse is 17 minutes. The TF magnet requires 20 minutes to cool after such a pulse.

The converter system ratings are summarized in Table 2.

Supply Name	Bipolar Current	Output Voltage		Maximum Current
		Open Circuit	Full Load	
TF	No	1550	800	260 kA
OH1	Yes	932	500	±50 kA
OH2U	Yes	243	100	±50 kA
OH2L	Yes	243	100	±50 kA
EF1U	Yes	418	200	±15 kA
EF1L	Yes	418	200	±15 kA
EF2U	No	341	300	7 kA
EF2L	No	341	300	7 kA
EF3	No	3645	2400	22 kA
EF4	Yes	1023	900	±10 kA
EFC	No	500	500	3 kA

Table 2: Power System Converters

The TF converter utilizes a dual-voltage power supply to combine rapid current ramp-up with lower alternator demand at full field. This technique, while utilized in some industry applications, [11,12] is new to fusion power supplies. The TF, OH1, OH2, and EF1 converters employ electronic fuse loss detection. This approach eliminates indicating fuses and allows detection of commutation failures as well as operation with 1 device inoperative in each phase group.

The OH1, OH2, and EF1 converters are bi-polar units, requiring no mechanical switching to double-swing their respective loads. Each unit is connected to an SCR switch that can interrupt the full converter output at voltages up to 2 kV. The thick, one-piece vacuum vessel encourages low-voltage start-up in order to limit the effects of eddy currents. Solid-state interrupting switches provide a cost-effective, reliable alternative to electromechanical devices at these voltage levels. The SCRs utilized in the switches are standard phase-control devices rather than high-speed devices utilized in inverter applications.[13,14]

The EF2, EF4, EFC, and alternator excitation power is provided by converters on long-term loan from Lawrence Livermore National Laboratory. These units were originally utilized on the TMX-U experiment. They have been refurbished and outfitted with new control systems.[15] The energy for these systems is taken directly from the utility supply.

All PF coils are protected by varistor assemblies rated for maximum stored energy. Most power supplies incorporate crowbar units to circulate the current during severe faults, but inversion of the stored energy back to the alternator is the preferred action. The TF magnet stores over 300 MJ at 9 Tesla, and inversion of the TF supply significantly accelerates the alternator/flywheel at the end of a pulse. All coils are instrumented with current detectors (small magnetic reed switches that close when the current exceeds 100 amps) that alert the control room operators. Each magnet is protected with ground fault sensors. All bus leads incorporate provisions for reversing the direction of current flow.

The auxiliary heating utilizes 2 transmitters operating at 80 MHz. The 2 MW output of each transmitter feeds a single-strap, movable antenna or a 2-strap antenna fixed to the outer vacuum chamber wall.[16] A proposed upgrade to 8 MW with variable frequency would increase the access to interesting heating regimes in addition to improving plasma performance.

Control System

Engineering control of the experiment is performed by relatively autonomous Allen-Bradley PLC-5 Programmable Logic Controllers (PLC's). The PLC's provide robust processors combined with a wide array of analog and digital I/O capability. Each PLC is linked to a personal computer located in the control room. All links to and from the control room are via fiber optic cables. The control room PC's are networked and can share real-time process information for purposes of coordination or interlocking. Each PC provides graphic display of equipment status, accepts and qualifies operator input, and performs data logging and trend monitoring. Commercial software packages were selected for the PLC's, PC's, and network.[17]

A hybrid analog/digital computer provides real-time control of plasma position and shape.[18] Up to 96 analog inputs may be assigned to up to 16 controlled variables. The feedback signal path from the magnetic pick-up coils to the power supply voltage programming inputs is entirely analog. The relative weight of each input and the operations performed on each channel are controlled by digital coefficients. Up to 400 sets of coefficients may be programmed prior to each plasma discharge. The hybrid software allows the operator to input the desired trajectories of each controlled variable, and utilizes a database of both observed and simulated equilibria to compute the necessary digital coefficients.

Data acquisition is via standard CAMAC instrumentation. Integration, isolation, and other analog signal processing functions are provided by specially developed hardware that utilizes standard Eurocard packaging.[19] The data is collected, organized, and manipulated with the MDS-Plus software package.[20] This database is hierarchical with both raw and processed data organized by experiment and parameter. MDS-Plus provides a pseudo-oscilloscope for viewing data as well as interfaces to other graphics packages.

Radiation Shielding

The neutron production rate with Ohmic plasmas may approach 10^{15} neutrons/s for 1 second. Rates with RF heating could be an order of magnitude higher. These rates represent potential health risks and could interfere with diagnostic electronics. Extensive calculations and modeling predict that the shielding presently in place will keep dose rates outside the experimental areas well below legal maximums for non- radiation workers.[21]

The experimental cell is constructed of reinforced concrete with 1.5 m thick walls. The floor thickness is 1 m and the roof is 1.2 m. The urban location of the experiment prohibits a large site; the site boundry is less than 5 m from the outside wall of the experimental cell. A movable 4.3 m by 4 m by 1.5 m thick concrete shield door closes the primary cell entrance. The magnet bus and cryogenic leads enter the cell through a 4.3 m tall by 1.2 m wide opening. The lower 2 m of this opening provides personnel and small equipment access. This opening is surrounded by 0.9 m thick walls. A separate emergency exit leads to another vestibule area.

Radiation doses inside the vacuum chamber may require short cool-down periods prior to personnel access. Residual activity from activated molybdenum first wall tiles could result in a dose of 410 mRem/hour after a year of maximum performance pulses. The dose is reduced to 50 mRem/ hour after 8 days.

The tokamak will be surrounded by a 0.6 m thick concrete structure dubbed the diagnostic igloo. This struture serves to support many diagnostics and attenuates the radiation dose to electronics located within the cell. The structure is composed of reinforced concrete with 0.5% weight boron frit as an aggregate. The attenuation varies from 8 to 30, being smallest near the port openings and largest between openings. No credit for this shielding was included in the health physics calculations. This approach allows modifications to the igloo without affecting the radiation protection plan for the experiment. The igloo is constructed of 30 sections stacked in 3 tiers, plus a large top cover. It is assembled with the overhead crane and may be removed from the experimental cell during maintenance periods.

Status

The tokamak is assembled and the first round of system integration tests are complete. The initial tests were at room temperature to facilitate observation and testing of the various bus sections and magnet motions. The cryogenic cooling system is presently being installed. The flywheel is scheduled for installation late in 1991. All flywheel auxiliary system (bearings, cooling, etc.) are installed and ready. Cryogenic operations at up to 6 Tesla toroidal field will begin late this year. Installation and testing of the diagnostics will begin as soon as cryogenic cooling system tests are complete.

References

[1] I.H. Hutchinson and the Alcator Group, "C-MOD, The Next Alcator," Proceedings IEEE 13th Symposium on Fusion Engineering, Vol. 1, p. 13 (1990).

[2] Feltmetal is a trademark of Brunswick Tecnetiks.

[3] W. Beck "Alcator C-MOD Toroidal Field Magnet Assembly," this conference.

[4] H. Becker, et al., "Superstructure for a Super Tokamak: Alcator C-MOD," Proceedings IEEE 13th Symposium on Fusion Engineering, Vol. 2, p. 1367 (1990).

[5] W. Burke, "Temperature Control and Magnet Instrumentation in Alcator C-MOD," this conference.

[6] J. Daigle, "Fabrication of the Alcator C-MOD Ohmic Heating Coil and Coaxial Bus," this conference.

[7] B. Labombard, B. Lipshultz, S. Kochan, "Design of Limiter/ Divertor First-Wall Components for Alcator C-MOD," this conference.

[8] R.S. Granetz, I.H. Hutchinson, J. Gerolamo, W. Pina, C. Tsui, "Magnetic Diagnostics in Alcator C-MOD", Rev. Sci. Instrum. 61 (1990) 2967.

[9] J. Murphy, et al, "Turbogenerator Flywheel for Alcator C-MOD," this conference.

[10] Bokelmann, D., Forch, K., Haverkamp, K.D., "Forging Technique for the Manufacture of a Heavy Flywheel with 108 t Forging Weight," Proceedings of the 11th International Forgemasters Meeting, 1991.

[11] K.H. Sueker, "Thyristor Autotapchanger Power Supply for Alcator C-MOD Toroidal Field," Proc. IEEE 13th Symposium on Fusion Engineering, Vol. 1, p. 555 (1990).

[12] S. Fairfax, "The Alcator C-MOD Power System," Proc. IEEE 13th Symposim on Fusion Engineering, Vol. 2, p. 1193 (1990).

[13] K. Sueker, S. Fairfax, "Design and Construction of Thyrsitor DC Circuit Breakers for Alcator C-MOD," this conference.

[14] S. Fairfax, K. Sueker, "Thyristor DC Circuit Breakers for Alcator C-MOD," this conference.

[15] J. Paranay, S. Fairfax, "Power Supplies for Poloidal Magnets in the Alcator C-MOD Tokamak," this conference.

[16] Y. Takase, et al., "Design and Analysis of the Alcator C-MOD Two-Strap ICRF Antenna," this conference.

[17] J. Bosco, S. Fairfax "The Alcator C-MOD Control System," this conference.

[18] Lister, J.B., Marmillod, Ph., Moret, J.M., "A Fast Response Hybrid Linearized Control System" Technical Report LRP 332/87, Centre de Recherches en Physique des Plasmas at the École Polytechnique de Lausanne.

[19] W. Parkin, "Signal Conditioning Electronics and Packaging for Alcator C-MOD Tokamak," this conference.

[20] G. Flor, G. Manduchi, T.W. Fredian, J.A. Stillerman, K.A. Klare , "MDS-PLUS - A Comprehensive Data Acquisition and Analysis System" in proceedings of the 16th Symposium on Fusion Technology, London, U.K. 1990.

[21] Fiore, C.L., "Calculation of Neutron and γ Production and Transport for the Alcator C-MOD Experiment," Proceedings IEEE 13th Symposium on Fusion Engineering, Vol. 1, p. 878 (1990).

ALCATOR C-MOD TOROIDAL FIELD MAGNET ASSEMBLY

William Beck
Plasma Fusion Center
Massachusetts Institute of Technology
Cambridge, MA 02139

Abstract: The Alcator C-MOD tokamak has been constructed by the Massachusetts Institute of Technology under contract to the U.S. Department of Energy. It is a compact(0.66 m major radius) high field (9 tesla) tokamak designed to produce diverted, elongated plasmas up to 3.0 MA for a flattop of at least one second. The toroidal field magnet is a cryocooled copper magnet incorporating several unique design features. Each rectangular magnet turn comprises four separate components, inner and outer vertical legs, upper and lower radial arms. The inner vertical legs of the magnet are bonded together into a wedged self-supporting unit. The radial arms and outer vertical legs carry the magnetic loads to an external superstructure against which the toroidal magnet forces are reacted. Although the superstructure is a massive structure(up to 0.66 m thick), these forces cause substantial deflection of the superstructure, resulting in several millimeters of motion at the connection between the parts of each turn. The electrical connections at each corner of the magnet are made with sliding joints utilizing silver plated felted and sintered copper pads. These sliding electrical contacts carry the full toroidal field magnet current of 0.26 MA. The unique design features are described in detail. The manufacturing processes for the various magnet components are outlined, and the assembly of the toroidal field magnet components into the tokamak is described.

Work supported by U.S. DOE Contract No. DE-AC02-78ET51013.

Sliding Electrical Contacts

The most revolutionary feature incorporated into the toroidal field magnet is the sliding feltmetal-copper electrical contact. Peak current density in the contact is 5 $\frac{kA}{cm^2}$ but it can operate safely up to 10 $\frac{kA}{cm^2}$. The contact resistance is between 10 and 20 $\mu\Omega - cm^2$ directly after installation and ends up around 5 $\mu\Omega - cm^2$ after several sliding operations.

The contacts are of a mortise and tenon arrangement. Tenons are located at the inboard end of the radial arms and at the top and bottom of the outer vertical legs. Mortising is at the central column and at the outer end of the radial arms. The electrical contact surfaces of the mortises are silver plated to reduce contact wear and resistance. The mating contact consists of 4 silver plated feltmetal pads which are soldered to the tenons.

Feltmetal was made by sintering 0.05 mm diameter OFHC copper wires onto 0.127 mm OFHC copper sheet to form a 30 cm x 68 cm pad 1 mm thick. The felt was then laser-cut into strips that were pressed between dies to form the contact shape. Laser cutting and crimping the edges of the pad proved to be an effective barrier to the molten solder during the bonding process. Solder wicking into the contact pad would have prevented the pad from seating properly against the mating surface.

The ability of the pad to operate at such high current densities can be attributed to the many small diameter wires which make up the feltmetal pad. The wires create many electrical contact spots, maximizing the number of current paths. The numerous contact spots minimize interface contact pressure which could lead to galling. Each contact pad is preloaded to 3 MPa contact pressure by spring plates that seat the contact (see Figure 1).

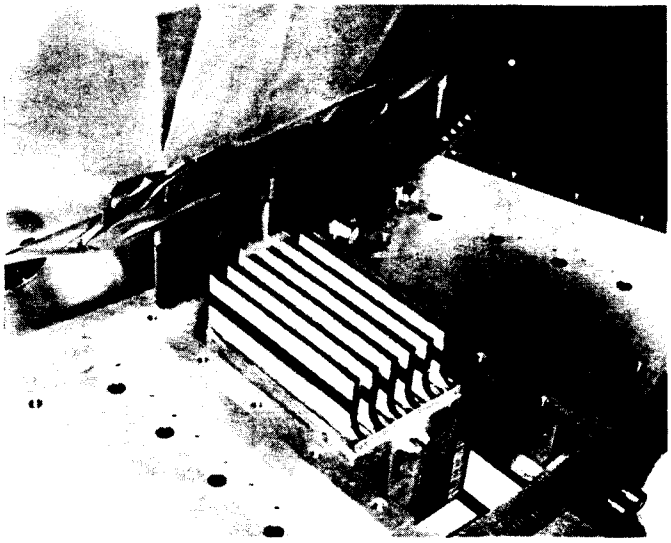

Figure 1. Upper Vertical Contact Aligned for Installation

Toroidal Field Magnet Components

The major components of the toroidal field magnet are the central column, radial arms, outer vertical legs, and superstructure. The central column is made up of the 120 inboard wedge shape turns. Each turn comprises 2 wedge shaped C-10700 copper plates bonded together with a 216 stainless steel reinforcement plate between them. The reinforcement plate prevents the copper from flowing under the wedging pressure that could exceed the copper yield strength. The 120 turns are electrically isolated from each other by a 0.64 mm fiberglass laminated sheet bonded between turns.

The central column was made up of 20 wedge shaped subassemblies of two different lengths. Adjacent subassemblies were offset vertically at each end by 2.54 cm to form wedge shaped keys which fit tightly into wedge shaped grooves machined into the covers for registration and support. This feature also dictated the vertical staggering of the radial arms, which help key the wedge plates to the covers.

Each radial arm and vertical leg bundle contains six C-10700 copper plates bonded together with a fiberglass laminated sheet between them for turn to turn insulation.

The radial arms are identical. Each bundle has a 1.5 degree offset bend in the radial plane to align the top and bottom mortises at the outboard end of the leg to accept the vertical leg (see Figure 2).

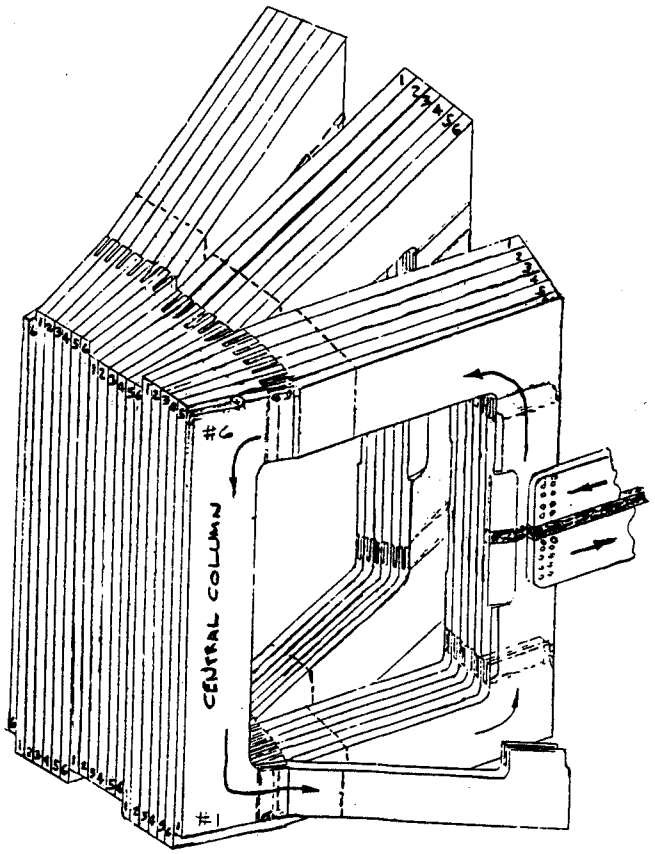

Figure 2. First Turn Transition Area

The turn to turn advance of the coil is incorporated in the central column and the radial arms (Fig. 2).

The superstructure is made up of top and bottom covers, top and bottom wedge plates, cylinder, and 96 drawbars, and the hardware to join the system together. The covers, wedge plate, and cylinder are forgings of 316 LN stainless steel and possibly represent the largest forgings of the alloy ever produced. The list of fasteners includes 96 oval pins and 40 tapered pins made of Inconel 718, 96 dowel pins, and two bolt rings made of 316 LN stainless steel.

The nominal length of the drawbars is 0.85 m. One end has a .20 m long, 4 inch diameter Whitworth thread at 1/3 inch pitch. The nut transfers the cover vertical load into the drawbars. The other end is paddle shaped with an elongated hole to receive the pin that transmits the tension load to the cylinder. Fastening the drawbars to the cylinder is accomplished by inserting the paddle into the annulus machined into each end of the cylinder and capturing them with the oval pins which fit through the elongated holes in the drawbar paddle and cylinder.

The covers and the cylinder react the outward magnetic loads exerted by the radial arms and outer vertical legs. The vertical outward force exerted on the cover is 110 MN. The covers are expected to deflect about 3 mm under this load during a 9 tesla pulse.

Proper alignment of the radial arms is determined by the wedge plates which are concentrically located within the cylinder and held in place by the tapered pins. Out-of-plane loads on the radial arms are reacted at the grooves in the covers and wedge plates. The dowel pins transmit the torque from the covers to the cylinder.The tapered pins carry the torque from the wedge plate to the cylinder.

Cooling/Ground Plane Insulation

The major requirement for TF magnet cooling (between 9 tesla pulses) is the reduction of the coil temperature from 120 K to 80 K in 20 minutes. Heat transfer at the radial arm surfaces is augmented by turbulators. They are surface upsets applied with a chisel to increase surface turbulence. In tests it proved to be beneficial for heat transfer to gas and two phase film flow. Experiments revealed that the rate of cooling was doubled over that without turbulators.

The radial arms are cooled by forcing liquid nitrogen through passages machined into G-10 ground plane insulation panels. Liquid nitrogen is supplied to each radial arm by two $\frac{1}{4}$ inch copper tubes. The tubes are connected to a manifold inside the cryostat and run parallel to the vertical ports. Liquid nitrogen enters through the outboard panel and is channeled to the inboard panel because of the of the high bearing pressure on the entrance panel. The inboard panel is divided into two chambers. Each is supplied liquid nitrogen by a separate tube. The inner chamber exhausts into the sliding contact region, continues toward the covers, through the 6.35 mm gap between the wedge plate and the cover, down between the vacuum vessel and the cylinder, through holes drilled in the dowel pins ending up in the bottom of the cryostat for recycling. Flow in the outer chamber is channeled back toward the covers and vented in the same manner as the inner chamber.

The outer vertical legs have cooling slots machined into the outboard surface. An outer G-10 panel was epoxied to the grooved surface to form the channel. A 1.3 m radius was machined into the back surface of the panel to bear up against the cylinder. Liquid nitrogen is fed into the bottom of the arm and exhausts out the top. It is directed through the cylinder, and collected in the bottom of the cryostat for recycling. The vertical legs were encapsulated with 1.5 mm fiberglass laminate for additional dielectric strength.

The central column has grooves machined into the inner vertical turns. The central column was wrapped with Kapton, and then with a unidirectional fiberglass reinforced B-stage epoxy wrap, to form the channel. The Kapton was applied to insulate the central column from the ohmic heating coil which was wound onto teflon coated shims. The shims were removed after epoxy impregnation leaving a 2.5 mm gap between the inside diameter of the ohmic heating coil and the outside diameter of the wrap on the central column. A cooling manifold was constructed on the bottom of the central column. Liquid nitrogen enters the manifold, is channeled upward through the central column cooling channels, and exhausts from the upper radial arms. A flexible fiberglass reinforced teflon barrier was bonded to the central column and attached to the inside surface of the upper wedge plate. The barrier directs the flow up through the toroidal magnet sliding contacts.

Cooling manifold plates are attached to the outboard surfaces of the covers to direct liquid nitrogen over them. A portion of the flow is directed down the bore of the central column for additional cooling.

Instrumentation

Due to a limited amount of space available in the ground plane insulation panels for wiring, instrumentation was held to a minimum. There was no space to install instrumentation

on the central column without jeopardizing the integrity of the magnet.

Voltage taps were mounted to each radial arm and vertical leg turn to monitor the condition of the sliding contacts. The outboard joints can be monitored individually. Inboard turns will be monitored in series since the central column could not accommodate any instrumentation wiring.

Thermocouples were installed on the radial arms and vertical legs. The temperature of the bundles will be monitored along with magnet resistance measurements to control cooldown and serve warning of cooling malfunctions.

Assembly Sequence

The first step in the assembly sequence was fabricating an assembly stand to support the vacuum vessel and the central column. The central column, along with the trapped ohmic heating solenoid, was positioned into the vacuum vessel bore onto the support column. The ohmic heating solenoid was centered and clamped in place. Then the upper and lower mounting plates were fastened to the vacuum vessel, clamping the solenoid and the equilibrium coils in place.

The lower wedge plate was then raised into position and supported by column jacks. Registration of the wedge plates was determined by three pins which were fit into the mounting plates. Three radial slots were machined into the wedge plates to mate with the pins. The slots assured that radial motion caused by thermal variations of the vacuum vessel relative to the cooled wedge plates would not be impeded. The upper wedge plate was installed to establish the radial position of the central column. Six 3 mm thick steel templates of the radial arms were inserted into the central column mortises (3 upper and 3 lower). The central column was adjusted until the side clearance between the templates and the wedge plates was even.

The lower radial arms were raised into position with a fabricated jacking fixture. The fixture contains four stationary lead screws that bolt to the wedge plate. An attached jacking plate contains four sprockets that mate with the lead screws. One crank drives all four sprockets in series, assuring that the radial arms remain parallel to the wedge plate while being raised into position. Once in position, the arms were clamped and the sliding joint spring plates were driven in place.

The central column ground plane insulation was epoxied in place and the assembly was positioned onto the bottom cover. The upper wedge plate was re-installed with spring washer stacks placed between the mounting plates and the wedge plate. The spring stacks will allow the vacuum vessel to expand when it is operated above cryogenic temperatures or baked at 150°C.

The cylinder was placed on the bottom cover to set the distance between the wedge plates. The lower wedge plate was secured into position by the tapered pins. Then the upper wedge plate was pulled down into position against the spring force until the tapered holes were aligned. The cylinder was removed after the alignment process.

The upper radial arms and spring plates were installed in the same manner as the lower arms, using a modification to the jacking fixture.

The vertical legs were installed with a fixture similar to the one used to install the radial arms. A 5 cm thick G-10 column was attached to the side of the leg opposite the horizontal experimental ports. Wedge blocks, that were bolted to the wedge plate, centered the tenons between the mortises. The column prevents the tenons on the leg from bottoming out against the backs of the mortises.

G-10 end caps were installed on the ends of the radial arms which will buck up against the cylinder. Each end cap was fitted individually to minimize clearance between it and the cylinder to limit radial motion of the arms during machine operation.

Prior to positioning the cylinder onto the cover the lower drawbars and the dowel pins were inserted into the lower cover. The cylinder was then installed and the upper and lower drawbars were fastened to it with the oval pins. The upper central column ground plane insulator was epoxied in place and the upper cover was installed. The bolt rings were lifted into place and the drawbar nuts were hand tightened.

The last step in completing the tokamak was preloading the drawbars. Each drawbar was hydraulically tensioned to 2.2 MN and the nuts were tightened against the cover to maintain the load. The preload minimizes the range of stress cycling of the drawbars thereby maximizing the life (see Figure 3).

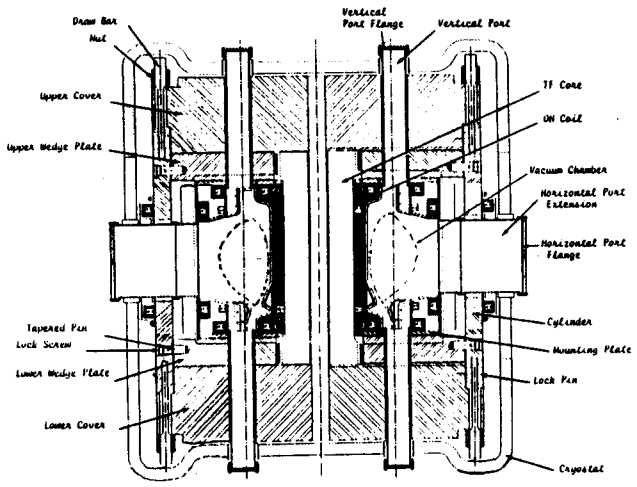

Figure 3: Assembly of Alcator C-MOD

References

[1] H. Becker, et al., "Superstructure for a Super Tokamak: Alcator C-MOD," Proceedings IEEE 13th Symposium on Fusion Engineering, Vol. 2, p. 1367 (1990).

[2] J. Daigle, W. Beck, "Fabrication of the Alcator C-MOD Ohmic Heating Coil and Coaxial Buss," IEEE 14th Symposium on Fusion Engineering, San Diego, CA, Oct. 1-3, 1991

[3] J.B.P. Williamson, "The Microworld of the Contact Spot," Holm Conference on Elect. Contacts (1981).

PROPOSED STANDARDS FOR MAGNET STRUCTURAL DESIGN

H. Becker
Plasma Fusion Center
Massachusetts Institute of Technology
Cambridge, MA 02139

P. Titus
Stone and Webster Eng. Corp.
Under contract to MIT PFC

Abstract: Mandatory Standards for Magnet Structural Design have been proposed.[1] They pertain to all phases of magnet technology from conceptual design through lifetime performance, and are intended for all magnet types.

The basis for development of the Standards is presented, together with extracted sections of the Structural Guidelines Document [2] that preceded it, and with a few examples to support conservatism in design of magnet systems.

Basis for Development of Proposed Standards

It is considered obvious that a major structural failure would have a world-wide negative impact on interest to continue development of fusion technology, particularly if it involves human injury. Accordingly, the Standards are based on human safety and operational reliability.

The ASME Boiler and Pressure Vessel Code (BPVC) regulates the structural design of pressurized equipment. It also is based on human safety and operational reliability.

A magnet under Lorentz load is somewhat like an item of pressurized equipment. It also must endure environmental loads (from temperature fields, earthquakes, and the like) as must a power plant.

A typical magnet system (such as a tokamak) is more complex than most items regulated by BPVC.

BPVC has been developed from decades of field experience combined with material property data, analysis, and a history of structural failures. No such background exists for magnet systems.

In light of those factors, it appeared prudent to base the proposed Standards on BPVC, with the same level of conservatism, and with the expectation that time will show whether that level should change.

Unknowns and Problem Areas

The following comments indicate the scope of unknown (or uncertain) factors that affect structural reliability.

Sometimes it is not clear if strength, force, or motion control should be used in material property tests.

It is not really clear how to evaluate combined mechanical and thermal stresses.

Data are needed on the effect on da/dN of time dependent crack growth phenomena (e.g., creep).

Small crack behavior is not well characterized for magnet structural materials.

Effect on crack growth of combined stress fields (operating, residual, thermal, fabrication defects, irradiation, etc.).

Influence of magnet load cycle on data from material property and structural tests.

This paper is derived from the Standards document [1] that was the outgrowth of the Structural Design Guidelines [2] produced under MIT/PFC DOE Contract DE-AC02-78ET51013. Peter Marston initiated the effort 12 years ago. He, Bruce Montgomery, and the first author, were the prime movers. Major inputs were provided by the second author together with John Mayhall, Bill Neef, Elmer Reis, Fred Puhn, Neil Mitchell, and Kyoshi Yoshida.

How to design an accelerated life test to obtain a proper evaluation of a prototype magnet structure.

Reliability of Miner's Rule for life evaluation under spectral loading.

Reliability of structural failure prediction using material property data and stress analysis.

Amplification of the base for fatigue data at R (minimum stress)/(maximum stress) other than -1, or 0.1, and at low frequencies or long hold times.

Relation of allowables to inspectability.

Effect on life of repairs during construction and operation.

Usefulness of guaranteed minimum properties and scatter band limits, and relation to subcontractor production capability.

There is further discussion of problem areas in the Quality Assurance section.

Need for Conservative Design

A popular approach to setting structural design criteria is to begin with the BPVC values, and then to diminish the factors of safety when that leads to a machine that is larger than planned.

The experience with the High Power Demonstration Experiment magnet [3] should serve as a warning against overoptimism in magnet structural design. The magnet was designed to be activated several thousand times to 6 tesla maximum field. It suffered a catastrophic structural failure after a few tens of cycles at field levels no greater than 4 tesla. The failure analysis revealed improper stress analysis, the use of a structural material with low fracture toughness and relatively rapid crack growth, and the presence of numerous stress concentrations.

That is an extreme case. However, it is the only documented major structural accident in a large magnet.

The following two illustrations of structural failure sensitivity to design parameters provide additional support to the need for conservatism in magnet system structural design.

Use is made of the linear elastic fracture mechanics relation for fatigue life,

$$N = \left[a_i^{-n/2+1} - a_f^{-n/2+1}\right] / \left[(n/2-1)CS^n\pi^{n/2}\right] \qquad (1)$$

in which a_i and a_f are the initial and final crack sizes. Eq. (1) is obtained by direct integration of the Paris Law [4].

$$da/dN = C\left[S(Q\pi a)^{1/2}\right]^n \qquad (2)$$

in which C is a coefficient, S is applied stress, Q is the crack geometry factor, and n is the slope of the linear range on log-log paper.

Case 1. Effect of Fracture Toughness

The point of this example is to show that fatigue life is relatively insensitive to fracture toughness, and that once the crack reaches only a small fraction of the theoretical critical size, little more life is left in terms of cycles to failure.

It is assumed that n=3 in the Paris Law, and that the material fracture toughness ranges from 110 to 440 MPa(m)$^{1/2}$. The initial crack size has been assumed to be 2.5 mm, and the stress range is between 200 and 700 MPa.

Figure 1 displays the relation of life to fracture toughness and stress. The numbers on the right side of the figure are arbitrarily selected values of final crack size. The left hand scale of the graph is the life-related crack size factor. It is the first term in brackets in Eq. (1). The critical crack size was calculated from the fracture toughness relation.

$$K_{IC} = S(\pi a_{cr})^{1/2} \qquad (3)$$

The crack shape coefficient was ignored for this example.

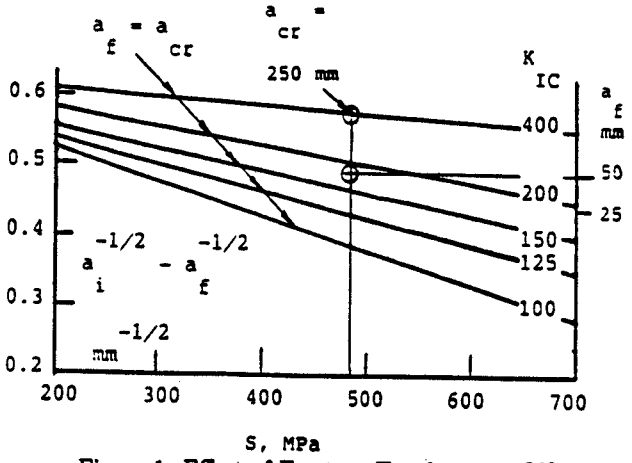

Figure 1. Effect of Fracture Toughness on Life

The total life-related crack factor range is seen to be from 0.28 to 0.60 $mm^{-1/2}$ over the large ranges of stress and fracture toughness. It also shows the small amount of residual life at 480 MPa between an assumed allowable crack size of 50 mm and the theoretical critical crack size of 250 mm. The life difference would be 14 percent (over that of 50 mm size)for 200 mm of additional crack growth. In other words, 86 percent of the life would be used up at 20 percent of the critical crack size.

This result is for illustration only. Some stress/crack-size combinations actually may be beyond the log-linear Paris Law range. In that case, more than 86 percent of the theoretical life would be used up at 50 mm crack size.

Case 2. Life Sensitivity to Inaccurate Data

The preceding example included the assumptions that the initial crack size is 2.5 mm, and that the stress is chosen at reliably identified values. The Paris Law exponent, n, was chosen at 3.0, and C was assumed to be some appropriate value not necessary to identify for this example. Now it will be assumed that the initial crack size, stress, and C value are different because of inaccuracies in calculation and measurement.

From Eq. (1) the ratio of "real" (r) life to expected (e) life will be

$$N_r/N_e = (a_{i,e}/a_{i,r})^{1/2}(S_e/S_r)^3(C_e/C_r) \qquad (3)$$

with n=3 as before.

Assume that the initial crack size is 3 mm instead of 2.5 due to limitations in UD measurement. Also, assume that the stresses are 10 percent higher than calculated because of factors such as fabrication tolerances, residuals, variations in material properties, and calculation uncertainties due to inaccurate temperature profiles. The value of C from da/dN data could easily be 25 percent greater than expected because of the steepness of the curve, and possibly larger scatter in the data than expected (due to dwell times, for example).

Substitution of those numbers into Eq. (3) leads to N_r/N_e = 0.5, or 50 percent lower life than expected.

These results provide one reason for the recommendation in the Standards that the stress intensity range should be limited to the log-linear zone of the da/dN curve.

Allowables

The preceding results, and the listed unknowns, provide the basis for the following allowables (m,y,u = membrane, yield, ultimate).

Table 1. METAL ALLOWABLES CRITERIA

A. Sm for STATIC LOAD

STRESS TYPE	SUPERSTRUCTURE	MAGNET COIL	
		Stand Alone	Within Superstructure
Membrane	Lesser of 2/3 Su or 1/3 Sy	Same As For Super-structure	Lesser of 3/8 Su or 3/4 Sy
Membrane +Bending	1.5 Sm		Su
Peak	3.0 Sm		Sy

B. ALLOWABLE N FOR FATIGUE BY FRACTURE MECHANICS
(W = With Inspection, WO = Without Inspection)

SUPERSTRUCTURE	MAGNET COIL
W, 0.2; WO, 0.1	Stand Alone: W, 0.1; WO, 0.1 Within SS: W, 0.4; WO, 0.2

C. ALLOWABLE N FROM S-N CURVES

SUPERSTRUCTURE	MAGNET COIL
W, 0.1; WO, 0.02	Stand Alone: W, 0.1; WO, 0.02 Within SS: W, 0.2; WO, 0.04

For non-metallic composites, all allowables are half the values shown in Table 1.

Buckling Allowables

If a structural part might be in danger of buckling elastically, the allowable buckling stress shall be 1/3 the collapse stress if the collapse stress also is elastic.

If a structural part were to begin deforming in a buckle mode, and if part of the increasing load were to be transmitted to adjacent structures, they also should be analyzed for instability.

If the collapse strength of a buckling part is in the inelastic range, buckling analysis may be based on strain rather than stress. In that case, the allowable strain shall be the smaller of 1/3 the collapse strain, or the strain at 2/3 yield, whichever is less. The collapse strain shall be calculated by taking into account the proper plasticity reduction factor for the structure.

Structural Adequacy Analysis

Survivability evaluation involves determination of applied loads, determination of structural response to those loads (through calculation or measurement), and comparison of applied quantities (q_{app}) with allowable quantities (q_{all}). The criterion for structural adequacy is the Margin of Safety,

$$MS = (q_{all}/q_{app}) - 1 > 0 \quad (4)$$

The quantities mandated in the Standards are stresses, or lifetimes Other quantities could be deflections, temperatures, voltage drop, current, or anything else that might lead to stresses. Allowables for those quantities are not mandated by the Standards. They are design specific. Values for those quantities should be identified in the Structural Design Criteria document for the device to be designed.

For static analysis, the effective applied stress, S, shall be based on the Tresca criterion,

$$S = S_a - S_b \quad (5)$$

in which S_a and S_b are the two principal stresses at a point (out of the three at that point) with the largest algebraic difference between them.

For fatigue analysis, the effective stress shall be the stress (from all conditions) normal to the plane of the crack, whether the crack is real, or assumed to exist.

Thermal stresses shall be summed algebraically with mechanical stresses, and the Peak criterion (Table 1) shall apply to static loads.

There are some data to indicate that time dependency may be accounted for through use of the equation,

$$da/dN = \partial a/\partial N + (\partial a/\partial T)\,/f \quad (6)$$

that relates cyclic crack growth rate, da/dN, to the fast cycle growth rate, $\partial a/\partial N$, the actual loading frequency, f, and the time dependent growth rate, $\partial a/\partial T$. The last quantity could account for any time-dependent phenomenon such as creep, relaxation, stress corrosion, and accumulated radiation damage. Some support for the use of Eq.(6)may be found in the test data of Pineau [5],for example.

The effect of R (min S/max S) on da/dN appears to be identifiable almost entirely from experimental data alone. In some cases, a Goodman diagram has been used to convert the stress range for R = 0 to ranges for other R's.

Load spectrum survivability often is determined through the use of Miner's Rule,

$$\Sigma(N_{app}/N_{all}) = 1 \quad (7)$$

in spite of data that indicate it may be optimistic. Eq. (7) was derived for fatigue analysis using S-N curves. Much work needs to be done before an accurate relation can be established for crack growth fatigue analysis under load spectra. In the meantime, it is recommended that the factor, 1, be replaced by 0.5.

Initial cracks may not be found at zones of peak stress. However, for life calculations it is required that assumed initial cracks do occur there as well. Lifetime should be determined by integration of Eq. (2) taking into account the changing background stress field as the crack grows. It could be decreasing due to reduction of the stress at the location of a peak (at a concentration, for example). It could be increasing due to loss of structural section. That procedure should lead to a more reliable prediction of survivability.

Material Property Testing

Ancient structures engineering most likely involved building and operating (or using) the desired device, and if it did not fail, well and good. Modern structures engineering involves determining the properties of the material candidates for the structure, performing a theoretical analysis of the structural response to the expected loads, and assessing survivability.

The latter procedure is intended to supplant the former. Implicit in the modern method is the expectation that the material properties represent reliably the behavior to be expected in the device under design. That criterion will be met most effectively if the test specimens are loaded in the same manner as the material in the magnet system during operation.

To a great extent, that is not the case today. It is necessary to repeat much of the material property tests so that they are conducted under the same time-load-temperature cycles expected in magnets under design. In addition, radiation effects have not been included in many tests of materials for fusion magnets.

Some magnet structural materials for cryogenic service were designed for elevated temperature applications. Insulators were developed for electrical properties but now are required to withstand severe structural loads. It was thought that creep need not be considered in structural steels at 77K, or at 4K. Tests during the last few years indicate that view may be incorrect.

One continuing controversy is whether tests should be performed under load control, strain control, or crosshead displacement control. For evaluation of survivability under stresses that stay elastic, it may be clear that load control data are needed. If the stress at a concentration should enter the inelastic range, under cyclic conditions there may be some measure of strain control required, depending on the amount of plasticity. Reliability of strain measurement by crosshead motion control may be questionable depending on the specimen shape.

There may be problems with structures that do not permit extracting specimens of a size commensurate with ASTM standards. Other problems include load rate effects (such as temperature rise during 4K tests, for example). New fracture toughness test standards are being developed. Mention already has been made of the need for expansion of R range in da/dN data.

It is conceivable that one of the biggest problems in material property testing is the ability of the personnel to perform the tests properly. Two cases may support that view. One involved 143 yield strength measurements at 298 K on the 304 LN used in MFTF-B [6]. The values ranged from 225 MPa to 376 MPa with the mean at 311 MPa. The coefficient of variation was 6.7 percent.

Another example is the result of a round-robin fracture toughness test program on an austenitic stainless steel at 4K [7]. The J_{IC} scatter was up to 35 percens, and the standard deviation was 22 percent for 12 measurements.

Structure Verification Testing

It has been mentioned that virtually no structural verification testing has been performed on magnets or magnet systems, and that such tests are needed to provide data for establishment of real allowables. They can be designed to reveal the relation of magnet survivability to inspection and maintenance.

That background should be merged with continuous efforts to develop a realistic Magnet Code.

Tests should be performed under real magnet conditions. That raises the question of accelerated life testing for fatigue-driven structures. One method is to increase stress levels and relate the observed life to predicted life based on S-N curves, and then slide along the curve to find the allowable stress for the design life as a check on prediction. Fracture mechanics could be used in comparable fashion. Those methods may be satisfactory if time-dependent phenomena are not involved. If they are involved, it also may be possible to increase those effects. That could be done by exposure to higher levels of radiation, or corrosion, than expected. Creep crack growth rate data would be required for applicable situations such as a superconducting TF magnet under long time full field loading between pulses of out-of-plane loads from poloidal field coils.

Temperature fields should be reproduced if thermal stresses act with stresses for Lorentz loads and earthquakes, for example. There is still uncertainty about the correct analysis of structural survivability under combined thermally and mechanically induced stresses. The solution to that problem will require tests ranging from simple elements to full scale prototype assemblies, combined with theory and material property tests.

Quality Assurance

In every field of technology, except magnets, there is an extensive data base on mechanical properties of materials, results of structure tests to failure, stress and failure analysis, operating experience, and correlation of those data. In aircraft engineering, for example, stresses are analyzed, material properties are measured extensively by the design organization, and structural testing is performed on most elements, components, and assemblies. Futhermore, prototypes of the completed craft are subjected to simulated flight cycles, including imposition of controlled damages, until failure occurs.

And yet, in spite of design standards plus that detailed evaluation process, airplanes fail. Also, buildings and bridges fall, and ships sink, although designs of those structures also are regulated, and despite the fact that they have existed for thousands of years.

With one exception, no structural failure test has even been conducted on a magnet element, component, or assembly. Consequently, real safety factors are unknown. Applicability of data from stress-strain curves and fracture mechanics tests is questionable since the test conditions do not duplicate the load-time-temperature functions found in magnets for MHD and energy storage, or in fusion magnets to be subjected to nuclear radiation.

Aircraft are subjected to rigorous inspection, as are ships and, to some extent, bridges. Inspectability and maintenance are important for any device to ensure survivability after it has been designed and built. One particularly long lived device is the Brooklyn Bridge. It has lasted primarily because of continuous inspection and maintenance, in addition to large safety factors. Stringent inspection and maintenance programs are required by the Federal Aviation Authority. Inspectability is a major design consideration, with lower allowables required for uninspectable regions than for inspectable regions. (Table 1.)

The Standards document requires thorough Inspection and Maintenance procedures, and calls out specific actions to implement them in a comprehensive program of Quality Assurance. Among them is the need for preventive maintenance as well as damage repair activities. An important feature of the Q/A program is FMEA discussed in the following section.

Failure Modes and Effects Analysis

The Standards recognize three classes of structural damage:

A. Total destruction of a magnet system, including human injury.

B. Large damage to a magnet system, with minor, or no, human injury. Extensive repair required to reactivate. Large downtime.

C. Slight damage to a magnet system, but no human injury. Minor repair required. Small downtime.

FMEA is a method for avoiding those types of damage and minimizing failure risk. It involves identifying every conceivable failure mode in a structure, assuming that failure will occur in spite of survival prediction, organizing the modes into damage classes, and assessing the human hazard level and structure survivability.

FMEA helps to identify design weaknesses that could lead to structural failure, and thereby avoid them. It helps to develop realistic programs for inspection and maintenance, including the types of measurements to be made. FMEA may be the cornerstone of repair plans that involve interaction of repair procedures with analysis and indicated testing to assess properly the remaining life of the structure.

As a formal discipline, FMEA should begin at the early stages of design, and continue throughout the life of the structure. It would also include other systems such as electrical and hydraulic.

Path to a Magnet Code

The BPVC is in continuous development and updating as new performance data and analysis methods become available. If the history of BPVC development plus the continuing activities are used as an example, then it is to be expected that evolution of a Magnet Code would be through a continuous cycle of material property testing, structure verification testing, stress analysis, failure analysis, field experience, and revision of the design controlling document.

The proposed Standards for Magnet Structural Design is offered as an instrument to start that process, and as a stimulus to continue it.

References

[1] H. Becker, Ed., "Standards for Magnet Structural Design," MIT Plasma Fusion Center Report, June, 1991.

[2] H. Becker, et al, "Structural Design Guidelines for Magnets," MIT Plasma Fusion Center Report, August, 1991.

[3] H. Becker, J.M. Tarrh, and P.G. Marston, "Failure of a Large Cyrogenic MHD Magnet," 8th International Conference on Magnet Technology, Grenoble, France, September 5-9, 1983.

[4] P.C. Paris, et al, "A Rational Analytic Theory of Fatigue," The Trend in Engineering, v. 13, 1961, pp. 9-14.

[5] A. Pineau, "High Temperature Fatigue: Creep-Fatigue Oxidation Interactions in Relation to Microstructure," Advanced Seminar In Fracture Mechanics-3, Ispra, October 19-23, 1981.

[6] R.P. Reed, "Progress in Cyrogenic Structural Materials," presented at the US-Japan Low Temperature Workshop,

Jaeri, Naka, Ibaraki, Japan, May 26-27, 1988.

[7] H. Nakajima, et al, "Round-Robin Tensile and Fracture Test Results for an Fe-22Mn-13Cr-5Ni Stainless Steel at 4K." Materials Studies for Magnetic Fusion Energy Applications at Low Temperatures - XI. NBS Report NBSIR 88-3082, May 1988, pp. 305-316.

THE ALCATOR C-MOD CONTROL SYSTEM

J. Bosco, S. Fairfax
Plasma Fusion Center
Massachusetts Institute of Technology
Cambridge, MA 02139

Abstract: The Alcator C-MOD experiment includes over 30 engineering and diagnostic subsystems. The control system hardware and software is a mixture of custom and commercial products which includes sensors, signal conditioners, hardwired controls, programmable logic controllers, displays, a hybrid analog/digital computer, networked personal computers, and networked VAX workstations. This report describes the computer-based portions of the control system.

The control system coordinates all C-MOD systems including power, vacuum, heating and cooling, access control, plasma shape and position control, and diagnostics. Programmable logic controllers (PLC's) are located near each subsystem. The control room is isolated by fiber optics. Functions that are essential to personnel or equipment safety (e.g. access control) are implemented in hardwired logic and monitored but not controlled by the PLC's. The initial configuration will include over 25 Allen-Bradley PLC- 5 units. The PLCs in each subsystem are connected to personal computers (PC's) in the control room. The PC's provide graphical displays and operator interface. The PC's are networked and share process data with each other and with a master control console and a large mimic panel. The PLC, PC, and network software are all commercial products. During each shot, control of the power supply voltage programming will pass to a hybrid computer designed and fabricated at Centre de Recherches en Physique des Plasmas (CRPP) in Lausanne, Switzerland. The hybrid computer has 96 analog inputs and 16 analog outputs. The hybrid performs several matrix multiplications on the analog data using coefficients stored digitally and loaded prior to the pulse. Each set of coefficients provides control laws for a particular phase of the discharge. Any one of 400 sets of coefficients can be selected in less than 1 millisecond. The software used for the hybrid computer is the result of a joint collaboration between MIT Plasma Fusion Center and CRPP.

Introduction

Alcator C-MOD is a tokamak with a shaped non circular plasma, a poloidal divertor and auxiliary RF heating. The basic plasma design parameters are:

Major Radius	0.66 meters
Minor Radius	0.21 meters
Toroidal Field	9 Tesla
Plasma Current	3 megamp
Flat-top duration	1 sec @ 9T
	7 sec @ 5T
Required energy	500 megajoules

The objectives of the Alcator C-MOD project are described in Reference 1.

Factors Affecting Control System Design

Some of the factors which affected the C-MOD control system design would be common to many large systems while some would be applicable to many large scientific experiments.

The factors that apply to many large systems are:

Remote operation for personnel protection
Distributed control hardware to reduce wiring
Modular control blocks to enable independent development
Central collection of control information

The factors that apply to large scientific experiments are:

A very flexible and fast responding system
A flexible and high resolution timing system
Interaction between control and data acquisition systems

Control System Components

The control system consists of a variety of components including hardwire logic, programmable logic controllers (PLC's), operator interface terminals (OIT's), a control room display panel, a hybrid digital/analog computer and Camac timing modules.

Hardwire logic is used for personnel protection (access control) and self-protection of individual pieces of equipment (e.g. power supplies). Hardwire logic is also used to protect protection between certain systems (e.g. coils and power supplies).

Allen Bradley model PLC-5 PLCs were selected. Each PLC is located near the equipment being controlled. There will be 25 to 30 PLC's used, with about half for engineering control and half for diagnostic control. The number of I/O connections to the PLC's is estimated to be in the range of 4000 to 5000 points – the modular nature of the control system makes adding additional I/O points straightforward. The basic PLC-5 model can accommodate up to 256 I/O points and the most powerful model up to 3072 I/O points. PLC's are a backup for systems which are hardwire protected and provide primary protection for some other systems (e.g. vacuum system). PLC's also provide status and accept control inputs from operator displays. The PLC's are programmed using Allen-Bradley ladder logic software.

The choice of PLC strongly affects the architecture, performance, and utility of the control system. Many PLCs utilize large central processors that handle thousands of remote I/O points. The Allen-Bradley PLC-5 is smaller, less expensive, and more limited in capability. The use of many relatively small, inexpensive PLCs instead of a single unit provides a degree of sub-system independence and security that would be difficult to achieve on a centralized system. This architecture is more suitable for an experiment than for a relatively static industrial plant. The distributed system allows many programmers to work simultaneously on the various systems. The programmers may vary in experience and talent from professionals to students and the only certainty is that the system software will change frequently. Failures in hardware or software are almost always confined to one PLC and its associated equipment. Each PLC processor and OIT is protected from unauthorized changes by both keys and passwords. Interconnections between sub-systems must be explicit either in network software or in hardware in order to function at all. Unintentional dependencies, a common problem with large software packages incorporating extensive revisions by many authors, are greatly reduced by this architecture.

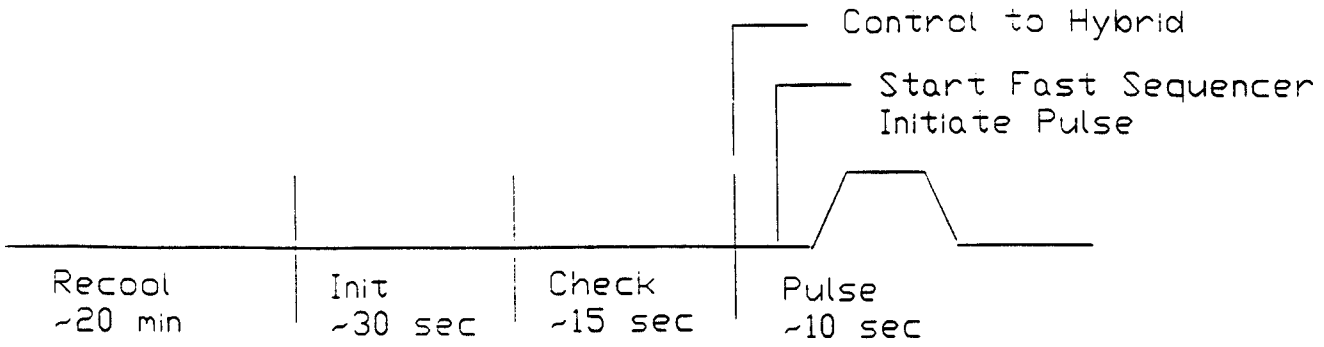

Figure 1: Duty Cycle

OIT's are located in the control room. Each OIT is an IBM®-compatible compatible personal computer with EGA color displays using Intec Paragon® control software. The OIT's are connected to the PLC's via a 57 kbaud serial link. The main function of the OIT's and the Paragon software is to provide a "user friendly" interface to the control system. Paragon software is used by a programmer to develop display "pages" which present the information gathered by the PLC's and enable an operator to input control values to a PLC. The complexity of a display page is limited by the amount of available memory in the PC but many display pages can be stored on disk. In addition to the OIT's, there will be a large mimic display in the control room.

The hybrid computer is a custom designed analog/digital system intended to provide the flexibility and speed needed for feedback control of a non-circular plasma. The hybrid computer is a collaboration between MIT and CRPP. CRPP designed and built the hardware and MIT is testing the system and supplying the user interface and software. The hybrid computer has a 3 kHz analog bandwidth and can adjust gains at a rate of once every few milliseconds.

The Camac timing modules are capable of providing synchronization and resolution of a few microseconds to all the C-MOD systems. The Camac timing modules are used during the C-MOD pulse. They are programmed through the VAX based C-MOD MDS Plus data acquisition system. The MDS Plus data acquisition system is described in Ref. 2.

Control System Configuration and Operation

C-MOD is a pulsed machine with the duty cycle shown in Fig. 1. The hardwired controls and PLC's are always in operation while the hybrid computer controls power supply output voltages, and indirectly the plasma shape and position, only during the pulse period. The operator sets a current limit for each power supply. This limit, communicated via the PLC, will override hybrid programming signals. Each power supply incorporates additional protective circuitry to prevent excessive output current or pulse length. The PLC's provide timing and sequencing in the period between pulses, but prior to the pulse, control of timing is passed to specialized Camac timing modules.

A block diagram of the control system is shown in Fig. 2. The OIT's, located in the control room, are connected to PLC's by fiber optic cables. There is one OIT dedicated to each major engineering or diagnostic system. Each OIT can be connected to one or more PLC's. Normally an OIT is connected to only one PLC. With this arrangement, a response time of about 1/4 second between the TF power supply OIT, for example, and the TF power supply PLC is achieved.

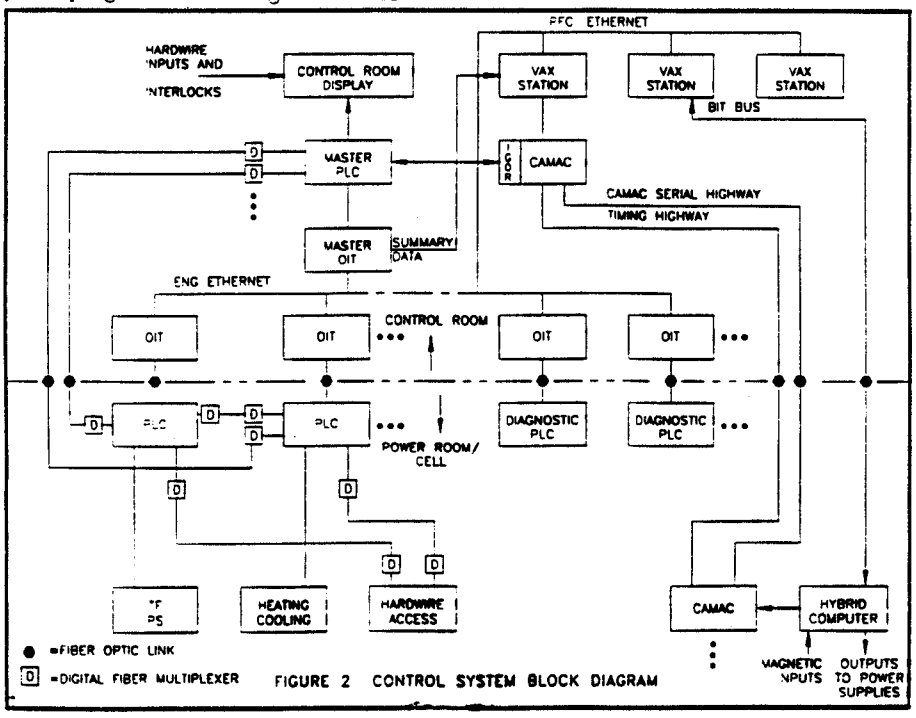

There is a need to supply information from one PLC to others or from one OIT to others. The Paragon software allows for a distributed database with individual PCs linked by Ethernet. The network utilizes Novell Netware®, a dedicated server PC, and Gateway Ethernet interface cards. The response time over this network is about 1 second but tuning may reduce this time.

Certain information which must be shared between PLC's is considered critical for equipment protection. The TF power supply PLC must know that the TF coils are sufficiently cooled before pulsing them. This type of critical information is supplied through a digital fiber optic multiplexer called a DFOL.

Most information shared between the PLC's and OIT's is carried over the network. There is one OIT/PLC combination which has been designated as the Master. The Master provides timing information to all the other PLC's in the form of States (discussed below). The Master also collects information from all the other OIT's and PLC's to drive the large mimic panel located at the front of the control room.

A set of control values and actual performance measurements will be transferred to the VAX-based data acquisition system. This transfer has not yet been implemented but several possibilities exist. One possibility is to use software available as part of Paragon which allows reading the Paragon database through a serial port on one of the OIT's. Another possibility is to use a Paragon feature that generates an ASCII compatible report which can be read by a VAX system.

Control System States

A series of States are defined to characterize the various phases of machine operation – see Fig. 3. The state is selected by an operator at the Master OIT subject to certain conditions. One condition is that only certain state transitions are allowed (as shown on Fig. 3) and another is that a transition to another state can only be made if all PLC's signal that they are ready for a transition. The state selected is communicated to all the other OIT's over the network. The other OIT's acknowledge that the state transition has been received. If any PLC fails or senses a severe fault which can affect other parts of the machine an Abort state will be generated. The Abort state can be generated by the Master operator, by the Master if it senses a fault or by any PLC by means of a hardwired DFOL connection to the Master PLC. In Abort state, all PLCs act to protect and shut down their equipment.

State changes (except Abort) are sent over the network, resulting in a response time of about 1 second. This time resolution is adequate for the actions that are taking place between shots but much better resolution is needed just before, during and just after the shot to enable various diagnostics and engineering systems to be accurately synchronized. This is accomplished by signalling the state transitions to a Camac input register. On the transition to the PULSE state, the MDS Plus system activates a set of Camac timing modules which can provide a resolution of a few microseconds. This system operates by sending an encoded 1 MHz serial timing signal throughout the facility where it is read and decoded by Camac modules as needed. The Camac timing modules are manufactured by MPB Technologies and were first used at the Tokamak de Varennes.

The PLC's are not fast enough to control of the shape and position of a non-circular plasma. During the PULSE state, control of each power supply's voltage is transferred to a hybrid computer.

Hybrid Computer

The hybrid computer provides real time feedback control of plasma current, position, shape and density. The analog inputs to the hybrid computer (up to 96) are mainly from magnetic pickup coils located inside the tokamak. The outputs go to the voltage programming inputs of 10 power supplies which drive 13 poloidal field coils. The computer is called a hybrid because it takes analog inputs and processes them in real time with a set of preloaded digital values. This approach provides speed and flexibility. Ref. 3 contains a more detailed description of the hybrid computer.

The digital values are preloaded into memory in the hybrid computer from a VAX computer through a Bitbus serial link. The digital values are selected by the VAX computer after a human operator provides the desired trajectory of each controlled parameter. The selection of digital coeffients uses both collected data and equilibrium models. The analog inputs, along with the digital stored data, is processed by microcontrollers, D/A converters and analog adders, integrators and differentiators. A so-called real time node determines the rate

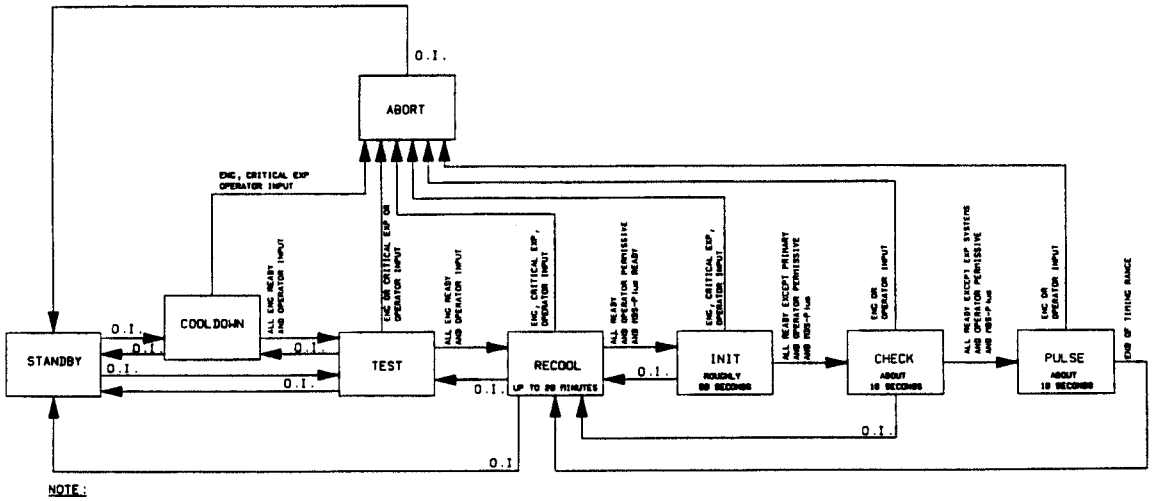

FIGURE 3
CONTROL SYSTEM STATE DIAGRAM

at which new digital values are taken from the hybrid memory and used. The real time node responds to external inputs. This feature may be used to intitiate pre-defined responses to selected conditions. For example, a real-time signal generated after a sequence of minor disruptions could cause the real-time node to jump to a set of coefficients that attempt a graceful shutdown.

References

[1] I.H. Hutchinson and the Alcator Group, "C-MOD: The Next Alcator," Proceedings IEEE 13th Symposium on Fusion Engineering, Vol 1 p.13 (1990).

[2] G. Flor, G. Manduchi, T. Fredian, J. Stillerman, K. Klare, "MDS-PLUS – A COMPREHENSIVE DATA ACQUISITION AND ANALYSIS SYSTEM," Proceedings of the 16th Symposium on Fusion Technology, London, U.K., 1990, pp. 1272-1276.

[3] J.B. Lister, Ph. Marmillod, J.M. Moret, "A Fast Response Hybrid Linearised Control System," Proc. of EPS Conference on Control Systems for Experimental Physics, Villam-Sur-Ollon, Switzerland, Oct. 1987 (LRP 332/87).

TEMPERATURE CONTROL AND MAGNET INSTRUMENTATION IN ALCATOR C-MOD

William M. Burke, Jr.
Plasma Fusion Center
Massachusetts Institute of Technology
Cambridge MA 02139

Abstract: The Alcator C-MOD tokamak is nearing completion at the M.I.T. Plasma Fusion Center. In C-MOD, a complex magnetic field is used to hold a hydrogen plasma in a vacuum. The toroidal field (TF) magnet which generates the primary field consists of copper conductors with glass-epoxy insulation and a massive stainless steel superstructure. The ohmic heating (OH) and equilibrium field (EF) field magnets are mounted directly on the vacuum vessel. These magnets are used to heat the plasma and to control its position

In normal operation, all of the magnets and the support structure are cooled to liquid nitrogen temperature (-200 °C) to take advantage of the low resistivity of copper at cryogenic temperatures. However the vacuum vessel, which is surrounded by cold magnets, must be kept relatively warm (0 °C) to maintain the integrity of the O-ring seals. The surface of the vacuum vessel is covered with 366 Kapton-foil electric heaters. Each heater is controlled and monitored individually using an integral K-type thermocouple.

During a plasma shot, the temperatures of the various magnets increase between 20 and 100 °C. The temperatures must be monitored to insure that the magnets are cooled properly before beginning another next shot. E-type thermocouples are used to measure local temperatures at several points on each magnet and on the support structure. The resistance of each magnet is also monitored between shots. This gives an excellent indication of average temperature.

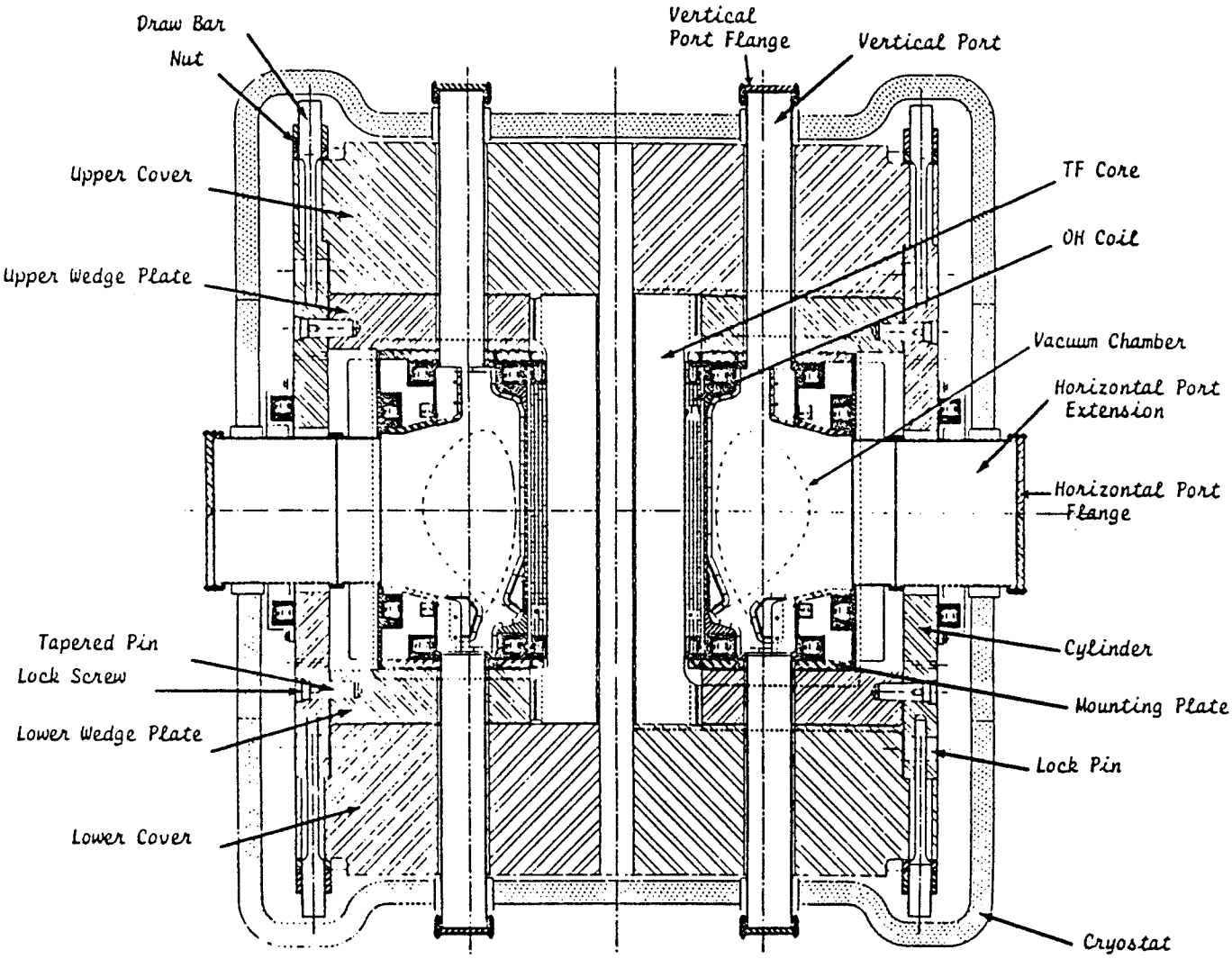

Figure 1. Cross-sectional View of Alcator C-Mod

The construction of C-MOD is described briefly with an emphasis on thermal considerations. The temperature limits for the various components and the overall performance requirements for the temperature control system are discussed. The design of the temperature control system hardware and software is presented in some detail.

Construction of Alcator C-MOD

The drawing in Figure 1 shows a cross-sectional view of Alcator C-MOD. The machine is nearly symmetric around the vertical axis and around the midplane. The TF magnet encloses the vacuum vessel and most of the other magnets. The OH magnets are wound directly on the central column of the TF, facing the inner cylinder wall of the vacuum vessel. Eight EF magnets are mounted directly on the vacuum vessel, four on the and four on the bottom. The massive structural components, the retaining cylinder and the top and bottom covers clamp the entire assembly together. A large fiberglass dewar provides insulation to keep the machine cold. 10 large horizontal ports, and 20 smaller vertical ports provide access to the vacuum vessel. The ports must pass through the TF magnet and the cylinder or covers to reach outside the dewar.

Figure 1 illustrates one of the problems with the compact design of C-MOD. There is very little free space between the vacuum vessel and the magnets for heaters or thermal insulation. Clearances are typically between 0.5 and 2.0 centimeters. A polyimide foam is used for thermal insulation wherever feasible. The outer wall of the vacuum vessel, the horizontal and vertical ports, and the EF coils are wrapped with the foam. However, is no thermal insulation between the OH magnets and the vacuum vessel.

Item	Mass (kg)	Capacity (J / °C)
Warm Components		
Vacuum vessel, coil mounting plate and internal hardware.	8690	**4.2×10^6**
Cold Components		
Top and bottom covers, cylinder, and misc hardware.	108,000	4.7×10^7
TF magnet	18,000	7.1×10^6
OH and EF Magnets	6100	2.4×10^6
Total	120,000	**5.7×10^7**

Table 1. Thermal Capacity of C-MOD Vacuum Vessel and Magnets

Thermal Analysis

The thermal parameters of C-MOD are summarized in Tables 1 and 2 below. The machine is very massive, approximately 130,000 kg. The vacuum vessel makes up about 10% of the total. The magnet coils and support structure make up the other 90%. Since the thermal inertia is large, the speed of the temperature control system is not critical. Response times on the order of 1 minute should be acceptable.

Operating Modes and Temperature Limits

When C-MOD is operating normally, the vacuum vessel will be at 0 °C and the magnets at -200 °C. The large surface area between the components allows for a substantial heat flow. Approximately 50 kW of the electric heating and 20 liters per minute of LN_2 cooling will be required to maintain a 200 °C temperature differential.

During a plasma shot, the magnet power supplies can deliver up to 300 MJ of energy to the machine in less than 10 seconds. 75% of this energy goes into the TF magnet, raising the temperature by as much as 70 °C. Most of the remaining energy goes into the other magnets, resulting in similar temperature increases. A small fraction of the energy goes into the vacuum vessel and the structural components via eddy current heating. Approximately 2000 liters of LN_2 are required to recool the magnets before the next shot. Since the desired time between shots is 20 minutes, the LN_2 flow must be at least 240 liters per minute.

Before C-MOD can begin operation, the vacuum vessel must be baked to no more than 150 °C to remove traces of water vapor, solvents, and other impurities. Since C-MOD requires a high vacuum, in the 1×10^{-8} Torr range, bakeout may take several days. Higher temperatures would reduce the baking time, but could also damage delicate Teflon wiring inside the vessel. The vacuum vessel heaters are used to bake the machine. However, the magnet cooling must also be active in order to keep the

	Area (m^2)	Resistance (°C / W)
Vacuum vessel to magnets and structure (foam insulation).	46.6	4.9×10^{-3}
Vacuum vessel to OH magnet (G10 and an air gap).	2.9	2.0×10^{-2}
Net Thermal Resistance		**3.8×10^{-3}**

Table 2. Thermal Resistance between C-MOD Vacuum Vessel and Magnets

magnet temperatures below 80 °C. The epoxy in the magnets will deteriorate at higher temperatures.

Approximately 80,000 liters of LN_2 are required to cool the magnets and structure from room temperature to -200 °C. The cooling rate must be limited to reduce thermal stresses in the structural components, particularly the top and bottom covers which are 66 cm thick. The heaters must also be active during cooldown to limit thermal stresses in the vacuum vessel.

Vacuum Vessel Heaters

366 Kapton-foil electric heaters are attached to the vacuum vessel. They cover an area of 36 square meters, approximately 75% of the total area of the vessel. The heaters are less than 0.2 centimeter in thickness. This was an important consideration given the limited space available. The heaters are also flexible; they can follow the simple curves of the vacuum vessel quite well. Heater power and thermocouple leads are routed along the surface of the machine to the closest port, then exit the dewar along the port.

Once C-MOD is assembled, the heaters are virtually inaccessible. Since a great deal of time and labor are required to tear down, repair, and rebuild the machine, the heater system design must be robust. Each heater includes two heating elements and two thermocouples. If a heating element or thermocouple is damaged during machine assembly or fails in operation, the spare may still be usable. The large number of heaters also provides a measure of redundancy. Loss of a single heater, or even several heaters at separate locations, will not compromise C-MOD performance and will not require a shut down.

The Kapton-foil heaters have a power rating of 7.5 kW per square meter with a single heating element in operation. This represents a nominal electrical load of 250 kW, although the available power is only 150 kW. The average duty factor for all the heaters must be restricted to 60% or less. But any single heater can operate continuously. This is five times larger than the nominal power requirement described earlier. The additional capacity will allow the system to perform in the face of small LN_2 leaks and other realities.

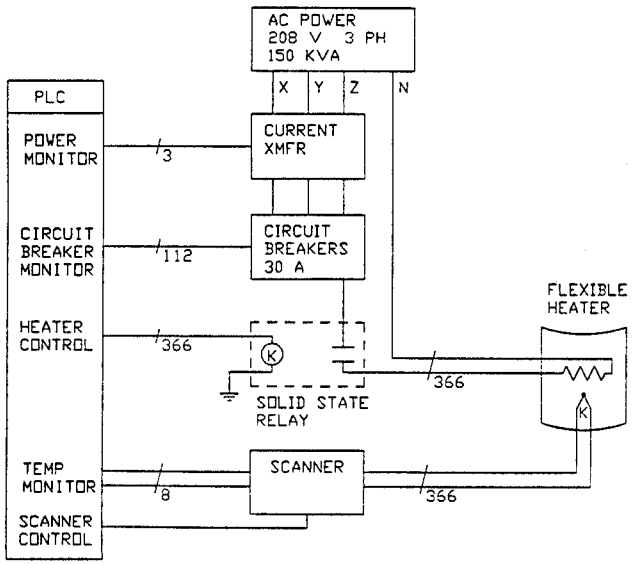

Figure 2 Block Diagram for the C-Mod Vacuum Vessel Heating System

A block diagram for the heater control system is shown in Figure 2. The heaters are run phase to neutral on a 208 VAC 3 phase service. They are fed by more than one hundred 30 A circuit breakers. An Allen-Bradley PLC (industrial controller) monitors the instantaneous power consumption and the status of all circuit breakers. The PLC controls the heaters via two racks of solid state relays, and reads groups of up to 8 thermocouples at a time using a reed relay scanner. The time required to read each group of thermocouples is approximately 1 second.

Instrumentation for Poloidal Field Coils

The OH and EF magnets each consist of a single continuous piece of copper. So a 4-wire resistance measurement will give a good indication of the average magnet temperature. In addition, E-type thermocouples are bonded to the EF magnets at several points to monitor the local temperatures. The OH magnets are not equipped with thermocouples.

A schematic diagram for a typical magnet resistance monitor is shown in Figure 3. A high voltage 4-pole normally open relay connects a 24 volt power supply and two voltage sense leads across the magnet bus between shots. Resistors in series with the power supply limit the current to approximately 5 amperes. One of the resistors acts a shunt to monitor the current in the magnet. The PLC monitors the shunt voltage and the amplified voltage from the sense leads to calculate magnet resistance and infer temperature.

Resistance measurements were made for all coils, in LN_2 and at room temperature. The cold values range from 1 to 16 milliohms. With 5 ampere drive current, the voltage drop on the magnets will vary from 1 to 80 millivolts. The signals will require amplification before going to the PLC.

Instrumentation for Toroidal Field Coils

The construction of the toroidal field magnet is much more complex than any of the PF magnets. It consists of 120 turns, and each turn is made up of 4 separate segments -- inside, outside, top, and bottom. All 120 inside segments form a monolithic central column. The other segments are bundled together in groups of six. The joints between segments are designed to slide when the magnet is pulsed. So the resistance of the magnet depends

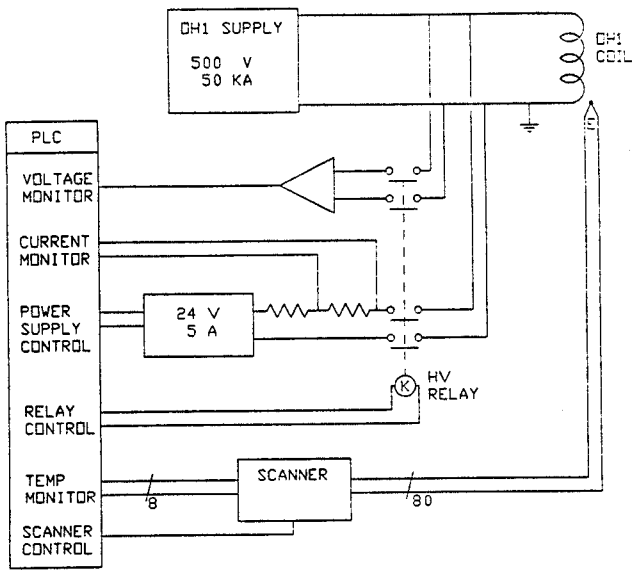

Figure 3. Block Diagram for the Alcator C-Mod Magnet Instrumentation

on the bulk resistance of the copper and on the contact resistance of all 480 sliding joints.

The instrumentation for the toroidal field magnet is similar to that for the PF magnets described earlier, but it is much more extensive. All of the magnet segments except for those in the central column have a voltage tap. So it is possible to monitor the resistance of outer sliding joints individually, and the inner joints in pairs. In addition, each bundle of six segments has a thermocouple. There are totals of 360 voltage taps and 60 thermocouples.

The resistance of the TF magnet at room temperature is 3.82 milliohms. The resistance of each segment is approx-imately 8 micro-ohms at room temperature, and 1.0 to 1.5 micro-ohms at normal operating temperatures. An auxiliary power supply will drive a current between 1 and 5 kA in the TF magnet between shots for monitoring the resistance (and for discharge cleaning). The PLC monitors the current in the TF coil using a shunt, and controls scanners to select the desired voltage tap and thermocouple. At this drive level, the voltage drop between adjacent taps will be in the range of 1 to 8 millivolts. The large number of signals will require a high voltage scanner for the voltage taps as well as the thermocouples.

Current Status

The construction of Alcator C-MOD is nearing completion. All of the heaters have been attached to the vacuum vessel. The magnets, the support structure, and the vacuum vessel have been assembled. The magnet power supplies and buswork have been installed and tested. Many elements of the computer control system are operational. The LN_2 cooling system components will be installed over the next few months.

Two heaters were damaged during machine assembly. One heater is open circuited, the other is short circuited to the vacuum vessel. In both cases, the spare heater remains functional.

The machine has been operated at low power levels and at room temperature. The heaters have been used to bake the machine to 70 °C, the maximum safe temperature without magnet cooling. Under these fairly benign conditions, the PLC can maintain a uniform vacuum vessel temperature to within ± 1 °C.

References

[1] W. Beck. "Alcator C-MOD Toroidal Filed Magnet Assembly," this conference.

[2] J. Daigle, "Fabrication of the Alcator C-MOD Ohmic Heating Coil and Coaxial Bus," this conference.

[3] A. Zhukovsky, "The Cooling System for Alcator C-MOD," Alcator memorandum, 28 August 1989.

FABRICATION OF ALCATOR C-MOD OHMIC HEATING COIL AND COAXIAL BUS

J. Daigle
Plasma Fusion Center
Massachusetts Institute of Technology
Cambridge, MA 02139

Abstract: The ohmic heating (OH) solenoid on Alcator C-MOD contains 3 separate coils, all wound in place on the TF magnet core. Each coil carries up to 50 kA at up to 4 kV. The winding geometry is complex, with the OH1 coil full length, 2 layers deep in some places and 4 layers in others. The two OH2 coils are partial length and 2 layers thick. The conductor is full-hard C-10700 silver bearing copper, 21 x 16 mm. The high stresses in this coil preclude brazing terminal plates or conductor lengths. The main coil conductor was fabricated by brazing several lengths together prior to final drawing. The terminal connections were made using soft solder and long scarf joints. The joining techniques and the terminal plate design were qualified with development and testing at both liquid nitrogen and room temperatures for a 100,000 cycle design life.

The OH solenoid, while trapped on the TF core, moves with respect to it. The TF core was covered with teflon-coated steel strips prior to winding, which were withdrawn after potting. Only millimeters of clearance are available between the solenoid, the core, and the vacuum chamber. Winding techniques were developed on a model coil that contained all the difficult layer-to-layer transitions but not the full height of the coil. Insulation is provided by 2 half-lapped layers of Kapton tape, overwound with glass fiber tape. Winding of the actual coil was carried out in the Alcator C-MOD experimental cell. After winding, the entire coil was vacuum impregnated with epoxy.

The very high magnetic fields (9 T on axis, over 18 T at the OH solenoid) require coaxial buss to all PF magnets. The OH coax is less than 40 mm in diameter yet carries up to 50 kA and withstands test voltages of over 15 kV. The coax has a 90 degree bend and contacts the coil through feltmetal pads.[1]

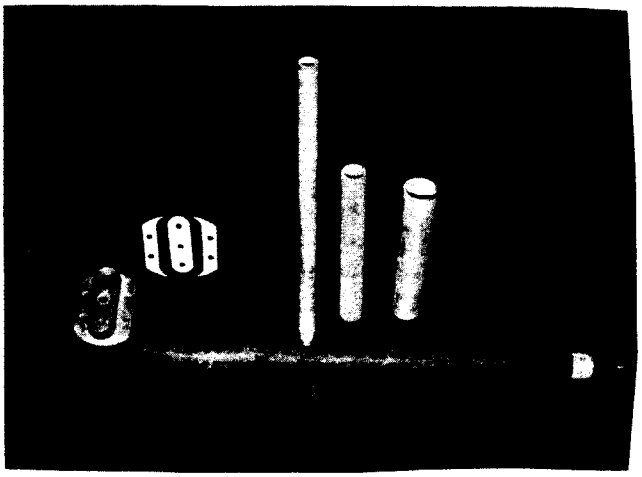

Figure 1: OH Coax with Extensions and Feltmetal Gaskets

Ohmic Heating Coil Description

The OH coils consist of 3 coils wound on the core of the TF magnet. The coils must operate in a background toroidal field of 18 T. This field is essentially parallel to the OH conductor except in the lead region, where substantial forces are generated. A coaxial lead carries the OH current across the toroidal field and through the outer steel cylinder to parallel buss bars.

The main OH1 coil has four layers over the central portion and two layers at each end. The innermost layer is wound over the full coil length. The second layer is then wound back on top of the first layer only until it passes under the eventual four layer section. The third and fourth layers of the center section are then wound. The OH1 coil is completed by taking the conductor from the fourth layer back to the unfinished second layer. The OH2U (upper) and OH2L (lower) coils are then wound into the notches in the main winding.

Conductor

The OH coils are wound from C10700 (1% silver bearing) copper. The conductor is drawn for full work hardening to a final size of 16mm x 21mm with 2mm radius corners. The length of OH1 conductor required two scarf joints brazed before final drawing. The OH2 coils have no conductor joints.

The C10700 bar conductor has a minimum yield strength of 290 MPA. The brazing of the scarf joints annealed the copper, but the full yield strength was regained after drawing. Sample joints were tested at 300°K and 80°K.

Insulation

The conductor was insulated at MIT using a tape-wrapping machine loaned by Princeton Plasma Physics Laboratory. The taping machine was installed on rails and pulled itself along the conductor as the insulation was wound. The insulated conductor was than wound onto the coil. Taping was much faster than coil winding.

The conductor was wrapped with two half-lapped layers of 0.076 mm Kapton with a dielectric strength of 10,000 volts and an ultimate elongation of 70%, and one half-lapped layer of .25 mm fiberglass cloth. The total turn-to-turn insulation thickness was 0.8 mm. The conductor was carefully de-burred and cleaned before taping.

Machined G-10 epoxy/glass fillers and transition pieces were utilized to avoid epoxy rich regions. Fillers were used to fill 70 gaps between layers. Ten transition pieces were used to support the conductor at layer transitions. The transition pieces also supported and aligned the terminal plates.

Machined G-10 insulating blocks surrounding the terminal plates were put in before vacuum impregnation. All liquid nitrogen cooling channels, terminal plate electrical connections, screw holes, etc., had to be filled with teflon inserts to prevent epoxy fill during impregnation. The outside diameter of coil the was wrapped with 0.05 mm Tedlar to keep epoxy build-up on the coil surface at a minimum for strength and cooling efficiency.

A two piece chamber was clamped onto the central column for epoxy impregnation of the OH solenoid assembly.

Winding of OH Coils

A 27-turn model OH coil was wound at in Allentown, PA in a collaborative effort between the M.I.T. Plasma Fusion Center and Everson Electric. The model coil was wound on a mock-up core with the same conductor used in the actual OH coils. The model coil included all transitions and geometry of the OH1 coil but omitted the long straight sections. The coil was wound on a double layer of teflon-covered stainless steel strips 1.25 mm thick by 9.5 mm wide. The strips were removed after epoxy impregnation of the coil to create a 2.5 mm cooling passage between the TF central column and the OH coil. Terminal plates were also installed on the model coil so that both coax and coil could be tested at operating voltage and current. The model coil was impulse tested to 15 kilovolts. A full current test was conducted at the MIT Francis Bitter National Magnet Laboratory. Four 10 kA rotating generators connected in parallel produced a 40 kA pulse for 4 sec. with a 3.5 sec. flattop. All tests were done with the coax installed. The model coil is now used as a high power test load for the TF, OH, and EF power supplies.

Winding the OH1 and the OH2 Coils

The central column of the TF magnet was installed in a surplus WWII-vintage lathe with protective covers over sliding joint region. The covers on each end of central column were used to fasten the central column to lathe face plate and to hold the terminal plates of the OH coils in their proper location.

The Central column has a 2.1 mm FRP (omnidirectional fiberglass) wrap around its diameter, extending about 100 mm beyond the OH coils. This wrap acts as the insulator between the central column and the OH and will be used as the inner wall of the cooling jacket for the OH coils.

The FRP wrap was coated three times with a semi-permanent release agent to prevent epoxy from bonding to the central column during impregnation. The FRP wrap forms the inner wall of the vacuum impregnation chamber.

Teflon coated stainless steel strips 1.25 mm thick by 9.5 mm wide were installed on the surface of TF's FRP wrap. They extend half the length of the OH coil from both ends and protrude 20 to 30 mm at each end. The strips were removed after coil impregnation by a tool that resembled the key on a tin of sardines. The strips were installed in two layers staggered by 2.5 cm at the center of the solenoid.

The first terminal plate was soldered to the conductor using a 95% tin 5% silver solder. The temperature of both the terminal plate and conductor was monitored to prevent annealing. Heating was applied with 300 watt electric bar heaters controlled by variable autotransformers.

After soldering, a V-shaped slot was cut in the conductor for the length of the engagement between the conductor and terminal plate. This equalized the shear stress through the whole length of the solder connection when in tension. The joint design was tested at both room and liquid nitrogen temperature at 67% of the conductor yield strength for 50,000 cycles, followed by another 50,000 cycles at 85% yield.

The terminal plate and conductor were then fed through the tensioning device and taping machine, and attached to the mounting plate of the coil winding fixture. The tensioning device uses friction clamps straighten the conductor and form it around the central column. The required tension was approximately 9000 N. The tensioning device was mounted on a pneumatic piston that aligns the conductor for placement on the central column.

At the end of the terminal plate a double offset bend in the conductor was required. Approximately ten such bends were made in the fabrication of the OH coils. Bends were made by clamping the conductor with a forming die clamp. The conductor was bent slightly too far to compensate for the spring-back of this hard material.

After installing the proper G-10 spacers and transition pieces we were ready to wind the coil. When winding the coil adjacent turns could damage the insulation if wound too close. Turns were tightened with a teflon block and mallet after each rotation of the lathe. The first layer was wound over the full coil length. At the end of the first layer a G-10 transition piece was installed. It guided the conductor to second layer in 45° rotation. The winding pitch was then changed to wind in the opposite direction. In winding the second layer we wound until it passes under the eventual four layer section. We then ramped up to the third layer, in 45° rotation and changed the winding pitch, to wind in the opposite direction.The third and forth layers are short, 18 turns compared to the 47 turns on first layer. At the end of the fourth layer, a combination of transition and filler pieces brought the conductor down to complete the second layer. Winding continued in the same direction until the first turn terminal plate, taking care to form the conductor to fit properly in the last turn terminal plate.

At this point, the windings were fastened in place with a number of steel bands, in order to release the tension and cut the conductor. The outer terminal plate is fitted to line up exactly with the existing inner terminal plate, before soldering.

Four 12.7 mm diameter G-10 dowels with .1 mm clearance align the terminal plates, with the dowels extending through mounting plate. Another V-slot was cut into the conductor after the second terminal plate was soldered on.

OH2U and OH2L were made in the same way. The assembly had to be rotated end for end in the lathe in order to wind OH2U with the proper field direction while keeping the outer jacket of the coax at ground.

The Fabrication and Testing of Terminal Plate in the Alcator C-MOD Ohmic Heating System

The two terminal plates make up the connection to the coaxial buss. They must operate for 50,000 plasma pulses, at stresses approaching while at 2/3 the yield strength. Each pulse actually stress the terminals twice, once during the initial charge and once during the double-swing. All operations start with the conductor at 77°K. The equivalent square wave is 50 kA for 3.5 seconds. Faults in the power system can produce peak voltages of 10 kV.

The terminal plates were insulated from each other by G-10 inserts in all through holes that tie the plates together. The inner terminal plate was covered with Kapton tape and multiple layers of pre-impregnated (B-stage) epoxy-glass insulation. The terminal plates were vacuum bagged and cured in an autoclave at three atmospheres.

The terminal plate insulation was machined to make it parallel to the terminal plate surface. An oval hole was cut through the insulation for the inner coax electrical connection. Oval insulators were fabricated with B-stage epoxy by vacuum bagging on a mandrel, then machining to size. They extend through the outer terminal plate and engage the oval hole in the insulator of inner terminal plate. The assembled terminal plates were Hi-potential tested to 10 KV.

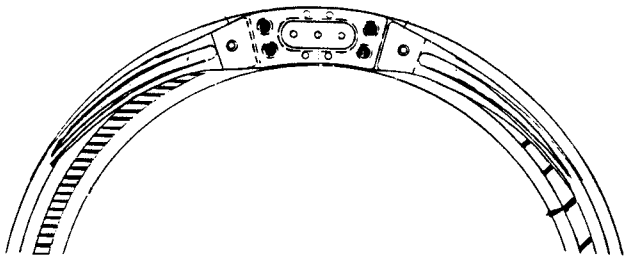

Figure 2: OH-2 Terminal Plates

The terminal plates are 12.5 mm thick at the coaxial end. The inner terminal plate has an additional 6.4 mm insulation. The total distance between the terminal plate surfaces is 16 mm.

The coax requires two parallel surfaces that mate perfectly with the terminal plates. Feltmetal gaskets compressed between the mating surfaces distributes the current evenly. The feltmetal is made up of C-20 OFHC 0.05 mm copper wires sintered in a random pattern to produce a steel wool-like material 0.9 mm thick. The feltmetal used has a density of 30% of copper. The feltmetal pads were then plated with 0.0025 mm Ag, without bridging fibers. The resistance of feltmetal was less than 10 micro-Ωcm^2.

We tested the connection with pressure sensitive paper. The feltmetal/coax interface has nearly complete surface contact. The feltmetal was compressed from .07 to .13 mm when the coax was bolted down.

The Epoxy Impregnation of the OH Coils

When the winding of the solenoid was completed it was vacuum impregnated in a large autoclave. This work was done at Everson Electric in Allentown, PA. The coil was wound and prepared for impregnation at MIT. All pockets were filled with teflon inserts, surfaces coated with a release agent, and all screw and bolt holes were filled with the appropriate teflon coated screw. The coil itself was wrapped with 25 mm wide tedlar with a small overlap. (This layer could not be very tight to allow epoxy flow in between wraps during impregnation, but tight enough to prevent epoxy rich areas). Glass matting and filler pieces were used to completely fill the mold.

The steel mold was clamped on to the FRP wrap of the central column. Silicon rubber RTV was used to seal all leaks. The package was then shipped to Everson Electric for the vacuum impregnation. The coil package was pre-heated to 40°C while the autoclave pressure was reduced to 150 microns. The coil was then potted with an epoxy mixture of:

DER-332	50 pbw	rosin
DER-736	50 pbw	rosin
NMA	90 pbv	hardner %
DMP-30	2 pbv	activator %

Once the mold was filled, the autoclave was pressurized to one atmosphere to force the epoxy into all voids in the coil. The coil package was than cured in an oven for:

4 Hrs.	@	60° C
4 Hrs.	@	80° C
12 Hrs.	@	93° C

After curing, the assembly was shipped back to MIT. The model was removed and the coils cleaned. All fillers were removed including the teflon-coated stainless steel strips. The assembly was fitted with an epoxy-glass cylinder. The space between the inner cylinder wall and the impregnated windings make the outside liquid nitrogen cooling chamber. Teflon coated glass-fiber boots were installed at each end of the OH coil inner diameter, to direct the flow of the liquid nitrogen. The cooling path forces liquid nitrogen along the outside of the solenoid and then over and down the inside.

OH Coax Description

Three identical coaxial leads were made to pass the high current pulse to the OH coils. The coaxes begin outside the retaining cylinder of the machine. Each coax has a 90° bend, with a 76 mm radius through the center of coax, 100 mm from the outer flange. The first coax section ends just inside the steel cylinder. Extensions pieces bring the coax through the cylinder after it has been installed. The inner coax sections have a 6.4 mm cooling hole through their length. Liquid nitrogen is passed through this channel.

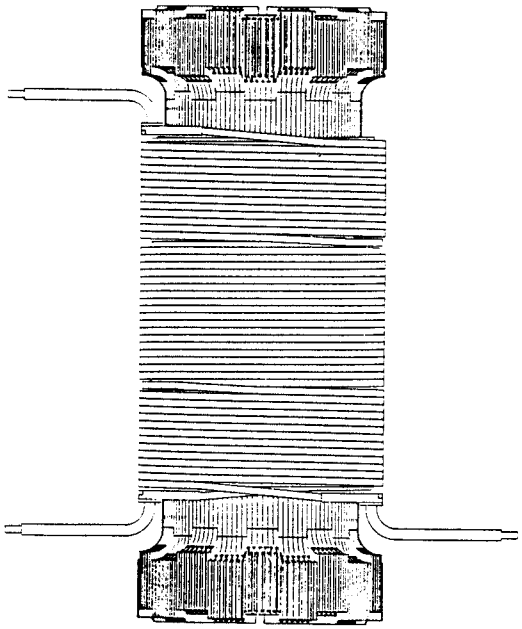

Figure 3. OH Coil with Coaxial Leads

Fabricating the Coax

The inner coax lead was gun drilled to make the cooling hole, then turned to 21 mm diameter. The oval inner coax flange was silver brazed to the inner coax at one end, and 3/8" NPT threaded female connection was cut at the other end. Both of these parts are made of OFHC copper. The outer coax lead is made of schedule 40 seamless copper pipe, with an OD of 33.4 mm and an ID of 25.4 mm. The outer coax flange was then sliver brazed on to one end and a 1" external NPT thread was cut at the other end. The parts were then silver plated for a better electrical connection.

The next step was to electrically insulate the coax. This had to be done in a way that would not damage the insulation while making the 90° bend. The insulation between outer and inner flanges was fabricated from B-stage epoxy in a manner similar to the terminal plates. This insulator extends through

outer terminal plate when installed.

The inner coax lead was wrapped with two half-lap layers of 0.09 mm bondable PTFE fluorocarbon film (teflon tape). This tape was used because of it's dielectric strength (9,000 volts), and elongation of 125%. Two half-lap layers of glass tape were then added to get a reasonably tight fit between the inner and outer coax, for epoxy impregnation.

We made special bending dies to be used with a hand metal bender to make our 90° bend. The fixture held the inner and outer coax firmly, as the coax was bent between dies.

The coax was then epoxy impregnated in a vacuum with the same epoxy mixture as the OH coils. The OH extensions were then made to accept the threaded pipe connections of the coax with a G-10 insert between them for voltage insulation.

The outer coax and the outer coax extension were also insulated with four layers of insulation. The first and third layers are one half-lapped layer of 0.08 mm by 25.4 mm Kapton tape. The second and fourth layer are a 0.25 mm glass reinforced B-stage epoxy. They were cured at 65°C for three hours.

Current and Voltage Testing of Coax

The coax was hi-potential tested to 15 kilovolts before and after cooling to 77°K. The test included potential from inner to outer conductors and from outer coax to ground.

The current testing was done at the same time as the high current test for the OH model coil at the MIT National Magnet Lab. The voltage drop was measured across the feltmetal connection, and across the coaxial threaded connection of coax to the coax extension. We ran this test at 40 Kiloamps. The results are summarized below.

.6u Ω across the feltmetal connection
2.1u Ω across the Threaded connection

Conclusions

Several items of importance emerged in the fabrication of the Alcator C-MOD OH coil system and the OH coax.

1. The yield strength of the full hard OH conductor was not compromised by the scarf joints.
2. Using Kapton tape as insulation for large conductors makes winding the coil easier because of it's strength, elongation, and insulation properties.
3. The technique of winding on teflon-coated steel strips, then removing the strips after winding and potting to create a freely moving assembly trapped on the TF core.
4. The cutting of the v-slot in the conductor at terminal plate to equalize the load distribution.
5. The excellent high voltage insulation provided by vacuum bagging and making parts from B-stage epoxy/glass in an autoclave.
6. Bending a large diameter solid coax 90° while maintaining it's electrical integrity.

References

[1] Feltmetal is a trademark of Brunswick Tecnetiks.

THYRISTOR DC CIRCUIT BREAKERS FOR ALCATOR C-MOD

S. Fairfax
Plasma Fusion Center
Massachusetts Institute of Technology
Cambridge, MA 02139

K. Sueker
Robicon Corp.
Division of High Voltage Engineering
Pittsburgh, PA 15239

Abstract: The Alcator C-MOD PF system requires DC circuit breakers in 5 poloidal field magnets for plasma initiation. Vacuum circuit breakers developed for the Alcator A and Alcator C experiments offered a proven technology but marginal reliability and relatively high maintenance costs. The thick vacuum chamber walls and heavy steel superstructure of Alcator C-MOD make relatively low start-up voltages attractive to limit eddy currents during plasma initiation.

A design based upon standard 77mm SCRs and diodes was chosen for several reasons. Bypass switches and other mechanical components were avoided to reduce maintenance costs and achieve high reliability on 5 separate systems. The circuit breakers will carry the full charging current pulse as well as the reverse swing current. Standard phase control devices offer superior current-carrying capability, low cost, and commonality with the devices, gate drives, and mounting hardware used in the magnet power supplies. Phase control SCRs have a longer turn-off time and require a larger counterpulse capacitor bank than inverter thyristors. The net cost of the additional capacitance is very small in a single-pulse, low duty-cycle system.

Design values and simulations for 3 switches are presented. Switch sections are rated 2 kV maximum interrupting voltage with bipolar current ratings of 50, 25, and 15 kA. A pulse-forming network provides the required 400 μsec turn-off pulse to the SCRs. The design is strongly influenced by the parasitic inductance in bus and circuit components. Time and cost limits precluded the construction of prototypes, so extensive simulation of the circuit was required. Two separate simulation approaches were cross-checked for accuracy and consistency.

Design Requirements

The commutation circuit provides the relatively high loop voltages required for plasma initiation. The C-MOD vacuum stainless steel chamber is over 2 cm thick in most places and contains no electrical break. Eddy currents in the vessel during any phase of the plasma complicate control. Eddy currents produced at start-up can be particularly troublesome, since they can easily exceed the total plasma current. There is a strong incentive to keep start-up voltages as low as possible while still providing the necessary electric and magnetic fields.

The design specification requires at least 20 Volts around the torus with limits on the magnitude of the vertical field, the field gradient, and the motion of the field null. The field null must be at either the inboard or outboard midplane as required, staying within an excursion of $\pm a/2$ for 5 mSec. The vertical field gradient at the null must be less than 0.01 T/m. Extensive modeling of the start-up [1], using a coupled filament model of the vacuum chamber and the surrounding superstructure, revealed that most magnets required less than 2 kV. The OH1 magnet requires terminal voltages up to 4 kV.

The relatively low voltages make solid-state switching competitive with vacuum contactor technology. Vacuum contactors can support recovery voltages up to 20 kV, and are more competitive at higher switching voltages. Single thyristors with voltage ratings exceeding 4 kV provide an ample safety factor for 2 kV switching duty. Vacuum contactors are subject to wear and failure due to a variety of mechanical problems. Analysis of Alcator C operating logs revealed that mechanical (as opposed to electrical) vacuum contactor failures resulted in about 3% of all shots that failed. The need for 5 commutation circuits on Alcator C-MOD made this failure rate intolerable. The maintenance cost of the mechanical contacts was also relatively high. A primary design requirement was reliability and low maintenance costs.

All of the DC converters associated with the commutation circuit are 4-quadrant, with bipolar output current. The OH2 and EF1 supplies are circulating current regulators that can cross 0 output current at any desired voltage. The OH1 converter is a standard lock-out dual bridge, where current and voltage to the load must be zero for some short time before the alternate bridge is enabled. Figure 1 shows the maximum performance load current pulses from the OH1, OH2, and EF1 power supplies. The commutation switch must pass bipolar currents. Mechanical switches suitable for 50 kA duty are expensive to buy and to maintain, so an electronic switch was preferable.

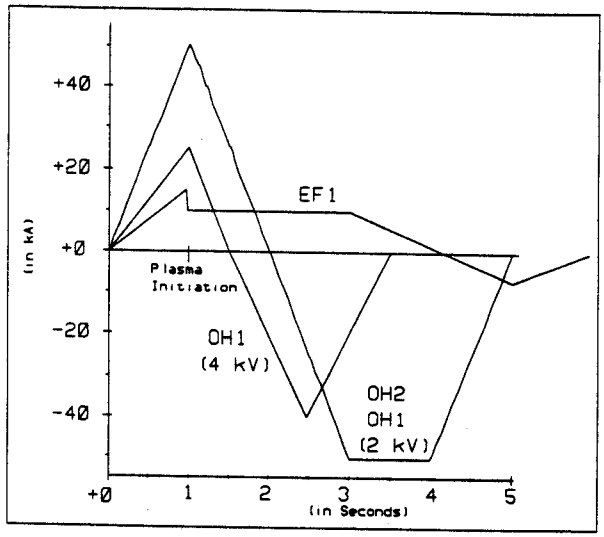

Figure 1: Maximum Switch Currents
OH1 Switch can be configured for 25 kA, 4 kV or 50 kA, 2 kV

The plasma start-up simulations predict that over 2 kV must be applied to the OH1 coil to provide 20 volts around the torus. The OH1 magnet and power supply rating is 50 kA with a 1-second flat-top. The simple solution of purchasing 2 50-kA switch sections and connecting them in series would have exceeded the already strained budget. Plasma initiation at lower electric fields is well documented and highly desireable for this machine. The OH1 switch is built in two sections. These sections may be connected in series to provide 4 kV switching at a maximum current of 25 kA. Connected in parallel, the full 50 kA current is available at a maximum voltage of 2 kV. This arrangement will allow for full voltage during initial operations,

while preserving the full charge and reverse-swing current once breakdown studies are completed.

Modeling

PSpice with the Behavioral Modeling option [2] is a powerful analog circuit simulation tool that includes ideal switches as circuit elements. These were used to construct behavioral models of thyristors.[3] The modeling process is aided by use of a schematic capture system to input the circuit rather than editing a text netlist. Teradyne offers the *Vanguard* [4] schematic capture package that provides translation to PSpice netlists. Vanguard includes a pseudo-oscilloscope to examine and manipulate the PSpice results, while MicroSim provides the Probe [2] Graphics package. The two products offer many complementary display and formatting capabilities. The circuit diagrams and waveforms in this paper were produced by the Teradyne package coupled with the PSpice simulator unless stated otherwise.

A completely separate simulation was undertaken by direct solution of the circuit differential equations. This simulation was done with numerical integration and carried out in QuickBASIC Version 7.1.[5] [6] The analysis was particularly critical in regard to the time allowed by the circuit for recovery of the main thyristors.

Run and plot time for the QuickBASIC model is only 3 seconds. This rapid execution and the simplicity of changing parameters allowed quick examination of many possibilities. Circuit modifications originating in either Cambridge or Pittsburgh were immediately applied to both models. The close agreement of the two simulations provides a high degree of confidence in the design.

SCR Selection

Currents in the main SCRs and diodes are defined by load currents and are not significantly affected by the breaker action. Their transient thermal impedance characteristic on small heat sinks were used along with an interative computer program which computed the junction temperature rise. The required number of parallel paths for each breaker was chosen to keep the peak junction temperatures below 100°C. This resulted in 12 parallel paths for the 50 kA units, 6 for 25 kA, and 4 for 15 kA.

Transient junction temperature rises for the switch SCRs were determined in like fashion but with the commutating current waveforms taken from the circuit simulation programs. Since switch current flows for only a millisecond or so, peak anode currents approaching 50 kA are permissible without excessive junction temperature rise. A high level gate drive of 40 V open- circuit, 4 A short-circuit, 500 nS rise time and 10 μS hold at 4 A is used to assure full device $\partial i/\partial t$ capability. Sustaining current is 500 mA. One switch SCR is used for the 15 kA and 25 kA breakers, 2 switch SCRs in parallel for the 50 kA units.

Reverse recovery characteristics of the SCRs and diodes were provided by the manufacturer. In both devices, the peak recovery current is a function of the circuit $\partial i/\partial t$ as the device current passes through zero. After reaching peak recovery current the device will develop an anode-cathode voltage such as to maintain an exponential decay of current in the circuit. The initial $\partial i/\partial t$ of this current may be as high as three times the circuit $\partial i/\partial t$ for the SCR and ten times circuit $\partial i/\partial t$ for the diode. Snubber circuits were designed to suppress the voltages produced as a result of this high $\partial i/\partial t$ passing through the circuit inductances.

This characterization permitted direct analysis by another QuickBASIC simulation. The devices were modeled as current sources forcing an exponential decay of device current. The RC networks were then designed to keep the recovery voltages well below the rated device peak reverse voltage. Snubber networks for the SCRs were limited by the 65A turn-on current limit of the C784. Saturating cores providing 2000 V-μS delay were added on each SCR anode to prevent discharge of neighboring RC networks on the paralleled devices. A 1 mΩ sharing resistor in series with each SCR/diode assembly assists in current sharing and provides a signal for the condution monitoring circuit (described later).

Basic Circuit

The basic circuit is shown in Figure 2. The main SCR conducts current in the forward direction, and the diode carries reverse currents. During commutation, the switch SCR connects the precharged capacitors and inductor to the main SCR forcing its net current to zero. A reactor in series with the diode has an inductance much larger than the parasitics associated with SCR or diode bus. The inductors and capacitors in the counterpulse network produce a trapezoidal pulse. Figure 3 shows the action of this circuit. The counterpulse current quickly rises to drive the main SCR current to zero, then provides a relatively constant $\partial i/\partial t$ through the diode and its inductor. The linear change in current provides a negative bias to the SCR, aiding in turn-off. Figure 4 shows the reverse bias across the main SCR during the recovery interval.

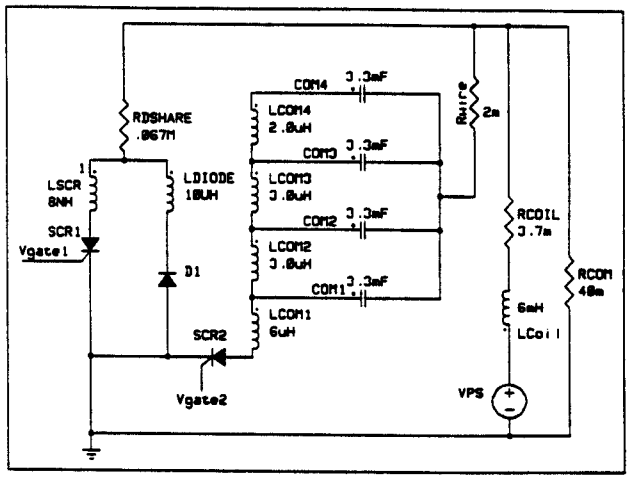

Figure 2: Basic Switch Circuit
The values shown are for the OH2 switch, rated 50 kA, 2 kV, utilizing 12 devices in parallel.

The pulse forming network was simulated using both 3 and 4-section designs. While 3-section designs were feasible they were much more sensitive to the element values and to mutual inductance than 4-section circuits. The size of the capacitor bank was not sensitive to the number of sections and so the 4-section design was chosen.

The choice of this particular circuit configuration was influenced by several factors. Using SCRs rather than diodes in the reverse circuit would have reduced the size of the commutation capacitor bank and the diode reactors. These cost savings would be balanced against increased costs for additional SCRs (the reverse current pulse is larger than the forward direction), firing circuits, and other controls. The use of SCRs in the reverse circuit would also have introduced a failure mode. If the

reverse SCR is not fired for any reason, particularly in the OH2 or EF1 circuits, the result will be loss of plasma position control and disruption. Failures in the forward circuit will result in no plasma being produced.

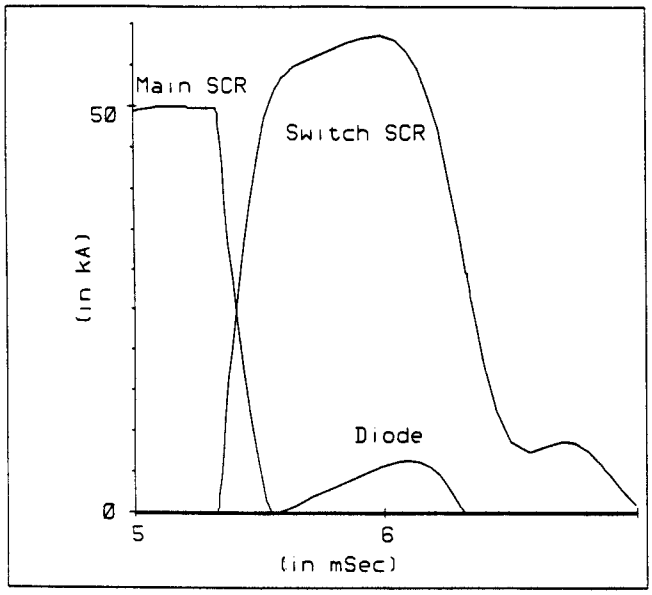

Figure 3: Currents in Switch Components During Commutation Interval

Controls and Interlocks

The basic commands for each switch are to close for charging of the coil and then open (fire the counterpulse network). Normally, the switches will be commmanded to close again after 20 msec. This re-closing operation can place high $\partial i/\partial t$ and $\partial v/\partial t$ stresses on the SCRs and influenced the choice of snubbers and saturable reactors. Switch controls are isolated from the power circuit by 30 m fiber optic cables. The control cabinets are further isolated by fiber optic links to the control room.

The Alcator control system utilzes both PLC's and CAMAC for control and monitoring of all systems.[8] The switches and the power supplies require simultaneous commands from both systems to operate. The PLC enables command responses while CAMAC timing signals close, open, and re-close each switch. The capacitor bank is charged before the pulse with the charge calculated and measured by the PLC. The charge is based upon the desired load current.

The switches protect themselves from most faults. All devices are fused, with electronic conduction monitoring. The conduction monitor circuits use the voltage drop across sharing resistors to drive an optical coupler. Fuse loss or failure of any device to conduct after application of a gate pulse is detected, with the offending device identified by an LED. A fault is signalled if a single device fires without command (and so attempts to conduct the full load current.) All other devices are gated on and the electronic conduction circuitry indicates which device failed. If voltages over 2200 volts are applied to the switch terminals (at either the main or commutating SCR's) a self-powered circuit fires the SCR's to prevent damage. This circuit uses the bus voltage to charge capacitors and fire the SCR gates, and is therefore independent of all external power or command signals. Operation of the self-powered circuit is signalled to the control cabinet. Loss or corruption of optical link data is detected and signaled as well as smoke, water or air flow loss, etc. A test switch in the SCR cabinet allows local firing of the devices to check gate pulses and perform maintenance. External commands are inhibited in this mode.

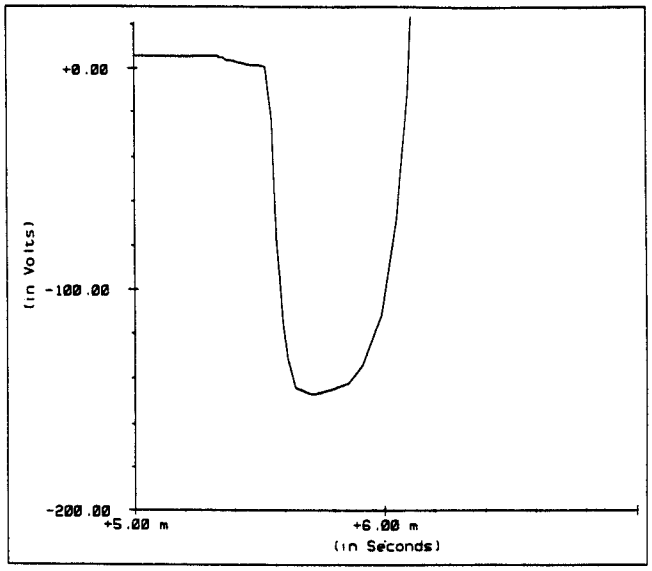

Figure 4
Voltage Across the Main SCR During the Turn-off Interval
The voltage is $\geq$ 100 volts for 420 μsec.

Resistors

The resistors that shunt each commutation switch are adjustable to provide voltages from a few hundred to 2000 volts at any current between 20% and 100% of the maximum. Each resistor is constructed of 91 $\times$ 152 cm Type 304 stainless steel plates cut in a labyrinth pattern. The cross section of each resistor varies with resistance. The resistors are designed with a worst case temperature rise less than 120°C. Normal operating temperatures, even at full current, are considerably lower.

The minimum voltage required for each resistor was determined by summing the minimum available inversion voltage (at maximum power supply current) and the coil resistance. (The heating of the coil and its resistance as a function of time was simulated with a PSpice model that assumes adiabatic heating of the copper. The model included both resistivity and specific heat variations as a function of temperature.) The minimum resistance will produce the same voltage across the coil (with the zero power supply voltage) as the power supply can produce at full inversion. All coils therefore have drive voltages ranging from 0 to 2 kV (4 kV for OH1) with zero power supply output when the switch is open. This allows for additional flexibility in "tuning" the drive voltage (by changing the power supply output voltage) during the plasma initiation interval.

Maximum and minimum voltages are determined, and maximum coil current is known. The minimum coil current determines the maximum resistance. There is no fundamental limit on the minimum current, but very low values will require a large, expensive resistor. The minimum coil current was set at about 20% of the maximum coil current. The actual value of I_{min} was adjusted slightly to allow for an integral number of resistor plates. Table 1 shows the values of each resistor. The units are kA, Volts, and milliohms.

Table 1

Coil	I_{max} (kA)	I_{min} (kA)	V_{max} (Volts)	V_{min} (Volts)	R_{max} (mΩ)	R_{min} (mΩ)
OH1	50	11.6	4000	564	345	11.3
OH2	50	13.7	2000	181	145	3.6
EF1	15	2.8	2000	250	718	16.7

The resistors are normally energized for only 20 msec or so each pulse, after which they are shorted out by the associated SCR switch. Normal temperature rise is less than 40°C, with forced air cooling between pulses. If the switch fails to re- close after commutation, each resistor will dissipate the maximum coil energy with a temperature rise of less than 120°C.

Counter-Pulse Networks

The main SCRs require a reverse bias of at least 100 volts for at least 400 μsec in order to regain forward blocking capability.[7] The counterpulse capacitors must drive the main SCR current to zero and maintain the reverse bias. Many commutation circuits use a simple LC resonant circuit to produce a half-sinusoid pulse. Breaking the resonant inductor into sections allows for finer control of the counterpulse waveform. The pulse-forming networks were simulated and examined for sensitivity to small variations in component values. Networks with 3 LC sections were considered but eventually rejected as too sensitive to component tolerance and mutual inductance. Networks with 4 LC sections allowed greater choice and tolerance in inductor selection.

The capacitors were chosen for economy and convenience in packaging. Each capacitor is rated 1,100 μF at 4 kV. The maximum charging voltage is 2 kV, but the capacitors are always fully reversed, for a total swing of 4 kV.

The values shown are not optimum. The primary goal was to produce a design that would work. Secondary considerations included reducing the number of different sizes of inductors and capacitors required. The schedule and budget pressures made it impractical to invest significant engineering time in careful parametric analysis and trade-off studies. The pulse-forming networks were verified to produce the required current and SCR reverse bias over the full range of allowable commutation resistance. This check revealed that the original specification of the minimum OH2 resistance was too low. The minimum OH2 resistance had to be increased to prevent the resistor from shunting too much counterpulse current away from the SCRs.

Table 2

Switch	$L_{com}1$ μH	$L_{com}2$ μH	$L_{com}3$ μH	$L_{com}4$ μH	$C_{com}1-4$ mF
OH1	3	3	6	12	2.2
OH2	2	3	3	6	3.3
EF1	6	9	9	12	1.1

Budget

The cost of the 6 SCR and diode sections, including controls, was $714K from Robicon Corporation. MIT provided the counterpulse networks and commutation resistors. The commutation resistors were plasma cut and drilled by an outside vendor for $45K plus $4K for hardware and assembly. The pulse forming networks cost $56K for capacitors and inductors. Capacitor charging power supplies, high voltage relays, bleed and dump resistors, and equipment stands totaled $50K. The total hardware cost for the 6 switches was approximately $870K. The marginal cost of the larger capacitor banks is clearly quite low.

Status

The full set of 6 switches have been manufactured, delivered, and installed. At the time of writing, the OH1 switch is configured for 25 kA, 4 kV operation. Preliminary tests at 10 kA, 1 kV were sucessful. The two EF1 switches have been tested at 8 kA, 1 kV. The switches will be tested at maximum design ratings as soon as the converters and loads are ready.

References

[1] Pillsbury, Jr., R.D. "Plasma Startup Scenario for the Alcator C-MOD Device." Proceedings IEEE 13th Symposium on Fusion Engineering, p. 642, 1990

[2] PSpice and Probe are registered trademarks of MicroSim Corporation.

[3] Giacoletto, Lawrence J., "Simple SCR and TRIAC PSpice Computer Models," IEEE Trans. Industrial Electronics, Vol 36., No. 3, August 1989.

[4] Vanguard is a registered trademark of Teradyne, Inc.

[5] Sueker, K. and Fairfax, S., "Design and Construction of Thyristor DC Circuit Breakers for Alcator C-MOD," IEEE 14th Symposium on Fusion Engineering, San Diego, CA, Oct 1-3, 1991.

[6] QuickBASIC is a registered trademark of Microsoft Corporation.

[7] Values from Data Sheet for GE784 SCR. General Electric Static Power Component Operation, Malvern, PA.

[8] Bosco, J., Fairfax, S., "The Alcator C-MOD Control System," IEEE 14th Symposium on Fusion Engineering, San Diego, CA, Oct. 1-3, 1991.

DESIGN AND CONSTRUCTION OF THYRISTOR DC CIRCUIT BREAKERS FOR ALCATOR C-MOD

Keith H. Sueker
Robicon Corporation, 100 Sagamore Hill Road, Pittsburgh, PA 15235

Stephen A. Fairfax
MIT Plasma Fusion Center, 175 Albany Street, Cambridge, MA 02139

Abstract

The detailed design of the Alcator C-MOD thyristor DC circuit breakers required extensive simulation and careful consideration of parasitic elements as well as device recovery and turn-on limitations. Simulations were performed both on commercially available packages and with direct solution of circuit equations with custom programs. The need for high reliability and minimum device count resulted in the choice of 77 mm devices normally used in phase control applications. Fast recovery devices offer modest savings in counterpulse capacitor and snubber networks, but these are more than offset by the higher losses and increased number of devices.

The circuit uses up to 12 parallel paths to carry pulsed currents as high as 50 kA. Maximum interrupting voltages of 2 kV are supported by devices rated 4.4 kV. Each SCR is shunted by a diode in series with an air core decoupling reactor. The counterpulse capacitor is discharged through 1 or 2 SCRs and utilizes a pulse forming network to quickly reduce the main SCR current to zero, then provide an relatively low and stable reverse voltage during the commutation interval. All devices are mounted with radial symmetry. The diode reactors are subject to modest forces under normal conditions but large lateral forces when adjacent paths are lost.

Circuit Details

The basic circuit for the DC circuit breakers is shown in Fig. 1. SCR1 carries the load current prior to interruption and diode D1 carries the reverse polarity load current needed for ohmic heating and plasma control. The pulse forming network (PFN) is precharged to a voltage appropriate to the expected load current, 2 kV for a 50 kA load, with the polarity shown. SCR1 is gated and the power supply is then energized to build up current in the load. Load current is interrupted by gating SCR2 which discharges the PFN into SCR1. Current in SCR1 is rapidly reduced to zero, after which PFN current diverts to D1 and continues to flow in that path. When PFN current falls below load current, the diode ceases to conduct and load current then flows through the resistor, RCOM, and the PFN.

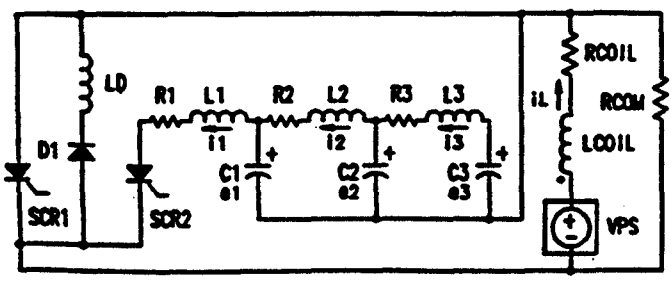

Fig. 1 Elementary DC Breaker Schematic

Finally, current in SCR2 ceases and it drops out of conduction. The circuit continues in a quiescent state until SCR1 is again gated, some 10-20 ms later. Current is forced into the ionized plasma as coil current is driven down and reversed at constant di/dt.

While this summary describes the basic circuit operation, there are many subtleties which must be considered in the design of the hardware. Computer simulation was used to study the various effects so as to assure success in the installation. Because the DC breakers are critical items in the operation of Alcator C-MOD, two independent studies were conducted simultaneously using two different simulation approaches.

Simulation in PSpice

PSpice [1] is a powerful analog circuit simulation and graphic display tool for personal computers and workstations. The package includes ideal switches as circuit elements, and these can be utilized to construct behavioral models of thyristors [2]. The modeling process is aided by the use of a schematic capture system to input the circuit. Teradyne offers the *Vanguard*[3] schematic capture package that provides translation of schematics to PSpice netlists and a pseudo-oscilloscope graphics package to examine and manipulate the results.

PSpice offers speed, flexibility and a large library of circuit elements. As with any simulation, the user must carefully test the results against empirical data or analytical solutions. The use of behavioral as opposed to physical models is particularly fraught with hazard. A few minutes spent in mathematical analysis of the circuit in question will often develop more insight than days spent varying parameters and topologies of a computer model.

The primary advantages of PSpice over high-level language simulation are the ease and simplicity of constructing and altering networks and the ability to view the results without the trouble of formatting or translating to a particular graphics package. The use of the schematic capture for netlist creation helps assure that the circuit under simulation is the same as the one the designer wishes to simulate. PSpice offers an option, called Behavioral Modeling, that allows the description of non-linear circuit elements in a variety of ways.

The switch elements in PSpice are actually voltage controlled resistors which exhibit gain in the transition region. Numerical instability was observed during preliminary work due to this effect. Decreasing the gain of the switch by reducing the ratio of on- to off-state resistance and increasing the voltage range over which the switch action occurred eliminated this problem.

PSpice utilizes default values for voltage and current accuracy that are well suited for small circuits and low-power devices. As discussed in the "Hints" section of the user's manual, high-power circuits need to adjust the desired accuracy of voltages, currents and charges so that the total dynamic range of the circuit under simulation is much less that 12 orders of magnitude. The circuits considered here utilize currents approaching 100 kA and charges in excess of 35 Coulombs; tolerances of 1 mA and 10 pC were found to produce satisfactory results in this work. Typical simulations required 100 seconds or less on a 80386 processor running at 20 MHz.

The behavioral model used for the GE C784 series SCR is shown in Fig. 2. The circuit is similar to the basic model given in [3], with additions for simulation of the forward voltage drop and the use of several devices in parallel. The parameters NUM_SCR and SHARE determine the number of devices in parallel and the maximum mismatch in current sharing between parallel devices.

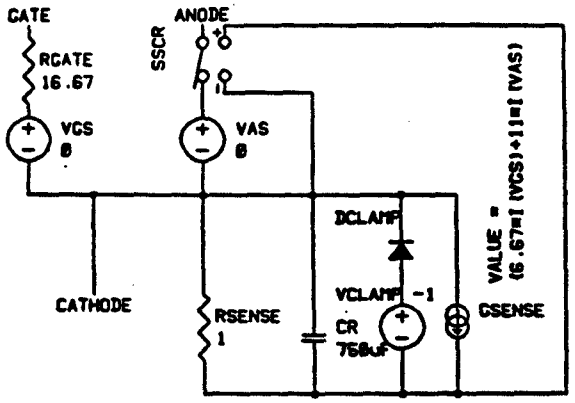

Fig. 2 Behavioral Model - GE C784 Thyristor

The current source is driven both by gate current and by anode-cathode current with voltage across the capacitor used to control the switch. The voltage source and diode clamp the capacitor's voltage to provide a consistent turn-off delay. The values shown provide for forward and reverse breakover at 4500 volts and turn-off delay of 350-400 μs. This circuit also exhibits reverse recovery currents similar to the real device, but the network shown was not adjusted to accurately simulate that characteristic.

Fig. 3 shows a diode network driven by SCR current scaled for the number of parallel devices and current sharing. This provides a forward voltage which is applied via the voltage-controlled voltage source to the SCR model. The forward voltage drop is also used to compute the peak power in the SCR.

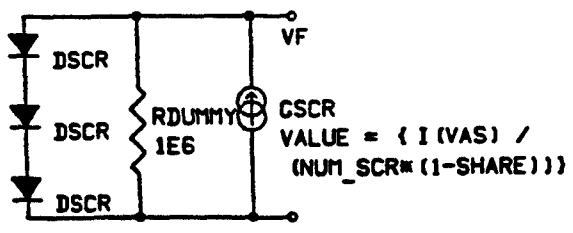

Fig. 3 Thyristor Forward Voltage Model

The network shown in Fig. 4 can be added to provide a quick estimate of the peak junction temperature. Resistors and capacitors are physical models of the SCR materials. The details of constructing and qualifying the thermal model are beyond the scope of this paper.

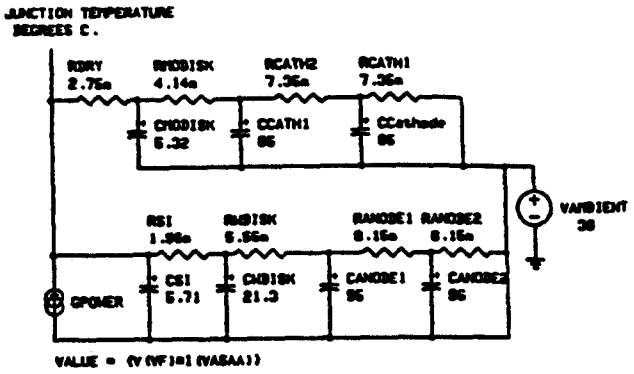

Fig. 4 Junction Temperature Network

Solution of Circuit Equations

Relatively simple circuit configurations can easily be simulated in a high level computer language by numerical solution of the circuit differential equations. Forward integration can be used instead of more complicated, but efficient, center value integration. The difference between a simple simulation running in five seconds and an optimized program running in five milliseconds is generally of no moment if programming time can be saved. The catch, of course, is that the circuit must be amenable to representation by simple equations.

There are several advantages to the direct solution of circuit equations over the use of canned software packages. First, nonlinear circuit elements can be incorporated easily, either by equations or simple interpolation routines from empirical data. Second, the circuit topology can be changed in response to time or circuit parameters by diverting to subroutines. Breakpoints can be set for options or partial solutions presented for inspection. Third, the output can be formatted, graphed or arranged in any fashion offered by the language and machine support.

Any circuit which can be expressed as a series of integral equations can be evaluated easily by numerical integration. For example,

$$e = L\partial i/\partial t \quad (1A)$$

$$i(t) = \int e\partial t/L \quad (1B)$$

$$i = i+e*d/L \quad (1C)$$

$$i = C\partial e/\partial t \quad (2A)$$

$$e(t) = \int i\partial t/C \quad (2B)$$

$$e = e+i*d/C \quad (2C)$$

where d = Δt and equations (1C) and (2C) are in computer format for discrete integration.

DC Circuit Breaker Simulation

By extension of these procedures, the behavior of the commutating circuit in Fig. 1 as SCR2 is fired can be described initially by equations (3) through (10) in computer form.

$$\text{(Start)}\quad i3 = i3 + (e3-e2-R3*i3)*d/L3 \qquad (3)$$

$$i2 = i2 + (e2-e1-R2*i2)*d/L2 \qquad (4)$$

$$i1 = i1 + (e1-R1*i1)*d/L1 \qquad (5)$$

$$e3 = e3 - i3*d/C3 \qquad (6)$$

$$e2 = e2 - (i2-i3)*d/C2 \qquad (7)$$

$$e1 = e1 - (i1-i2)*d/C1 \qquad (8)$$

$$iSCR1 = iL - i1 \qquad (9)$$

$$t = t+d \quad \text{(Return to start)} \qquad (10)$$

The circuit currents and voltages can then be developed by choosing initial conditions plus a value for d and then solving iteratively. A d value of 2.5 μs proved satisfactory.

Circuit Operation

Assuming the current from the PFN reaches a value greater than iL, SCR1 will be driven out of conduction. Reverse recovery phenomena in the thyristors and diodes, although critically important in snubber design, do not affect the pulse forming network to any great extent and can be ignored in the simulation.

Following current zero in SCR1, SCR2 will drive a net current through D1, the value of which is governed by the characteristics of the PFN when driving LD as a load. At some point, the PFN starts to run out of energy and the current through SCR2 decreases. Since load current is constant, the net current through D1 decreases and the voltage across Ld then reverses. This voltage reversal forward biases SCR1 and must occur at a time long enough after current zero, roughly 400 μs, so that SCR1 has regained blocking capability. During this time period, LD is simply added to L3 as far as circuit simulation is concerned.

When the current from the PFN falls below the load current, iL, the diode will recover and load current then flows through RCOM. The PFN capacitors become charged in the opposite polarity. Finally, the current through SCR2 falls to zero and it, too, recovers. The entire process is shown in Fig. 5 where the principal voltages and currents are identified and graphed over the commutation period. This simulation runs and plots in 3 seconds on an 80386SX at 16 MHz with Microsoft QuickBASIC v7.1 [3].

Junction Temperature Rise

The number of semiconductor devices required in parallel can be determined from their transient thermal impedance characteristics and the current waveform. The pulse lifetime curve for the C784 shows that the junction temperature rise should not exceed 75°C. for a 100,000 cycle load life. Thyristors at SCR1 in Fig. 1 must carry a load current rising to 50 kA in 1 second and falling to zero in another second. Those at SCR2 share the wave-form shown in Fig. 5 which rises to a peak value of some 65-70 kA. Diode current is primarily a load current rising to 50 kA in 1 second, holding for 1 second, and then falling to zero in another second.

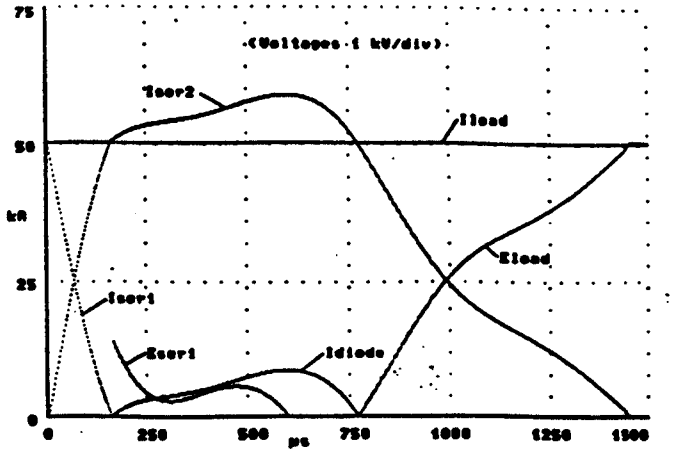

Fig. 5 DC Breaker Voltages and Currents

The thermal system of the semiconductors can be represented by the log-log plot of the transient thermal impedance for the device and a line of slope +½ drawn asymptotic to the TTZ curve. The conduction current waveform is divided up into a suitable number of time intervals and iterative procedures described in the various SCR handbooks used with a computer program[4]. A representative curve of current/temperature/time is shown in Fig. 6.

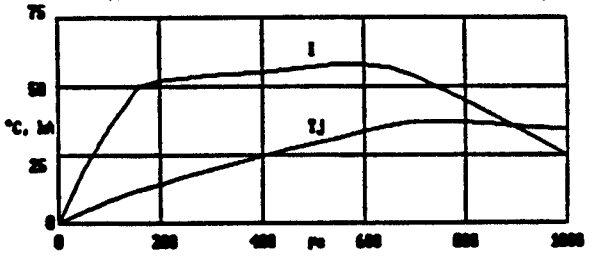

Fig. 6 Thyristor Junction Temperature Profile

Recovery Simulation and Snubbers

Since the load circuit has been taken as a current source, both SCR1 and D1 recover with e3 as a voltage source. SCR1, the first to recover, sees L3 and LD in parallel as a source inductance whereas D1 sees LD and L3 in series. SCR2 is driven by e3 plus the load drop across RL with LD and L3 in series as source inductance. Since recovery takes place in a time frame short relative to circuit time constants, the source voltages can be regarded as fixed during the recovery interval, and all three devices can be represented by a single circuit with parameter changes. Values for circuit variables can be taken from the main program output at appropriate times.

Fig. 7 shows a semiconductor recovery characteristic. There is no significant voltage drop across the device until recovery begins at a peak reverse current determined by the circuit di/dt. The semiconductor then acts as a current source which drives an exponentially decreasing current with initial di/dt

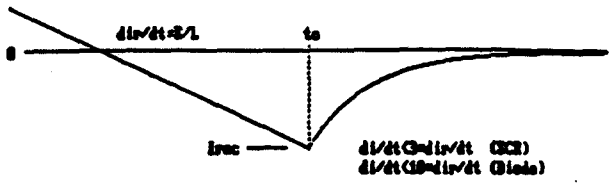

Fig. 7 Semiconductor Recovery Characteristic

set at 3X (thyristor) or 10X (diode) current zero crossing di/dt. The R/C snubber appears in parallel with the series circuit of source voltage and source inductance. An iterative computer program is used for simulation.

Snubber resistors for the thyristors must be selected so that the initial snubber discharge current on turn-on does not exceed the 65 A rating for the C784 devices. This duty occurs not at the start of load current but when SCR1 is re-gated to establish plasma current after ignition. Since neither thyristors nor diode have been conducting, snubber capacitors for SCR1 are charged to the full load voltage of 2 kV, and a minimum resistor value of 30 ohms is required for each device. A capacitor value can then be selected from the recovery simulation to limit thyristor peak voltage. Recovery voltage is shown in Fig. 8 for a 30 ohm resistor and 2μF capacitor on each thyristor.

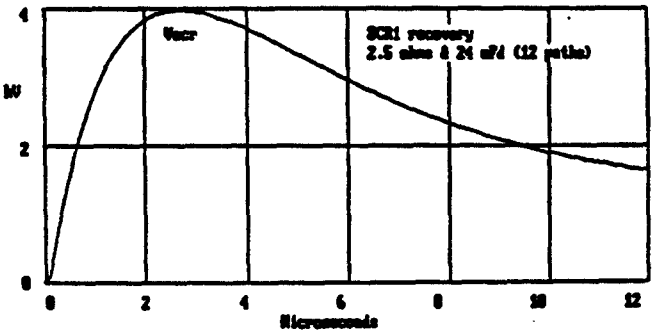

Fig. 8 Thyristor Recovery Voltage

SCR2 will have a snubber charged to the difference between e1 and load voltage. The duty is less severe. Diodes have no restrictions on snubber ratings, so a more cavalier approach can be taken with cost and size as the only constraints. Snubber values of 4 μF and 10 ohms were used on each diode.

Design Details [5]

Thyristor Gate Drive

In paralleled thyristors, it is imperative that all devices turn on simultaneously so that the circuit di/dt can be shared. Also, any one device turning on early will tend to discharge the adjacent R/C networks and may encounter excessive turn-on current. These problems can be minimized by installing a saturating core in series with each device so as to delay anode current for a time long enough to account for dispersion in intrinsic thyristor turn-on times and variation in gate drivers.

In the poloidal switches, saturating cores are used to provide 2000 V-μs minimum delay. Gating circuits have optical couplers with low delay dispersion as well as a pulse rise time of less than 500 ns. Isolation within the 2 kV switch potential is furnished by integrated circuit optical couplers whereas fiber optic couplers are used to furnish the required 5 kV operating voltage to ground.

Gate drive is supplied from a small power supply at each gate with a series transistor driven from an optical isolator. Two such circuits are used on each gate with the pair alternating drive at a rate of some 200 Hz. The result is a continuous gate drive which is never less than 500 mA and which applies a drive of 40 V, 4 A for about 20 μs every 5 ms. The gate drive for SCR1 is removed for plasma ignition, and the drivers then recharge to provide a full rated gate drive (40 V, 4A) immediately upon receiving a control signal for plasma current drive.

In addition to the controlled gate drives, each switch thyristor is connected to a second gate drive circuit which derives its operating power from the thyristor anode voltage. This circuit is set to fire the thyristor gates automatically if the anode voltage exceeds a preset level. It is intended to protect the thyristors from circuit misadventures.

Conduction Monitoring

Thyristor and diode conduction are monitored by LEDs connected across the current sharing resistors. Logic circuits incorporate gating and load current information to assure that all devices are actually conducting at proper times and that no parallel paths have been lost. Status signals are sent continuously to the ground level communications circuits.

Pulse Forming Network (PFN)

SCR1 is reverse biased and can recover so long as the current through the diode path is increasing. Therefore, it is desirable to have a slowly rising current in the diode so as to minimize energy storage requirements and limit peak currents in the commutating thyristors. The PFN serves this purpose.

Three capacitors and three inductors are proportioned so as to provide the desired discharge characteristic. A total of 6.75 μH and 10,000 μF are used. Stored energy is a maximum of 20 kJ.

Mechanical Layout

Twelve parallel thyristors are required to carry the 50 kA load current and two parallel devices for the commutating current. Current sharing under both static and dynamic conditions is assured by the use of stainless steel sharing resistors providing some 4 volts drop, and by the use of radial symmetry to balance all self and mutual inductances. The high di/dt rates inherent in these switches would make the dynamic current distribution uncertain with a linear mechanical layout.

Diode reactors, mounted radially, are subject to modest radial forces under normal conditions of balanced conduction. When several adjacent paths are lost, however, lateral force reaches 4300 lbs at the reactor center. Accordingly, the reactors are wound with impregnated solid windings and are mounted with reinforced, hot rolled structural steel angle to a ¼" thick steel cabinet floor.

The breakers are cooled with forced air circulation and air-to-water heat exchangers. Centrifugal fans are used to handle the relatively high head loss inherent in compact heat exchangers. Air flow switches are used for protection, and the power cabinets are also equipped with smoke and water detectors. The two power cabinets for the OH2 breaker are mounted on opposite sides of a common control cabinet. They will be connected in series to break 4 kV at 50 kA.

Communications

All signals between the control cabinet and a remote control cabinet are carried on two fiber optic cables. Although the control cabinet circuitry is already isolated from switch potentials, the fiber optic cables furnish a second level of isolation safety. Control signals from the host computer are carried on two eight-bit data words at a 225 kbit/s rate. Status and interlocking signals return on two concatenated words, six data bits each, at the same rate. The return multiplexing circuitry can easily accommodate additional data words.

Other Breakers

The description above covers the two 50 kA OH2 DC circuit breakers, each of which has 12 parallel thyristors and 12 parallel diodes along with 2 parallel switch thyristors. The overall system also requires two 25 kA DC breakers for the OH1 coils and two 15 kA DC breakers for the EF1 coils. Each of these breakers uses a single switch thyristor with six paralleled main thyristors and diodes for OH1 and four paralleled sets for EF1. The smaller breaker pairs are mounted in common power cabinets adjacent to control cabinets.

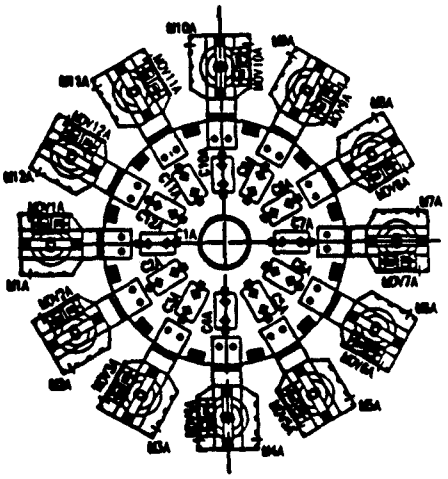

Fig. 9 Section View - OH2 DC Breaker

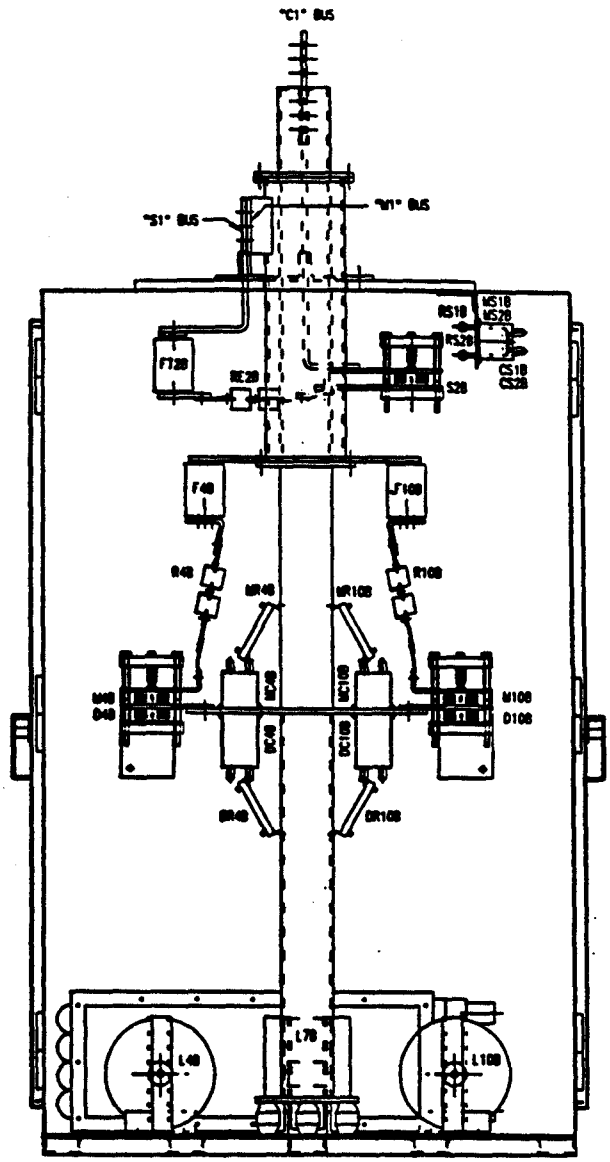

Fig. 10 Elevation View - OH2 DC Breaker

References

[1] PSpice is a registered trademark of MicroSim Corporation, Irvine, CA

[2] *Vanguard* is a registered trademark of Teradyne Inc., Santa Clara, CA.

[3] Giacoletto, Lawrence J., *Simple SCR and TRIAC PSpice Computer Models*, IEEE Trans. Ind. Electronics, Vol. 36, No. 3, August 1989

[4] QuickBASIC is a registered trademark of Microsoft Corporation.

[5] Newell, William E., *Transient Thermal analuysis of Solid-State Power Devices - Making a Dreaded Process Easy*, IEEE Trans. Ind. Appl., Vol. IA-12, No. 4, Jul/Aug 1976

[6] Fairfax, Stephen A. and Sueker, Keith H., *Thyristor DC Breakers for Alcator C-MOD*, 14th IEEE/PSS Symposium on Fusion Engineering, San Diego, CA 1991

ALCATOR C-MOD
ENVIRONMENTAL HEALTH AND RADIATION PROGRAM DEVELOPMENT

T.P. Fuller, C.L. Fiore

Plasma Fusion Center
Massachusetts Institute of Technology
Cambridge, MA 02139

Abstract

The challenge of providing an integrated health and safety program for an advanced fusion facility within the university atmosphere is addressed in the Environment, Health & Safety program design for the Alcator C-Mod project at MIT. The hazards common to all fusion experiments such as radiation, cryogenics, high power and voltage, confined spaces, hazardous chemicals, and heavy mechanical and machine equipment must be controlled in an acceptable manner with the coordination of university and facility programs. The development of this program is detailed.

Introduction

The Alcator C-Mod experiment (Reference 1) provides a work environment of a pulsed fusion experiment which presents a challenging mix of occupational hazards to the team of professionals responsible for the health and safety of experiment workers. Combinations of these hazards and the difficulties in personnel monitoring and protection must be addressed together for the first time in these fusion experiments, using the coordinated efforts of university and facility staff.

The roles of individuals and organizations responsible for occupational health and safety at the Alcator C-Mod have been defined. Hazards have been identified and prioritized. Methods for surveillance and monitoring of work areas and personnel exposure to various hazards have been developed. Programs and procedures needed to effectively implement safe working conditions and practices have been identified and initiated. Most of the considerations and practices undertaken to address conditions and concerns at the Alcator C-Mod experiment will be directly applicable to the safe operations at other pulsed fusion experiment facilities.

Organization

An integrated team approach between several departments and individuals has been taken to address the safety needs identified at the Alcator C-Mod experiment as shown in Figure 1. This method provides the experiment with knowledgeable and experienced professionals to address discrete specialty safety issues and topics while at the same time it provides the basis for a broad oversight function as the various groups communicate and interact.

The focal point for all health and safety issues at the project is the Plasma Fusion Center (PFC) Office of Environment, Safety, and Health (ES&H). This office is responsible for coordinating safety activities and projects at the experiment and provides a dedicated staff to address ongoing programs at the Alcator C-Mod experiment. This Office and all other division heads, including Torroidal Confinement, report directly to the Plasma Fusion Center Office of the Director who has ultimate line responsibility for safety.

The Massachusetts Institute of Technology (MIT) Department of Environmental Medical Services (EMS) provides support to the PFC from the Radiation Protection Office (RPO) and Industrial Hygiene Office (IHO). The RPO maintains licensure for both ionizing and nonionizing radiation sources with state and federal regulatory agencies. The RPO is responsible for measuring radiological exposures and effluents, reporting to government agencies, and overseeing activated product management and radioactive waste disposal. The RPO performs all radiation training, bioassay, whole body counting, dose assessment, and air sample analysis. The Industrial Hygiene Office (IHO) of EMS provides ongoing support in the development and implementation of chemical and solvent safety programs and all other industrial hygiene issues.

Another organization that provides support to the E,S&H Office is the MIT Safety Office. One of the primary functions of this group is to oversee the university fire safety systems and procedures. This group also assumes responsibility for mechanical, cryogenic, and general safety hazards. When necessary the Safety Office interacts with regulatory governmental agencies.

A PFC Safety Committee was developed to support the E,S&H Office in its responsibility for overall safety at the PFC. The group provides a comprehensive organization capable of influencing policy, performing inspections and accident investigations, reporting status of safety programs and communicating or coordinating information and activities with other key MIT organizations.

Other MIT groups which may support the E,S&H Office include the Physical Plant Department and the Radiation Protection Committee. Recently a position of Plant Engineer and Assistant Safety Officer was instituted at the Plasma Fusion Center to support the activities of the E,S&H Office Head.

Identification of Hazards

Electrical systems are significant hazards of concern at the PFC, not only due to the high voltage and high power needed to run

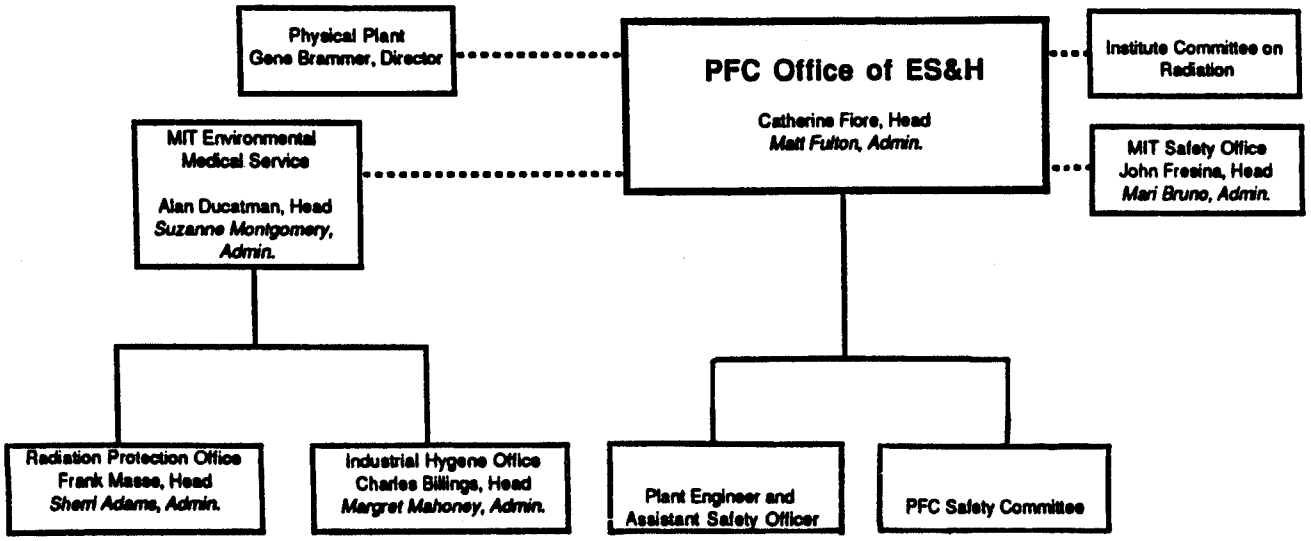

Figure 1. Health and Safety Organization

the pulsed experiment, but because of the numerous laser and other high power systems used to support the experiment. The power room contains 10 to 12 converter systems (10 to 40 MW) each for the poloidal field system. The input AC voltage is 13.8 kV. Power for the torroidal field is obtained from a 200 MW alternator which, after rectification, supplies up to 265 kamps to the magnet. High power lasers are located in several locations at the center which operate with up to 10 kV. High energy laser capacitor banks and transformers may be energized by workers at any time to support experiments or to perform maintenance. Two independent AC feeds are used to support emergency backup to the alternator. A 250 KW diesel motor-alternator has also been installed as an emergency power source.

Cryogenic hazards exist in close proximity with the high power electrical areas such as the buss tunnel and the cryostat in the cell. The experiment is expected to use as much as 15,000 gallons of liquid nitrogen per day. During cooling the maximum inventory in the torus may approach 1,000 gallons. Liquid nitrogen is stored in a large dewar located outside the experimental cell building. Liquid helium will be obtained and used as needed in small quantities. The primary occupational concerns associated with the use and storage of these materials include oxygen depletion, freezing or damage to safety systems or equipment, skin damage due to direct contact with transfer lines or the materials themselves, and explosion.

Potentially hazardous chemicals used at the facility include solvents such as alcohols, acetone, and freon. A variety of other toxic acids, epoxies, and electroplating solutions may be used or stored throughout the center. These materials pose an inhalation and skin contact hazard as well as possible flammability hazards.

Fire hazards at the PFC are evident due to the use of high power electrical systems, flammable gases, metals and liquids, and welding operations. Flammable gases used include; hydrogen, deuterium, and oxygen. They are contained in pressurized cylinders and stored at several locations in the facility. Flamable liquids include acetone, alcohols, and some uncured epoxies. Lubricating and pump oils may also release flamable vapors when heated to operating temperatures. Flammable metals include the use of lithium wire in some systems. Welding operations could be undertaken at unlimited locations including the cell, power room, and laboratories. In addition to being an ignition source, welding operations may produce highly toxic gases when airborne concentrations of chlorinated hydrocarbons, such as freon and 1,1,1-trichloroethane are present.

Confined spaces which have been identified as hazards include; the vacuum vessel, oil lubrication tank, alternator, and freon cleaning tank. The area under the vacuum vessel within the shielding igloo may eventually also be identified as a confined space. The primary concerns with these areas involve the depletion of oxygen or the creation of hazardous atmospheres, difficulty of access for personnel rescue, and radioactive contamination.

Mechanical hazards exist throughout the facility. The power room has a number of heavy buss structures suspended approximately 15 feet above the floor. Several converter cabinets in this area are over 10 feet tall. Falling equipment or hardware in these areas could cause serious personnel injury. Machining activities present general safety and inhalation hazards. Three cranes rated 35, 3, and 2 tons are used at the facility. Other mechanical hazards at the facility include the use of various machine tools and operation of the forklift to move heavy objects and to support personnel working overhead.

Several radiological hazards have been identified and estimated (Reference 2) which will result from high performance deuterium operation. Neutron rates as high as 5E15 neutrons per second are expected during one second experiment pulses about every 20 minutes. This results in significant neutron and gamma hazard in the cell during pulses as well as potential hazards to Alcator workers and the public in areas surrounding the cell. Residual activity in machine structures following high performance deuterium operations will present radiological hazards to Alcator personnel working in the vicinity of the experiment. For example; the dose rate at the midplane of the machine after a continuous one year high performance operation has been estimated to be 7.7E-1 mSv/hour (77 mrem/hour), primarily from Mn-56. This dose rate is expected to decline to 1.0E-2 mSv/hour (1 mrem/hour) after 24 hours, predominately from Cu-64. Inside the vacuum chamber residual activity in the molybdenum tiles could lead to a torus center dose rate of 4.1 mSv/hour (410 mrem/hour). After an 8 day cool down period this dose rate may be reduced to 5.0E-1 mSv/hour (50 mrem/hour). The activation and self shielding of experiment equipment will present challenging situations for source identification and control during maintenance of the systems and transfer of materials from the cell to other PFC areas.

Airborne radionuclides resulting from the pulsed neutron fluence is estimated to include 1.78E-2 Bq/cm^3 (4.8E-7 uCi/cm^3) Ar-41 immediately following each pulse. This would result in a maximum possible production of 1.36E11 Bq (3.69 Ci) based upon a total of 3750 high performance pulses per year. Since the air in the cell is changed once per hour the stack exit Ar-41 release rate will be 2.04E-3 Bq/cm^3 (5.52E-8 uCi/cm^3). This release would result in an annual dose to a person standing at ground level of 4.9E-2 mSv/year (4.9 mrem/year) due to Ar-41. Similar calculations for tritium production rates indicate the potential generation of 5E15 tritons per pulse. This would result in a ground level annual dose due to tritium of 1.0 uSv/year (0.1 mrem/year). The proposed use of an igloo surrounding the vacuum cell has been estimated to reduce offsite ground level dose rates to 5.25 uSv/year (0.525 mrem/year) from Argon and 1.238 uSv/year (0.124 mrem/year) from tritium per 3750 pulses.

Sealed sources used for instrument calibration and special nuclear materials in fission chamber detectors present another radiological hazard at the Alcator project. A Cf-252 source will be used in Alcator C-Mod to calibrate the neutron detection system with a neutron fluence of approximately 1.98E8 neutrons per second and a dose rate of 2.46 mSv (246 mrem/hour) at one meter. U-235 fission chambers are used at two different levels in close proximity to the vacuum chamber. The fissile material is contained and enclosed within these detectors. Special controls over the access to these chambers, as for all special nuclear materials, will minimize exposure risks to workers. Numerous smaller sources of varying radiations and strengths are used at the facility to calibrate instruments.

Several diagnostic experiments will utilize high power lasers with sufficient power to cause serious burns or eye damage to personnel exposed to the direct beams or to scattered light from the beams. A list of the most powerful lasers used at the facility are provided in Table 1.

Alcator C-Mod will be heated with 4-8 MW of RF power at 80 Mhz. The main sources of ambient RF radiation are the DC break in the transmission line between the experiment and the transmitters, leakage of RF excited by the antenna in the vacuum chamber out of windows in ports, and poorly connected joints in the transmission system that allow RF leaks. The Alcator C-Mod system produces up to one second long pulses with a 0.1% duty cycle. Average power is 2 kW for 2 MW pulsing per transmitter.

When 80 MHz RF is excited in the vacuum chamber significant RF levels might exist at adjacent ports. Estimates of RF outside horizontal ports indicate a possible exposure rate of 34 mW/cm^2 assuming that the port opening is completely transparent to RF. Based upon window attenuation of RF and isotropic diminution of the RF it is estimated that the exposure level would reduce to safe levels at 56 cm. Vacuum chamber top and bottom ports are smaller and longer and thus represent low RF leakage hazards. Electron Cyclotron Discharge Cleaning (ECDC) will use 3 kw power at 2.45 GHz in the vacuum chamber and should result in a higher leakage rate due to the smaller wavelength. Initial use of this equipment has indicated widow contact RF leakage of up to 20 mW/cm^2. Survey results of C-Mod area ECDC RF levels are shown in Figure 2.

Surveillance, Monitoring and Access Control

A Kirk safety interlock access control system designed to protect power systems and personnel plays a major role in the protection of personnel from a variety of identified hazards. Audio and visual signals indicate violation of interlock systems along with the location of the violation through a PLC system connected via a PC network to the control room. The PLC logic prevents restart of the power system without manual reset of the system through a search and lock procedure. Communications are provided electromechanically between all parts of the interlock system to ensure that a violation of any subsystem will effect a controlled shut

Table 1. **Lasers used as Diagnostics on Alcator C-MOD**

Diagnostic	Type of Laser	λ	Power or Energy	Location	Danger	Precautions
Two Color Interferometer	CO_2	10.6μm	5 W CW	Experimental Cell	Eye Damage	Enclosed Interlocked Path
	HeNe	0.6328μm	0.01 W CW	Experimental Cell		Enclosed Path
CO_2 Scattering	CO_2	10.6μm	200 W CW	Diagnostic Laboratory	Burns Eye Damage	Enclosed Path Room Interlocked
Laser Blowoff	Ruby	0.6943μm	1 J (20 ns)	Diagnostic Laboratory	Eye Damage Electrocution	Interlocked Room & Cell Lab. Area Restricted
Thomson Scattering	YAG	1.06μm	1 joule/pulse (20 ns) at 50 hz	Diagnostic Laboratory	Burns Eye Damage Electrocution	Enclosed Beam Lab & Cell Interlocked Light Tight Beam Dump

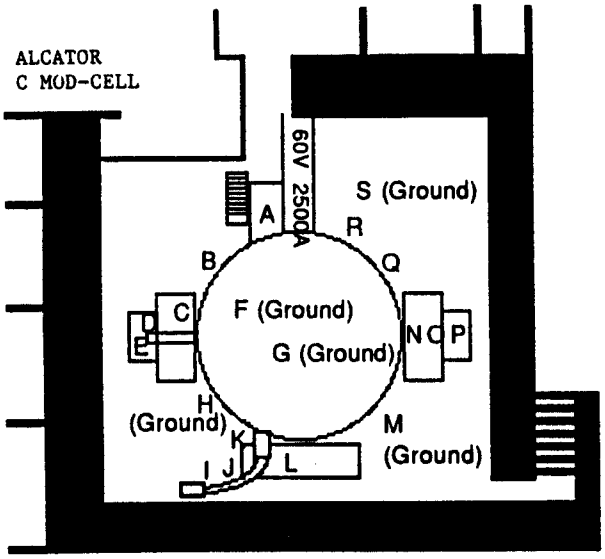

	(mW/cm^2) Without Plasma	With Plasma		(mW/cm^2) Without Plasma	With Plasma
A	0.0	0.0	J	0.3	1.0
B	1.8	0.0	K	10.0	5.0
C	5.0	0.1	L	0.2	20.0
D	2.0	0.7	M	0.0	0.0
E	-	20.0	N	20.0	1.0
F	0.3	-	O	11.0	0.2
G	0.0	-	P	5.0	0.1
H	0.2	-	Q	0.1	-
I	0.4	0.4	R	0.3	-
			S	0.2	0.0

Figure 2. ECDC RF Leakage

down of power systems. If a violation occurs during a pulse sequence, the system will shut down and all breakers will open in a controlled manner. The interlock safety system is tested monthly and the results are documented. The power room and cell are also monitored by closed circuit television during operation. The alternator is protected by a redundant interlock control and monitoring system. Critical temperatures, pressures, and flows are continuously monitored.

The radiological monitoring program provides a mix of various passive and active monitoring systems and equipment. Figure 3. illustrates the locations of several of these monitors.

Eleven Tracer Lab monitors have been installed in the C-Mod cell and adjacent laboratory areas to detect area radiation dose rates due to activation of machine structures and facilities. The range of these instruments is 2.58E-8 C/kg/hour to 2.58E-4 C/kg/hour (0.1 to 1,000 mR/hour). They provide hardwired real time monitoring of radiological conditions with readout in the control room and power room. Alarm set points are included at power room control panels.

Forty environmental/area thermoluminescent dosimeters (Li-6F,Li-7F) are used at locations inside and outside of the PFC. These dosimeters currently provide baseline dose data. During initial plasma testing in H-2 up to 40 self reading dosimeters will provide an indication of possible bremsstrahlung interactions from runaway electrons hitting the vacuum limiter. During pulsed fusion runs they will provide an indication of maximum total dose rate in the cell and adjacent public areas. They may also be changed out between shots to provide additional data regarding the dose rates exhibited at test locations for varying pusle power levels or operating conditions.

Six fission chamber detectors will be located near the vacuum chamber and are used to provide diagnostic information for the experimental operations (Reference 3). These will measure neutron production rates and fluence at the ranges from 10E10 to 10E17 neutrons/second. Data from these detectors will be recorded continuously during operations and will be used to track neutron inventories and support site boundary dose measurements.

Airborne Ar-41 and tritium effluent monitors will be located off of the Alcator stack release flow path. Tritium that may be generated in the vacuum chamber will be drawn off directly from the torus to the stack. Ar-41 generated in the surrounding cell will be drawn to the stack with a cell air change rate of once per hour.

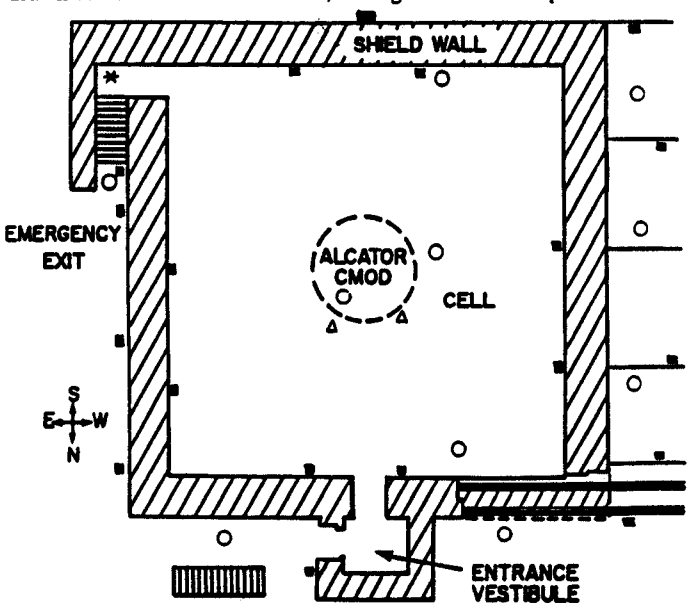

Tracerlab Area Monitors ○ Environmental TLD's ■
Ar-41,H-3 Effluent Monitors ✱ Fission Chamber Detectors △

Figure 3. Radiological Monitor Locations

Neutron sensitive personnel thermoluminescent dosimeters will be used to monitor exposures for all Alcator C-Mod workers who may be exposed to neutrons or other ionizing radiation on a continual basis as part of their normal job assignments. Forty self reading personnel dosimeters with ranges from 0 to 2.0 mSv (0 to 200 mrem) will be used to monitor worker exposures in addition to assigned personnel TLDs when they are in radiation areas. Alarming dosimeters will also be used to provide additional health physics coverage to workers in radiation areas.

Additional radiation monitoring will be completed using various portable survey meters with integration capabilities. A portable neutron detector will be used to survey PFC areas during pulsed experiments and during neutron fluence calibrations with the Cf-252 source. Hand held friskers will be used to minimize the spread of activated materials outside of controlled areas.

Portable air samplers will be used to collect samples from the vacuum chamber prior to any entries by workers. Samples will be analyzed on multichannel analyzers for airborne activation products. If tritium swipes from the chamber indicate the possible presence of airborne tritium an air sample may be collected and analyzed through the use of a portable tritium bubbler.

Various meters and probes are used to measure and control RF hazards at the facility. Surveys will be conducted for all identified hazardous areas during initial start-up operations to obtain a basis for RF conditions throughout the facility. RF measurements will also be taken whenever machine or structural changes are made which could alter the amount of leakage from various ports or connections.

Programs and Procedures

Electrical safety will be encouraged through the use of safe electrical practices, the implementation of electrical safety procedures, and the provision of personnel with adequate training. Electrical work is supervised by licensed engineers. Well controlled lock out and tag out policies will be used to ensure that the possibility of electrical shock is minimized. Access control checkpoints will be incorporated into operational procedures to ensure personnel are evacuated from hazardous electrical areas before systems are energized. Hazardous areas will be posted to inform PFC workers of electrical hazards. Policies are implemented which limit the number of personnel working in hazardous electrical areas at any given time. Fusing and breaking requirements are developed which will also work to minimize occupational electrical hazards throughout the facility.

Cryogenic, chemical confined space, fire, and mechanical hazards are controlled through the use of procedures to address appropriate activities. These procedures have been developed on an as needed basis with the advice and assistance from MIT Environmental Medical Services and Safety Departments. Special postings and protective equipment are also used to reduce risks in these areas. Figure 4. demonstrates some of the controls used during a recent alternator entry such as primary and backup air supplies, safety harnesses, air regulators and alarms.

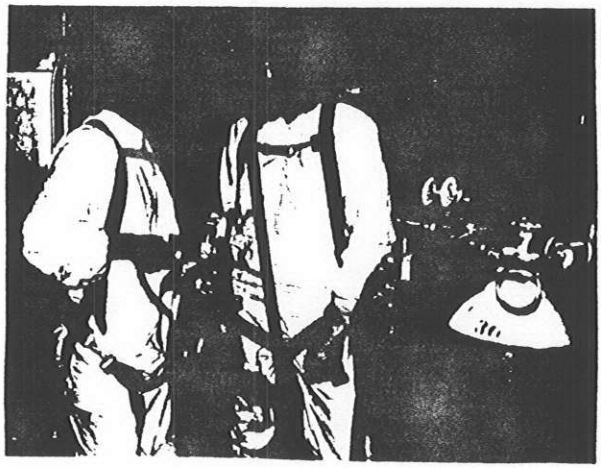

Figure 4. Confined Space Entry
Photo by D. Webster

An Alcator C-Mod Radiation Protection Plan provides an overall description of health physics program responsibilities and requirements. Radiation Protection Procedures are developed to support Plan objectives. These procedures will be implemented through the coordination of efforts by several different departments.

The first set of procedures developed are those which address Alcator C-Mod specific radiation protection problems. These are written as PFC facility oriented procedures to address the specific working conditions of the Alcator project.The topics covered in this initial set of procedures include; ALARA, Radiological Surveys, Contamination Control, Monitor Calibration, Access Control, Sealed Source Control, Respiratory Protection, Posting and Labeling, Training, Incident Reporting, Radioactive Material Control, External Dosimetry, and Internal Dosimetry. Additional procedures to address specific details for protection from RF hazards, provide a basis for the environmental monitoring program, and address facility emergency response activities are also being developed.

Radiation protection activities which are not specific to Alcator C-Mod operations are covered within the MIT Radiation Protection Office program and procedures. These include the following areas of: Laser Safety, Laboratory Analyses, Radiological Waste Handling and Shipment, Radioactive Material Receipt, Bioassay, Whole Body Counting, X-ray Safety, Accelerator Safety, and Magnetic Field Safety. Required activities may include combined and coordinated responses from RPO and the Alcator project.

Training

Alcator C-Mod personnel receive training from a variety of sources. Upon assignment each employee receives initial training from their supervisor regarding the hazards associated with their specific job. They are also informed of the appropriate protective measures during this session. Hands-on training and area job site walk throughs are also provided to new employees.

Formal training is also provided in various technical areas or for specific activities. Some examples are; radiation protection, respirators, electrical safety, site evacuation, and crane and forklift operations. The Industrial Hygiene Office provides specific training on the safe handling and use of hazardous chemicals, as necessary.

Conclusion

The programs, procedures, equipment, and training described above provide for the development and implementation of an integrated safety program to ensure the health and safety of PFC workers. This includes effective control and coordination of activities when different types of occupational hazards occur on one job such as a confined entry into a radiologically contaminated area or during machining of potentially contaminated materials. Procedures provide a means for documentation of required activities and a means to ensure that checks and controls are in place before work begins at a hazardous job site. The combination of programs, procedures, equipment, and training also provides a basis for an ongoing safety program which ensures the safest working environment possible for a modern facility with a wide range of hazards.

Acknowledgements

We would like to thank S. Golovato and A. Eckmann for their technical input.

References

(1)I.H.Hutchinson and Alcator Group,"C-MOD: The Next Alcator", Proceedings of the IEEE 13th Symposium on Fusion Engineering,1989.

(2)C.L.Fiore, "Alcator C-MOD Final Safety Analysis", PFC/RR-89-8,June, 1989.

(3)C.L.Fiore and R.S.Granetz, "Neutron Diagnostic Experiment for Alcator C-MOD",in Proceedings of the 8th Topical Conference on High Temperature Plasma Diagnostics,1990.

This work was supported by the US DOE Contract No. DE-AC02-78ET-51013.

DESIGN OF LIMITER/DIVERTOR FIRST-WALL COMPONENTS FOR ALCATOR C-MOD

B. LaBombard, B. Lipschultz, S. Kochan
Massachusetts Institute of Technology
Plasma Fusion Center
175 Albany Street
Cambridge, Ma. 02139

Abstract

A molybdenum first-wall heat shield will be employed during the first phase of Alcator C-Mod operation. The heat shield is composed of approximately 7000 tiles (2 cm thick by approximately 2.5 cm x 3.5 cm) and extends over three plasma-wall interaction zones: inner limiter, shaped-divertor, and flat-plate divertor (see fig. 1). Over 120 unique shapes of tiles are used to match the tile's surfaces to the cylindrical and conical geometries of the vacuum vessel. The heat shield and its support hardware are designed to withstand plasma disruption forces and, for the case of the shaped-divertor, to spread plasma exhaust of heat and particle fluxes over a large first-wall surface area. Peak surface heat fluxes are conservatively estimated (assuming no edge radiation) to be in the range of 6 MW/m^2 for the limiter and shaped-divertor tiles surfaces with total input powers in the range of 6 MW. Flat-plate divertor surfaces are projected to experience the highest heat loads, exceeding 40 MW/m^2. The first-wall armor features a regular pattern of poloidal and toroidal "tunnels" which are used to run cabling for magnetic pick-up loops (mounted on the vacuum vessel walls) and thermocouple wires. The present design allows the outer shaped-divertor tiles to be electrically isolated from the vacuum vessel. The electrical break reduces loop currents during disruptions, enables scrape-off layer currents into the outer divertor to be monitored, and provides for future divertor "bias" experiments. Details of the mechanical design and an outline of the principal design considerations are presented.

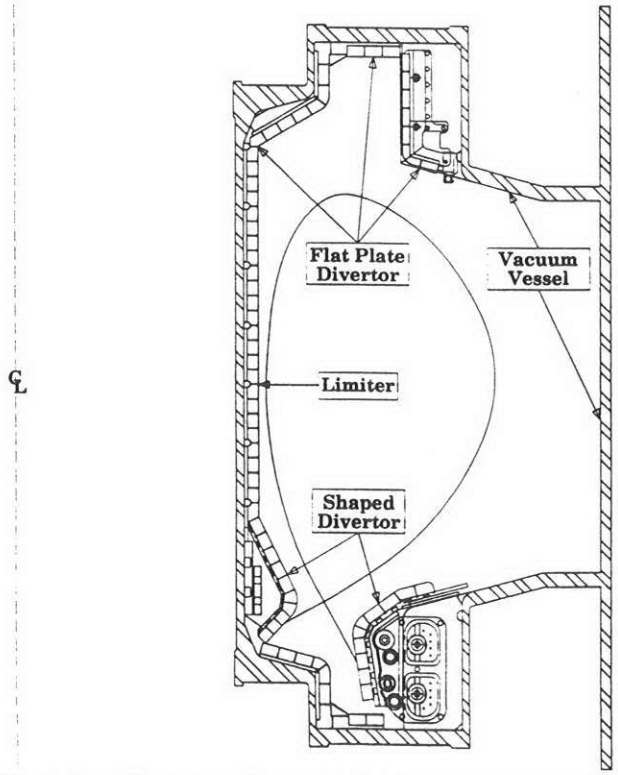

Figure 1 - Cross-section of C-Mod showing three principal plasma-wall interaction zones

Design Goals

Alcator C-Mod is a compact (R = .67 m, a ~ .21 m), high magnetic field (B ≤ 9T on axis), high plasma density ($n_o \leq 10^{21}$ m^{-3}) tokamak [1].The goals of C-Mod include the investigation of plasma confinement physics and essential plasma-wall interaction physics in diverted, elongated (κ ~ 1.8), and auxiliary heated (P_{OH} ~ 4 MW, P_{RF} ~ 4 MW) reactor-relevant plasmas. As in most tokamaks operating today, the limiter/divertor first-wall is expected to play an important role in determining the cleanliness and ultimate plasma performance parameters in C-Mod. The routine reactor-like first-wall heat fluxes anticipated in this compact tokamak (q_{surf} ~ 5 - 10 MW m^{-3}) will directly test the viability of high heat flux materials and operational techniques for the next generation of burning plasma and ignited tokamaks such as BPX and ITER.

The design of the first-wall armor for C-Mod presents a challenging task owing to the compact, high magnetic field, high power density environment. Principal requirements for the limiter/divertor first-wall may be summarized as follows:

Power Handling

- 5-10 MW/m^2 nominal surface heat fluxes (limiter, shaped divertor)
- 3 second heat pulse followed by a 20 minute cool-down period between pulses
- heat removal via indirect liquid nitrogen cooling of stainless steel vacuum vessel
- approximately 3,000 heat pulses per year

Disruptions

- 1MA/msec current decay rate at 3MA total current and 9T toroidal field on axis (14.6T at the inner wall)
- Up to 5,000 disruptions over lifetime

Materials

- accommodate molybdenum or graphite armor (molybdenum for first phase)
- structural support materials must retain strength at operating temperatures and be high vacuum compatible

Geometry

- first-wall armor surface must accurately conform to the cylindrical and conical shapes of the limiter, shaped divertor, and flat-plate divertor surfaces
- minimize impact of tile misalignments, thermal expansion, and gaps in the heat shield for diagnostic access
- allow for a network of diagnostic cabling (magnetics, thermocouples, probes) below the surface of the heat shield
- provide the capability to electrically isolate the outer shaped-divertor from the vacuum vessel (for current measurement and future bias experiments)
- provide the capability to actively pump gases in the shaped divertor chamber

Mechanical Design

Fig. 1 shows a cross-section of C-Mod with the arrangement of first-wall armor tiles that form the (a) inner limiter, (b) shaped divertor, and (c) flat-plate divertor surfaces. This arrangement will allow a comparison to be made between discharges in contact with each of the three surfaces. The primary mode of operation is expected to be with the shaped divertor. The total tile surface area facing the plasma is 6.7 m^2. The mass of molybdenum installed as first-wall tiles is approximately 1.4×10^3 kg. Plasma is expected to directly contact the heat shield over surfaces areas of approximately 0.8 m^2 for the inner limiter, 0.8 m^2 for the shaped divertor, and 0.2 m^2 for the flat-plate divertor.

We have chosen molybdenum as the first-wall material for C-Mod's first phase. This is based on a number of considerations: (1) good experience with molybdenum limiters on Alcator C (improved density control, lowest Zeff, minimal molybdenum radiation at high density), (2) lower start-up cost with molybdenum (It requires no extensive baking/wall conditioning. Also the vacuum vessel bake temperature in C-Mod is limited to 150°C.), (3) high-Z divertors may be necessary in reactor plasmas and, (4) molybdenum is a readily available and fabricated refractory material with good thermal shock characteristics. The C-Mod program also includes plans to test carbon in the high heat flux environment. A carbon flat-plate divertor will be installed, nominally two years into operation or as the total input power (Ohmic plus RF) approaches full performance values.

The mechanical design of typical first wall tiles and support plates is shown in figs. 2-4 . All molybdenum tiles are 2 cm in thickness, cut from sintered, cross-rolled, and annealed molybdenum plate stock [2]. A typical poloidal and toroidal extent of a tile is 2.5 cm and 3.5 cm respectively. This small size is required to reduce the eddy currents and forces which result during a plasma disruption. Thermal expansion and machining tolerances of the tiles are accommodated by a 0.5 mm gap between tiles. Each tile has a 15° by 0.4 mm chamfer to smooth over the toroidal "leading edge" formed by this gap.

The plasma-facing surfaces and back mounting surfaces of the tiles are machined to closely follow the conical shapes of ideal limiter/divertor surfaces. However, they were not machined as true conics since this would have required the use of expensive 5-axis CNC machining equipment. Rather, the conical surfaces on each tile were locally approximated as a cylinder with an optimized radius. In this way, readily available 3-axis CNC milling techniques could be employed. Typical overall dimensional tolerances (chord lengths, thicknesses, etc.) are within ±0.12mm (±0.005 in). The total deviation due to non-ideal curvature of a given tile surface is typically within ±0.01mm (±0.0004 in).

All support plates (excluding the shaped outer divertor and "gusset" protection tile assemblies) are plated with 37 μm of silver. This coating increases the thermal contact conductance between components (up to a factor of 10) and reduces the bulk operating temperature of the tiles (which is estimated to approach 500°C in high heat flux areas). A thin silver coating (12 μm) is also used on fastener hardware as a dry, vacuum compatible lubricant.

Tiles at the same poloidal location have the same basic shape yet they typically are machined with a variety of different "features" that depend on their toroidal location. Examples of such features are: cutouts for the nuts that fastening the backing plate, tunnels for diagnostic cables, holes for probes, cutouts for gas tubes or optical viewing dumps, and bevels on the "leading edges" that result when there is a gap in the tiles.

Each tile is held to its support plate via an Inconel 718 [3] screw, an Inconel 718 threaded cross-pin, and a lock washer. As a result, there are well over 30,000 parts for the first-wall armor assembly. In addition to fasteners, keys, nuts, and structural support hardware (wedge plates, spacers, support gussets, etc.), assembly of the heat shield involves:

Limiter -	1950 tiles,	140 backing plates
Shaped divertor -	3282 tiles,	90 backing plates
Flat plate divertor -	1602 tiles,	80 backing plates

Approximately 1000 stainless steel studs (304 SS) were accurately positioned, welded to the vacuum vessel, and pull tested. These provide fastening points for the heat shield (excluding the outer sections of the shaped divertor and flat-plate divertor).

All molybdenum tiles, silver plated backing plates, and support hardware were individually scrubbed with chlorethane, washed and wiped with alcohol, ultrasonically cleaned in freon, and baked in a vacuum oven at 500°C. The components were then assembled into "modules", approximately half of which include thermocouple sensors. Modules of tiles were carried into the vacuum vessel, positioned, thermocouple cables and/or probe cables routed, and bolted down.

"Cut-outs" on the back of each tile-module assembly interconnect to form a network of "tunnels". Wires for thermocouple sensors and an extensive array of magnetic field sensors [4] including poloidal magnetic field coils, poloidal flux loops, Rogowski coils, and diamagnetic loops are accommodated by the tunnel network.

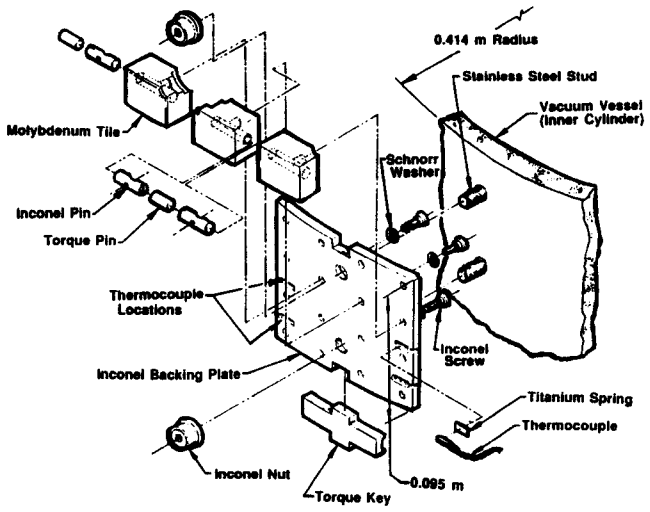

Figure 2 - Limiter module assembly

Limiter Modules

The inner limiter consists of 140 modules, 120 of which are similar to the one shown in fig. 2. This module shows the design philosophy which is typical of the entire heat shield, namely, an array of tiles fastened to a backing plate which is in turn fastened in some way to the vacuum vessel. Every tile has a 7.76 mm diameter cross-drilled hole which accepts a cross-threaded Inconel 718 pin. A silver plated Inconel 718 screw with #10-32 UNF threads fastens each tile/pin assembly from the vacuum vessel side of the support plate. For the limiter module shown here, sixteen molybdenum tiles

are mounted on an Inconel 718 support plate which is fastened to the vacuum vessel via stainless steel studs. The support plate has a radius of curvature which is slightly smaller than the vacuum vessel, allowing the plate to act as a "spring", tightly conforming to the vacuum vessel. "Torque pins" and "keys" are used to handle tile torques induced from plasma disruptions (as well as to provide a backup mechanism to restrain tiles from falling out should their screws become loose!).

An array of 220+ thermocouples will be used to follow the poloidal and toroidal variation and the long time history of the heat shield temperature after a discharge. Since the time for front-to-back temperature equilibration of a given tile is on the order of seconds, a thermocouple pressed to the back of a tile suffices for this measurement. Figure 2 shows one of two thermocouple attachment methods which are used. The thermocouple consists of a twisted pair of chromel-alumel wires that each have a ceramic fiber "sock" insulation. Bare ends of the thermocouple wires are spot-welded to a stainless steel block. The block is held against the back of a tile by spring force of approximately 250-350 Nt (60-80 lbs). The spring consists of either a strip of titanium as shown or a stack of 7 or 8 stainless steel belleville washers (6.35 mm O.D.) which employs a different cut-out feature in the backing plate than the one shown here. The titanium strip deforms and yields during assembly, accommodating machining tolerances.

We had originally planned on using stainless steel clad thermocouple wire with a powdered magnesium oxide insulation. However, the ceramic powder insulation proved to present a vacuum pumpout problem since it could not be easily sealed to vacuum.

Shaped Divertor Modules

The contour of the shaped divertor was designed with two primary objectives in mind: (1) distribute heat fluxes over a large surface area and (2) provide as much as possible a particle recycling and impurity trapping zone which is separate from the main plasma. To accomplish the latter objective, we contoured the shaped divertor to have surface normals at the strike-points which point away from the x-point. In this way, most sputtered impurities will not be directed to the confined plasma. We also chose the angles of intersection of the separatrix with the shaped divertor at the strike points to be of opposite sign to the more commonly used configuration (see fig.1). With this configuration, recycled neutrals have a higher probability of being ionized near the separatrix, potentially leading to a higher density, lower temperature divertor plasma.

Inner Modules: A portion of the shaped-divertor near the inner strike point is shown in fig.3. Components in the exploded view portion of the figure correspond 1/20 of the inner shaped divertor. Shaping and support of the inner divertor tiles on the vacuum vessel is achieved by a specially contoured "gusset block". These silver plated, stainless steel gusset blocks are fastened to the vacuum vessel via stainless steel studs. Stainless steel wedge plates span the spaces between gusset blocks and handle magnetically induced torques that would otherwise lead to unacceptably high shear stresses on the studs. Special Inconel keys and interlocking tabs are used extensively to eliminate the effect of these rotational moments elsewhere on studs and fasteners.

The upper backing plates (fig. 3) were cut from two conical rings of Inconel 625. The conical rings were rolled

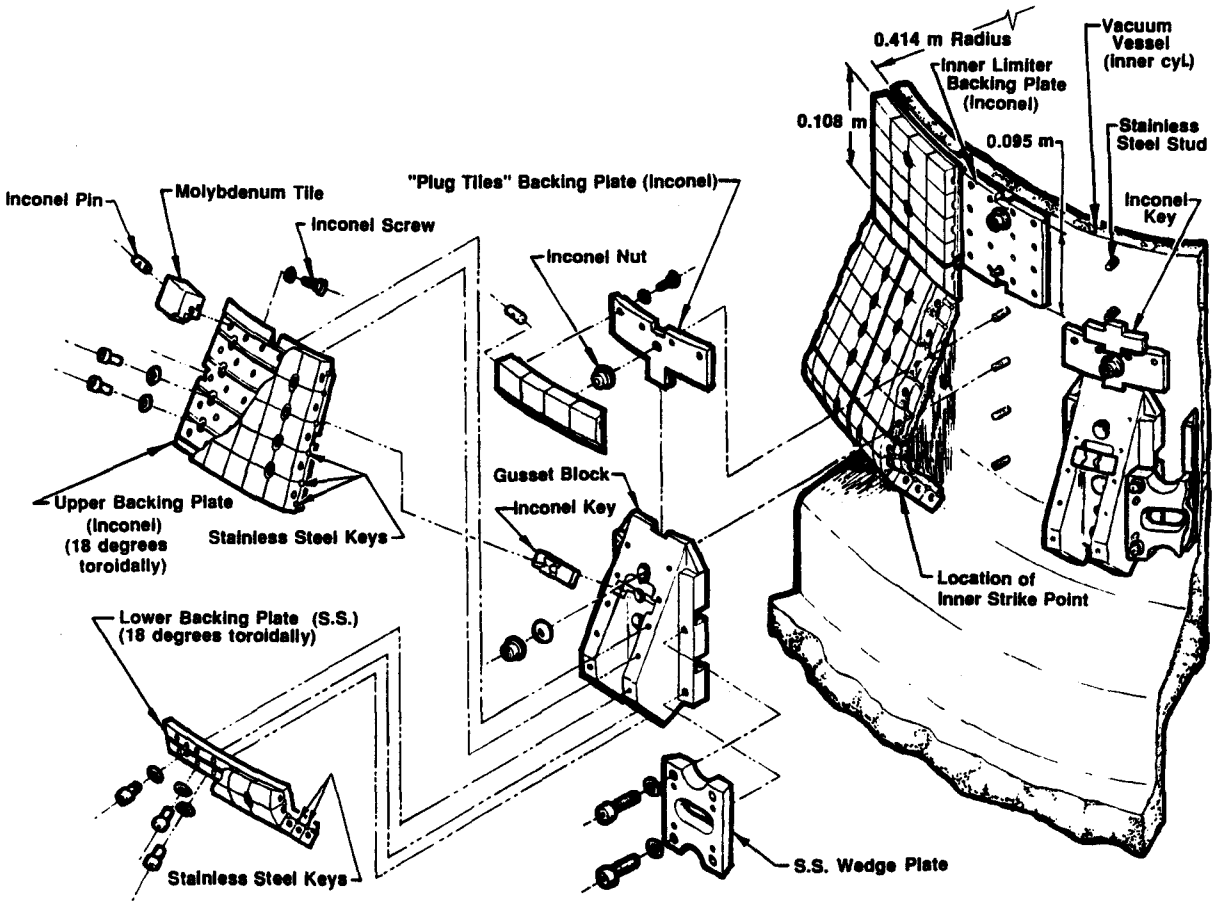

Figure 3 - Portion of shaped divertor assembly about inner strike-point

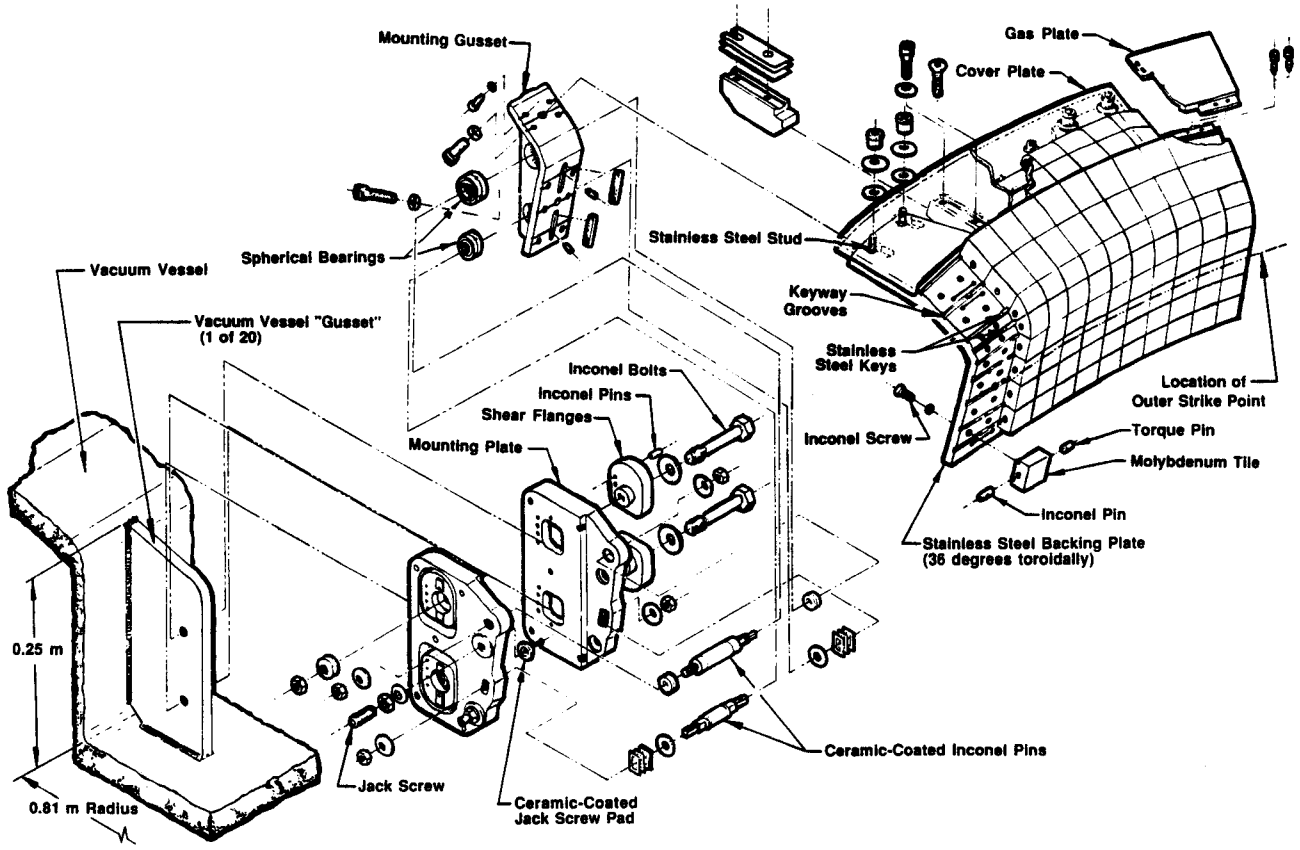

Figure 4 - Portion of shaped divertor assembly about outer strike-point

from a sheet, welded, stress relieved, and finish machined. The lower backing plates were machined from two forged rings of 304 stainless steel. Both backing plates have keyway grooves running toroidally between tiles. Electropolished stainless steel keyway stock is bent and pressed into the keyway grooves, engaging similar grooves machined into the back of the tiles. These keys keep the tiles from rotating about their fasteners during a disruption. The transition between the inner limiter and inner divertor tiles is made through special "plug tile" modules.

Outer Modules: Figure 4 shows an exploded view of tiles and support hardware that forms 1/10 of the outer major radius segment of the shaped-divertor. Specially contoured stainless steel backing plates provide the overall shape and support to the outer divertor tiles. These backing plates were machined from nearly square cross-section, 1.6m diameter forged rings of 304 stainless steel. Keys and keyway grooves are employed to interlock the backing plate and tiles, similar to the inner modules.

Unlike the inner modules, the outer modules are not bolted directly to the vacuum vessel. Instead, the outer backing plate is secured by a set of four ceramic-coated Inconel 718 pins via two intermediate assemblies, each consisting of a mounting gusset, two spherical bearings, two mounting plates, four shear flanges and associated pins and fasteners. This seemingly complex support hardware is actually quite efficient in its utilization of space and components as it provides for: (1) toroidal thermal expansion of the tile/backing plate assembly relative to the vacuum vessel (up to 3.5 mm), (2) low voltage electrical isolation of the tile/backing plate assembly relative to the vacuum vessel, eliminating potentially large loop currents during a disruption and providing for future divertor bias experiments, and (3) a method to accurately position the outer modules relative to the inner modules. (It turns out that without correction, variations in the radial, vertical, and angular position of the vacuum vessel gussets shown in fig. 4 would result in the array of tiles positioned far outside the accepted tolerance range of ± 0.5 mm.)

The ceramic-coated Inconel 718 pins are clearly critical components in this design. A testing program was implemented to qualify vendors' ceramic coating processes and to assure ourselves that the design was structurally sound. We subjected a total of 12 prototype pins from three different vendors to fatigue fracture tests. Each pin underwent 20,000+ cycles at 1.5-2.3 times the maximum load expected during a disruption. One pin showed a crack initiated at the edge of the ceramic. However, even after 100,000 cycles the pin did not fail structurally. In any case, we eliminated a stress-riser feature at the ceramic-Inconel interface that may have contributed to the crack initiation. A magnesium aluminate spinel applied by a flame-spray method was selected for the coating. The final sizing of the ceramic and Inconel diameters was achieved by grinding.

The mounting gussets, and sections of the mounting plates were also coated with approximately 0.5 mm of magnesium aluminate to eliminate direct electrical connection from arcs along magnetic field lines. For the first phase of C-Mod operation, each of the ten outer divertor modules will be hard-grounded to the vacuum vessel at a single point via a current shunt.

Since the outer divertor modules' support hardware provides for electrical isolation, it also thermally isolates the outer divertor from the vacuum vessel. Thermal isolation was chosen for two reasons: (1) to reduce the heat into the vacuum vessel behind the outer divertor where the liquid nitrogen is most critically needed for cooling the poloidal field coils, (2) to eliminate "hot spots" and associated thermal stresses on the vacuum vessel at the "gusset" locations, and (3) to simplify the electrical isolation aspect of the design. With radiation being the primary heat transfer mechanism, the entire outer segment of the shaped divertor is projected to approach a bulk temperature of 500°C during a series of full power discharges. Should the bulk temperature of the outer divertor rise above 500°C, more time between high power discharges may be mandated.

The cover plate shown in fig. 4 provides access to the mounting hardware and later to getters which may be installed behind some of the outer shaped divertor modules. In this case, the getters would pump gases through the toroidal opening (area ~ .1 m^2) under the outer segment of the shaped divertor (see fig. 1). The gas plate shown in fig. 4 restricts the neutral transport through unused diagnostic access openings.

A fully assembled outer divertor module weighs in excess of 55 kg (120 lbs), requiring an in-vessel hoist system for installation and service.

Magnetic Forces

The structural integrity of any plasma-facing component is perhaps most severely tested during a plasma disruption. C-Mod's first wall is designed to withstand the magnetic forces accompanying a full current (3 MA), full field (9 T on axis) plasma disruption with a current decay rate of 1 MA/msec. A 3 msec current decay time implies a characteristic magnetic diffusion skin depth of 4.2 cm in stainless steel and 1.1 cm in molybdenum. In order to minimize the magnetic forces on support structures and tiles, one is compelled to minimize the dimensions of these electrically conducting components. As the dimensions are made small relative to the magnetic skin depth, a significant portion of the poloidal magnetic flux due to the plasma current that is trapped inside these structures is able to diffuse out over the timescale of the disruption. Poloidal magnetic flux that remains trapped in a tile or support structure interacts with the external magnetic field. The effect results in a torque on the tile or support structure that attempts to realign the "frozen in" dipole field with the external field, much like a permanent magnet's response. The backing plate and fasteners must be able to support not only the magnetic forces of the plate itself but also of the array of tiles mounted on it.

The table below shows typical values of the rotational moment (torque) on molybdenum tiles which result from a full performance plasma disruption (with strike points on the shaped divertor). The moments are resolved into two components: "rotation" about the Inconel screw, and "rocking" which tends to lift one toroidal edge of the tile off the backing plate. These values were used for design purposes only and are based on a fairly crude, conservative model which does not take into account the holes and other features which are cut into the tiles. Preliminary laboratory mock-up tests suggested that these estimates may be too high by as much as a factor of 4 [5]. Uncertainties in the plasma disruption characteristics of C-Mod renders more detailed studies of this magnetic diffusion problem pointless at this time.

Tile Location	"Rotational" Moment	"Rocking" Moment
Limiter:		
Top	27 Nt-m (240 in-lb)	25 Nt-m (220 in-lb)
Midplane	80 Nt-m (700 in-lb)	~0 Nt-m (~0 in-lb)
Shaped Divertor:		
Inner Strike Point	~0 Nt-m (~0 in-lb)	21 Nt-m (190 in-lb)
Outer Strike Point	17 Nt-m (150 in-lb)	25 Nt-m (220 in-lb)

Heat Fluxes

Heat Flux Mapping

The contour of the shaped divertor was optimized to distribute the plasma exhaust over a large area and at the same time allow for variations in plasma position and separatrix shape. To accomplish this, a simple magnetic field-line following program was written to map the poloidal flux at the outside midplane to any limiter/divertor surface. In this way, by specifying the plasma conditions at the outside midplane, a rough estimate of the heat flux at any limiter/divertor surface could be obtained. The estimate is "conservative" in the sense that scrape-off layer power loss from radiation and charge exchange is neglected.

Based on data from the Alcator C scrape-off layer, the power flux e-folding distance at the outside midplane in C-Mod is projected to be 4-5 mm [6]. Heat transport into the divertor's private flux region is crudely modelled by including a half-gaussian power flux profile for that region with a width of approximately 1/3 the decay length of the globally connected scrape-off layer (i.e. 1.3 to 1.6 mm at the outside midplane).

Shaped Divertor Optimization

Figure 1 shows the geometry of the poloidal cross-section of the shaped divertor tiles. This geometry was kept as a simple as possible for fabrication purposes. It is specified as series of straight line segments connected by tangent arcs. The optimization procedure involves specifying the shape of a test surface, computing the heat fluxes for a variety of equilibria, and modifying the test surface shape if necessary. An important consideration is the change in separatrix surface shape as the plasma evolves. A divertor shape that is optimized for a particular time in the discharge becomes less than optimum at another time.

Flux surface positioning inaccuracy is also an important consideration. The shaped divertor is designed to tolerate a positioning inaccuracy of ±3 mm in major radius and ±6 mm in vertical position. For some large displacements, the strike point can move from the shaped tiles to the flat tiles on the floor.

First-Wall Heat Flux Estimates

Figure 5 shows estimates of the heat fluxes on the inner limiter, shaped divertor, and flat-plate divertor surfaces. The solid and dashed lines correspond respectively to equilibrium flux surfaces at the beginning and end of the constant plasma current phase of the discharge. Assumptions in this estimate are: (1) total power on limiter/divertor surfaces of 4.5 MW and (2) equivalent heat flux e-folding length on the outside midplane of 4.25 mm. The anticipated heat fluxes for these conditions may be summarized as:

Location	Nominal value	With strike-point sweeping
Shaped Divertor	6 - 8 MW/m^2	4 - 5 MW/m^2
Flat-Plate Divertor	30 - 50 MW/m^2	10 - 30 MW/m^2
Limiter	6 - 8 MW/m^2	

Note that the flat-plate divertor heat flux may be too high without separatrix sweeping. (For reference, molybdenum surface melting occurs for a heat flux of 50 MW/m^2 and a duration of 0.7 sec.)

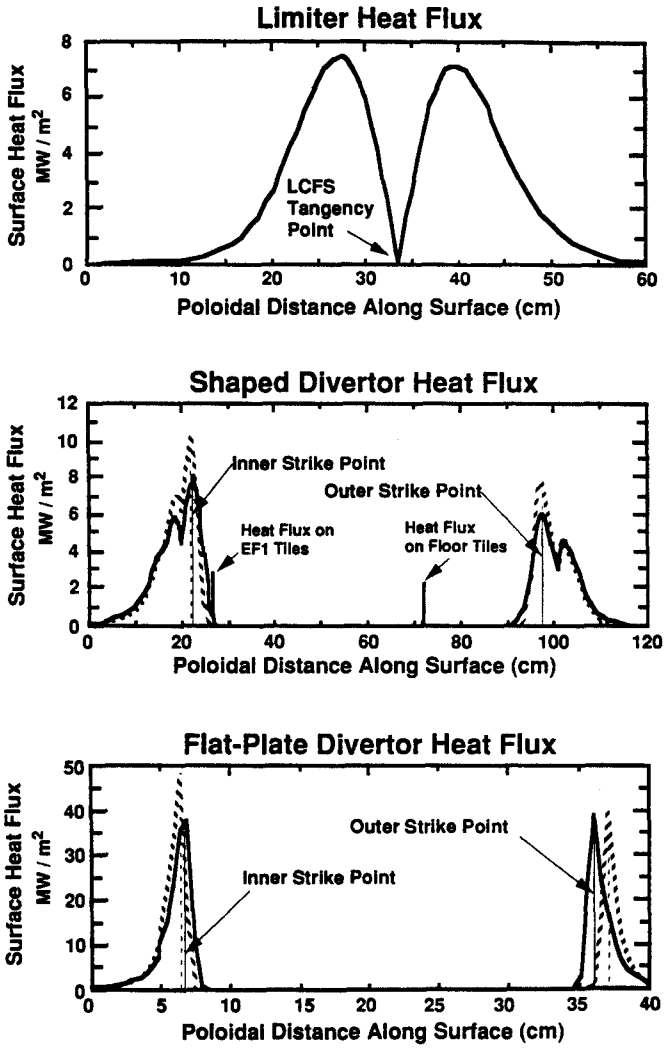

Figure 5 - Heat flux profile estimates

Special First-Wall Tiles

It is necessary to "bevel" the edges of some tiles around the diagnostic access openings. Such beveled areas result in local heat flux enhancements of a factor of 1.5 or more. Figure 6 shows two approaches which we have considered. We have chosen the "directional double bevel" for the highest heat flux areas such as the flat-plate divertor. A symmetrical "double bevel" is used around the Thomson viewing dump on the inner limiter. The location of the leading edge of the beveled tiles is determined by mapping the "shadow" cast by the trailing edge of tiles across the opening.

Options for "Beveling" Around Openings

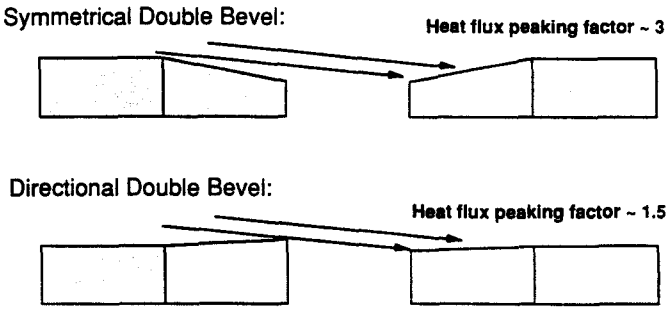

Figure 6 - Beveled tiles

Acknowledgements

The C-Mod limiter/divertor design, fabrication, and installation project could not have proceeded without the help of many people on the C-Mod team. The authors are especially grateful for the help from Dr. H. Becker, Dr. D. Gwinn (design), D. Gilbert (fabrication), J. Murphy (mechanical testing), Dr. J. Rice, R.A. Childs, and T. Toland (vacuum preparation), J. Gerolamo and W. Pina (assembly).

This work is supported by U.S. DOE Contract No. DE-AC02-78ET51013.

References

[1] S. Fairfax, et al. , " Alcator C-Mod", this conference.

[2] Molybdenum was supplied by Climax Specialty Metals, Cleveland Ohio.

[3] All Inconel 718 components were precipitation hardened to achieve a minimum yield strength of 950 MPa (140 ksi).

[4] R.S. Granetz, et al., "The Magnetics Instrumentation on Alcator C-Mod", this conference.

[5] Based on a laboratory "hack" experiment performed by D. Gwinn and B. Lipschultz

[6] B. Lipschultz et al., "Alcator C-Mod: A High-Field Divertor Tokamak", J. Nucl. Mat., vol. 162-164, pp.793-798, 1989.

POWER SUPPLIES FOR POLOIDAL MAGNETS IN THE ALCATOR C-MOD TOKAMAK

J.S. Paranay, S. Fairfax
Plasma Fusion Center
Massachusetts Institute of Technology
Cambridge, MA 02139

Abstract: The highly flexible plasma shaping and diverter configuration of Alcator C-MOD necessitate the use of many separate magnet power supply systems. Eleven separate systems are used to power the fourteen magnets in the tokamak. The severe budgetary constraints prevented the purchase of an entirely new converter set for each of these eleven systems. The solution to this dilemma was the long-term loan of the TMX-Upgrade magnet power supplies from Lawrence Livermore National Laboratory to MIT. The converters operate in groups of two or three to power four of the ten poloidal field magnet systems and to provide excitation to the alternator.

The "TMX supplies" have been completely overhauled and redesigned for their use in the Alcator program. All have new control logic, PLC interface, and gate drive circuits. Several have been modified to provide 2-quadrant operation. The AC and DC bus have been redesigned and simplified. Twelve of the units are mounted in a double-high rack to preserve floor space. The AC unit substations are located near the converters to minimize resistive and reactive losses.

This report details the overhaul and use of the TMX supplies in the Alcator C-MOD experiment. Some test data from rebuilt supplies will be presented along with details of the interface to the Alcator control system.

Strategy

The main purpose of rebuilding the power supplies was to custom fit them into the Alcator C-MOD system. In addition, converting from single to two quadrant operation was incorporated into the design.

The original TMX power supply was a single quadrant, line commutated AC-DC converter. Its source, 480 volts 3 phase, connected through a circuit breaker and contactor. The contactor fed 6 water cooled pressure mounted thyristors mounted in-line inverse parallel. The SCRs fed 2 power transformers connected delta-delta and delta-wye. Water cooled, pressure mounted rectifiers formed a 12-pulse bridge which could be connected in series or, through the interphase reactor, in parallel. Over-current protection was provided using 2 current transformers on the AC line. For DC feedback, some TMX supplies used Hall effect transducers, but most used a voltage divider and current shunt with isolation amplifiers. The regulator offered local voltage limit and remote current command. The gate drive consisted of a wye-connected power transformer and 3 gate boards designed specifically for 6-SCR in- line control.

The re-built power supply falls into one of three categories. The "TMX" is still a single quadrant converter, the "TMX-2" is a 2-quadrant supply, and the "TMX-2i" is a 2-quadrant supply with an air-cooled transformer. Four power supplies were set aside for spare parts. Once all the components were tested, one TMX power supply was rebuilt and tested as a single quadrant prototype. The major design changes were made in the areas of gate drive, regulator, control logic, isolation, AC and DC bus.

Control Section

The control circuitry, test phase reference, heaters and fans are powered from a three phase 208 volt source separate from the 480V power section. A 208V line to neutral tap supplies single phase 110VAC to the 24VDC, ±15VDC, and gate drive power supplies. The 24VDC ladder logic allows the use of blocking diodes for global circuits such as RESET and LAMP TEST. The control panel announces faults with latched relays and indicator lamps.

The 480V line is monitored by a three phase detector which checks phase loss and rotation. The rear doors to the power section are safety interlocked and key locked. 480 volts is not present in the front section to make troubleshooting easier and safer. The cooling water is flow checked so that any leaks will close the water flow solenoid. Normally closed temperature switches are located on each rectifier pair for thermal protection. Over-current trip is accomplished by comparing the shunt feedback to a pre-set level. The ±15V power supply for the isolation amplifiers is monitored. The emergency circuit opens the main circuit breaker and then the contactor. This is an active open local and remote signal. An unscheduled output circuit checks that current flows through the DC bus only when the gates are enabled. This helps confirm that all TMX supplies connected in the same DC circuit get proper command signals from the PLC.

Fault 1 is a summation of 3 phase 480, over current, ±15V, emergency, and unscheduled output. Fault 2 sums doors, water flow, and over temperature. Three modes can be selected by local control panel switches: run local; run remote; and test. For safety, test disables the 480V circuit breaker and remote commands, and enables the gate drive circuit. The gates are then referenced to the 208V control power through a phase reference switch assembly. The remote commands to close the contactor and activate gates are active high. The contactor is not allowed to open under load. This is accomplished by sensing current via a reed switch mounted on the DC bus which provides an active output signal. All emergency burdens are taken by the circuit breaker.

The regulator was manufactured by Enerpro, Inc.[1] The modified circuit provides automatic switching of current or voltage mode regulation. It incorporates integral plus proportional control for both voltage and current and has a built-in adjustable soft-start circuit.

The gate drive circuit is also manufactured by Enerpro. It is a general purpose firing circuit for phase controlled thyristors using CMOS LSI gate array technology. It is relatively inexpensive, versatile, and proven reliable. For the TMX it is configured as a 6-thyristor in-line AC controller. For the TMX-2 and TMX-2i, it was easily changed, with the addition of an auxiliary firing board, to a 12-pulse, 2-quadrant series bridge controller.

The isolation amplifier assembly consists of two dual isolation amplifier boards, a distribution amplifier board, a ±15V power module, and simple card-cage. The first isolation amplifier board is dedicated to remote current and voltage command signals from the PLC. The second isolates the output bus from the regulator for feedback. The distribution amplifier buffers the feedback signals for monitoring at the local control panel and in the control room. It also provides over current trip and isolation amplifier power supply monitoring.

Power Section

Each circuit breaker was inspected, cleaned and adjusted. The main contactors were checked mechanically and tested. Contacts and arc-chutes were replaced where needed.

The SCRs and rectifiers were ohm-checked and high-potted to 600 volts before being reused. Since the two quadrant power supplies do not use rectifiers, there were ample replacements for the single quadrant supplies. The TMX-2 and TMX-2i power supplies, however, require twice the number of thyristors as the original supplies. New SCRs were selected based on compatible specifications with the original, and cost. The thyristors are 53mm General Electric [2] type C750 PB1 phase control SCRs, 1200V. The rectifiers are Westinghouse [3] R9G0, 600V, 2200A, 15us recovery. Snubber networks on the in-line AC switch are 50 ohm, 0.5uF. Snubbers on the controlled bridge are 5 ohm, 0.5uF.

The transformer core is a laminated "E" and would be costly to rebuild, therefor all of the rework was done with the core intact. The primary had been wound with solid copper wire and the secondary is half inch copper tubing. Water is passed through the secondary for cooling (the TMX-2i uses an air-cooled transformer with a foil-wound secondary). Some of the insulating spacers between the windings were replaced and secured with epoxy. The tubing and connections were leak-checked and pressure tested to 100 PSI. The impedance was tested with the secondary shorted phase-to-phase and the primary driven with a three-phase variac. The resistance was tested using a 10 amp DC source driving each coil independantly, all others open. The average resistance was calculated to be 57.5m Ω primary, 1.3m Ω secondary wye, and 2.2m Ω secondary delta. The insulation was tested using a megger and hi-pot power supply. Any shorts were repaired by lifting the coils along the core and adding insulation. The turns ratio was tested and results confirmed 48:7 wye, 48:13 delta. The excitation current was tested by energizing the primary, secondary open. All transformer terminals and bus are now silver-plated for low resistance connections and stainless steel hardware with compression washers are used throughout.

Control System Interface

All TMX power supplies used in the PF system are controlled by an Allen-Bradley PLC-5 programmable logic controller. The PLC is connected via fiber-optic link to personal computers in the control room. The PLC provides information to the operators on the status of all interlocks as well as trend and performance data from past pulses. The PLC also provides the current limit programming and voltage programming for test pulses. A system of hard-wired interlocks provides functions for personnel protection. The access control system, for example, disables the converters irrespective of PLC commands if the area is not secured. Several additional systems are used for timing, data collection, and voltage programming of the power supply output during the tokamak pulse.

The C-MOD control system uses a simple state machine to coordinate the action of all the various subsystems.[4] Standard CAMAC digitizers collect data on power supply output voltage and current. A fiber-optic distributed timing highway provides the initiate and end pulse signals with microsecond accuracy. The power supplies require start pulse signals from both the PLC and fast timing systems, while either system can force a supply to shut off. The voltage programming for each power supply comes from a hybrid analog digital computer built for Alcator C-MOD.[5] The hybrid can implement simple PID loops as well as more complex multivariate control algorithms. The PLC controls the power supply current limit at all times, and will force the power supply off if the hybrid fails to do so.

Magnet Systems

The EF2 coils are powered by 2 TMX units operating in parallel. These coils are used primarily for diverter control, though they do couple into plasma position as well. The upper and lower coil have independent supplies. The EF2 coil is closely coupled to the nearby EF3 coil. The EF2 coil

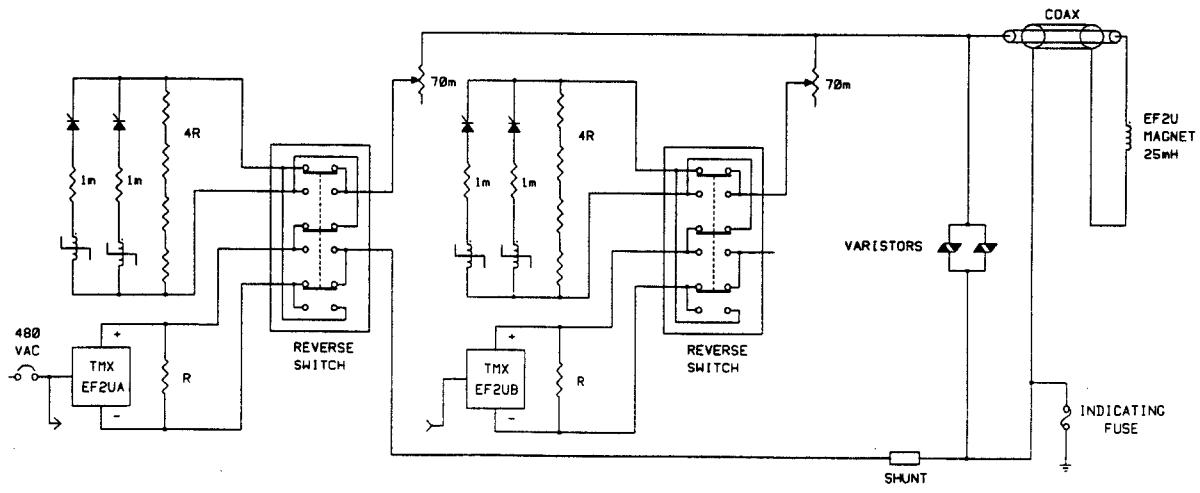

Figure 1: EF2 Upper Magnet Power Diagram
(EF2 Lower is identical)

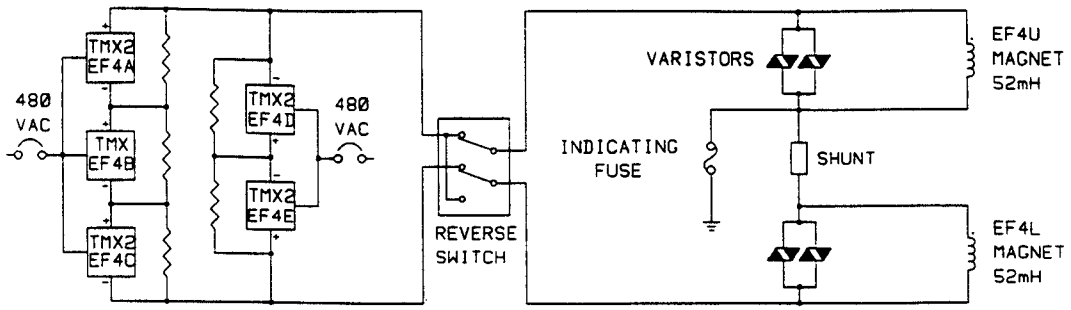

Figure 2: EF4 Magnet Power Diagram

power supply must generate negative voltage during most of the plasma pulse to counteract the effect of EF3 drive. A ballast resistor is inserted in series with each supply, as shown in figure 1. The value of the ballast resistor is adjustable to accommodate different plasma operations, such as no diverter, upper diverter only, dual diverter, etc. The resistor provides the necessary negative voltage, while the single-quadrant power supplies provide a controllable positive output. The SCR and voltage dividing resistors are necessary to protect the TMX supplies from the output of the much larger EF3 supply. Each EF3 coil is normally driven with over 1800 volts, and the coupling to the EF2 coil is nearly unity. The EF2 supplies can withstand at most 600 volts across their output terminals. So long as the supplies are conducting current, the output voltage is limited, but the action of the EF3 supply or a plasma disruption can force the current in the EF2 magnet to 0. The EF2 circuit would also tend to conduct during the initial charging of the OH and EF coils. The SCR in series with the output is rated 4400 volts and protects the supply from excessive voltage.

The EF4 coils are located outside of the 15-cm thick stainless steel outer cylinder. The coils are connected in series and provide a vertical field for plasma radial equilibrium. The penetration time of the magnetic field through the liquid-nitrogen-cooled cylinder precludes feedback control using the EF4 coils. The EF3 coils are similarly connected but can respond to plasma radial position changes much faster. The EF3 coils are closer to the plasma and driven by a 3600 volt power supply. The EF4 coils are powered by 5 TMX converters as shown in figure 2. Two of the converters provide reverse current for biasing of the vertical field null. The remaining converters provide forward current following a pre-programmed waveform during the discharge. A lockout circuit enables the forward converters only after current feedback signals in the reverse converters have been at zero for at least 100 msec.

The EF4 coils may require more power than the TMX supplies can give when the experiment is operated with full 9-Tesla, 3 MA discharges. The TMX supplies now connected to the EF4 coil would be used to drive 8 large DC traction motors purchased from Los Alamos National Laboratory. Each motor is outfitted with a flywheel and stores over 3 MJ at maximum speed. These motors were previously overhauled and evaluated for pulsed duty applications.[6,7] Each can provide up to 1200 volts at up to 2 kA. Two of the TMX supplies would be used to provide a 4-quadrant field supply, while the remaining supplies would be used to accelerate the motor/generators prior to the pulse.

The EFC coils provide plasma vertical position control. They are driven by a chopper to achieve fast response (Figure 3). The chopper supply was purchased from General Atomics and is essentially identical to those used on DIII-D.[8] Three TMX supplies in series are used to provide the DC input to the chopper.

Alternator excitation was formerly provided by a shaft-driven exciter. The addition of the flywheel to the alternator eliminated the space for the exciter, and a static exciter was required. Two TMX supplies in series now provide the excitation. A DC circuit breaker, also loaned by LLNL, protects the alternator field. The circuit breaker was purchased for protection of MFTF magnets. A network of silicon carbide varistors limit the field voltage when the breaker opens under load.

Summary and Conclusion

All power supplies have been pulse tested to 300 volts at 5KA into an inductive load. The 12 EF units are mounted in the power room and DC connections have been made to the magnets. PLC and CAMAC wiring has been tested and the supplies were operated from the control room. The alternator exciter supplies are in place and connected.

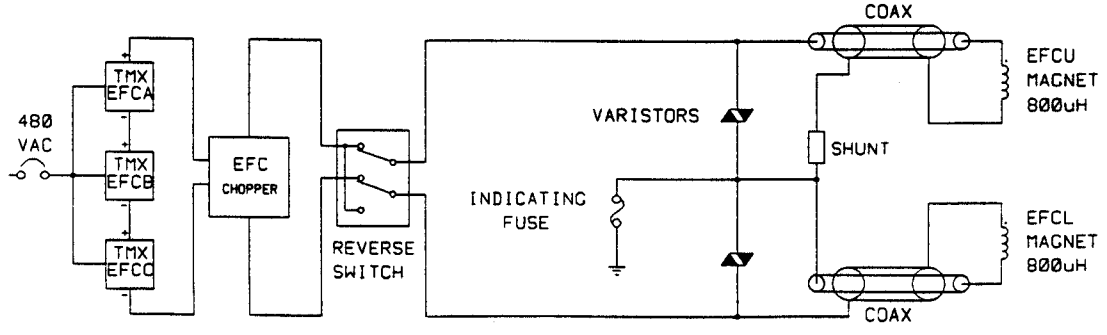

Figure 3: EFC Magnet Power Diagram

References

[1] Enerpro, Inc., Goleta, CA.

[2] General Electric Static Power Component Operation, Malvern, PA.

[3] Westinghouse Electric Corporation, Pittsburgh, PA.

[4] J. Bosco, S. Fairfax, "The Alcator C-MOD Control System," IEEE 14th Symposium on Fusion Engineering, San Diego, CA, Oct. 2-4, 1991.

[5] J.B. Lister, Ph. Marmillod, J.M. Moret, "A Fast Response Hybrid Linearized Control System," Technical Report LRP 332/87, Centre de Recherches en Physyique des Plasmas at the Ecole Polytechnique de Lausanne.

[6] P. Thullen, "Operating Limits on Commutator DC Machines Used as Electromechanical Capacitors," IEEE Proceedings 9th Symposium on Engineering Problems of Fusion Research, Vol II, pp. 1418-1421 (1981).

[7] P. Thullen, D.M. Weldon, "Commutator DC Machines Used as Mechancial Capacitors in a Series Resonant Ohmic-Heating Simulation, IEEE Proceedings 8th Symposium on Fusion Engineering, p. 729 (1979).

[8] P.J. Rock, J.C. Wesley, "1.5 Megawatt D.C. Chopper Power Supplies for Plasma Shape Control on Doublett III," IEEE Proceedings 8th Symposium on Fusion Engineering, p. 1289 (1979).

SIGNAL CONDITIONING ELECTRONICS AND PACKAGING FOR THE ALCATOR C-MOD TOKAMAK

W. Parkin
Plasma Fusion Center
Massachusetts Institute of Technology
Cambridge, MA 02139

Abstract: Engineers and physicists are collecting more data and looking at more signals with each new fusion machine. Most of these signals need some form of processing, amplification, integration, isolation, etc. An economical way of handling signals is needed that avoids the redundancy of individual power supplies and packaging. The system has to accommodate both large and small numbers of channels with a variety of inputs and outputs.

A design utilizing industry-standard EURO card packaging, connected via ribbon cable to a custom I/O backplane, accommodates the many different circuits to be used on ALCATOR C-MOD. The chassis approach eliminates packaging, powering, and mounting problems associated with one of a kind circuits and allows dense packaging of multiple circuits. The separate I/O backplane allows easy removal and replacement of circuit cards, while leaving front panel space available for circuit-specific indicators. The DIN pin-and-socket connectors are considerably more robust and reliable than edge connectors. The pin-out was chosen to allow up to four circuits per card, allowing up to eighty channels in one 5 1/2" tall, rack mountable chassis. The 11" I/O backplane provides the user with Lemo and screw terminal connectors.

A variety of general purpose signal conditioning circuit cards have been designed and built for engineering and diagnostic systems. Four channel circuits include low drift integrators, analog multiplexers, temperature controllers, instrumentation amplifiers, trans-impedance amplifiers, and an eight-pole Bessel filter for anti-aliasing applications. A two-channel card provides thermal electric cooler control. Fiber optic interface is provided by an 8-bit digital transceiver and an analog fiber optic link.

Standardization

This is the third fusion machine built by the Alcator group at MIT. In the past, circuits were designed and built by engineers, physicists, and technicians, one at time, as needed. Each circuit was put in a box or chassis, usually with its own power supply. It would be mounted in an equipment rack and left there until maybe years later, it failed. The circuit would have to be found, the schematic looked for (hopefully the person who designed or built it still worked for the group), fixed, then re-installed. My apologies, I made it sound a worse than it was. Alcator A and C were great machines, with great results. With all the different circuits around, it made preventive maintenance and calibration difficult, not to mention Quality Assurance!

Today safety, Quality Assurance (QA) and budgets are major concerns. By standardizing, QA is made simpler, and time and money are saved by going to Printed Circuit Board (PCB) design. The problem with standardizing is it is difficult to please everybody. With this in mind, engineering has tried to put options into the design and layout of the boards, to make them usable in as many applications as possible.

By using a computer to to make schematics and PCB layouts, documentation is simplified. All good design packages will generate parts list and net lists. Schematics can be printed out on laser printers or plotters. Assuming proper computer back-up, schematics will never get lost. The software can generate plots that can be photographed. The photographs can then be used to make the PCB's. The software can also make Gerber and drill list files. These files can then be put on a floppy disk and sent out to PCB manufacturers.

All the PCB's for C-MOD were made by outside vendors. In the past, boards were made in house. Due to the high cost of chemical disposal, maintaining a dark room, venting of fumes, and time, this is no longer economical. Boards are typically made in two weeks, but can be rushed, at a premium, to three days. The cost for a four layer board with silk screening and soldermask runs from $25 to $50 depending on quantity and complexity. On large orders of 50 boards, we usually have the vendor make up five boards to be tested first. Once they have passed testing the remainder of the boards are made. The finished boards are then sent out to be loaded and wave-soldered. Our typical four channel circuit boards cost around $20 each to be loaded. This is less expensive than we can do it in the lab, and frees up technicians for other work.

All the circuit boards designed to date are 2 or 4 layers, with through plated holes, solder mask and silk screen for component designations, title, date, and revision number. The backplanes and most circuit boards were designed in house using Teradyne Case Vanguard schematic capture and printed circuit board layout software on a DOS based personal computer. This has made QA and documentation a much less painful job.

Most boards contain four circuits and a power supply regulation section. The power supply section contains 15 volt input filtering capacitors, 12 volt regulators and 12 volt filtering capacitors. Filtering and de-coupling caps are used generously on all cards. By using voltage regulators on each PCB, a short circuit on one board is less likely to effect the other boards in the rack.

The Euro Backplane (EPB)

The EURO backplane is a six layer printed circuit board designed at the MIT Plasma Fusion Center. It attaches to a standard EURO rack. The EBP consists of 21 press fit DIN connectors, filtering capacitors, and power connectors. To assure a good electrical contact between the press fit pins and the EBP, the board is 0.125 inches thick. The thicker board is also stronger and is less likely to flex while plugging and unplugging circuits.

The six layers are ground, +5V, +15V, -15V, ± 24V, and the solder side which contains 12 bussed lines, common to all 21 connectors. These bussed lines can be used for resets, address lines, enables, or common inputs.

All 21 DIN connectors are electrically identical. All inputs, outputs and power, except fiber optics, go through the connectors. The connectors have 3 level wire wrap pins. The last level of the pins are gold plated and is used for making connection to the I/O back plane. The wire wrap pins can also

The Mini Back Plane (MBP)

With the wide variety of standard circuits that have been or are planned to be built, we found that we wanted to use them in places that were to small for the rack mount backplanes. There are also places where only two or three circuits are needed, and a smaller back plane would more cost effective. So the MBP was created. This is also a 6 layer board. The layout of this backplane was simplified by the computer layout software. Instead of starting the layout from scratch, the file that was used to make the EBP was edited down to six slots. Then the Phoenix connector was replaced with the 37 pin "D" connector.

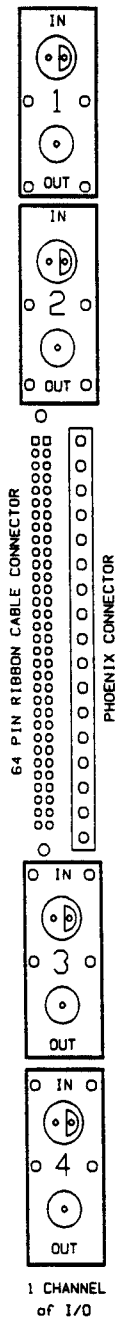

Figure 2: 1 Channel of I/O

Since size was the major issue, this is a one board backplane. All the I/O comes off the MBP through a 37 pin "D" connector. An IDC connector will then be used to bring out all I/O through a ribbon cable. The first twenty wires of the ribbon cable are used for analog signals. Care was taken to make sure there were ground wires in the ribbon cable between inputs and outputs and between channels to prevent oscillation and crosstalk. The last 17 wires on the ribbon cable are for other signals that are handled by the Phoenix connector on the I/OBP.

The MBP is electrically the same as the EBP and I/OBP combined into one board. The MBP is 7.0" wide by 5.1" tall. With a card cage attached it is 8.5" deep. It will hold six circuit boards. There is also a bus section that is the same as the one on the I/OBP.

Description of Circuit Boards

Low Drift, Precision Integrators

This circuit was designed by Prof. Ian Hutchinson (Toroidal Confinement Division Head). There are four integrators on the printed circuit board. The circuit consists of a low DC offset op-amp, LF411A and a sample and hold chip, AD582. There are 25 turn potentiometers on the input to adjust the time constant and common mode. The integration is done using the LF411A and metalized polyester film capacitors. Other types of capacitors caused output overshoot. The sample and hold provides a small amount of negative feedback, eliminating drift.

The Alcator C-MOD machine, when in operation will need over 200 integrators. Located between the first wall and the vacuum vessel are 171 diagnostic coils. These coils are used for sensing plasma position and current. The output of these coils have to be integrated very accurately. The outputs from the integrators go to an analog hybrid computer. The computer analyzes these signals to provide feedback information to plasma positioning power supplies. A 1% error in these signals can affect plasma position by more than a half centimeter. Using precision analog instrumentation and CAMAC, they have been calibrated to 0.3%, with drift as low as 0.1 mVolts per second, and input common mode rejection (CMR) of > 80 dB. The integration time constants range from 1 milliseconds to 5 seconds. Each board has four integrators and a power regulation section. The integrators will also be used on Ragowski coils used for monitoring bus currents from the power supplies to the machine.

Quad Differential Instrumentation Amplifiers

This circuit was designed by Joe Bosco (Alcator C-MOD design engineer). Amplifiers are used everywhere, and by everyone. Some users need precision, high CMR amplifiers. Some need output impedance of 50 ohm loads. Some outputs will go into CAMAC, some into PLC's. Instead of making four different PCB's, one board was designed to try to handle all requirements. The circuit board has four channels and a power supply section The inputs are protected with diodes connected to the plus and minus power supplies. The op-amp chosen was a Burr-Brown instrumentation amplifier INA101HP. One resistor sets the gain. The output of the 101 is then buffered using an LF356 and LH4001 buffer. There is an optional short circuit protection resistor in series with the final output. The inputs and outputs are jumper selectable to I/O through the Lemo connectors or the Phoenix connector on the I/OBP.

Quad Analog Multiplexer

This circuit was designed by Joe Bosco. This circuit was designed to be used in testing, calibrating, and setting up the analog hybrid computer. This computer will calculate, in real time, plasma position and provide feedback information to the power supplies. The multiplexer board has four channels and a power section. Each circuit can choose from four different inputs, a "high" input, a "low" input, a test waveform input and the "real" input from the integrators. These boards were designed for the hybrid and offer few user options. This board was designed to be used by the backplanes but because of the amount of signals being digitized by CAMAC, a separate backplane was designed. The hybrid computer was designed with 37 pin "D" connectors, using ribbon cables to handle I/O. The new backplane has 37 pin "D" connectors and some control circuitry, specific for this application. CAMAC digitizers were bought with same type of connector, making cabling a lot simpler.

Quad Trans Impedance Amplifier

This circuit amplifies current inputs and converts them to voltage outputs. These are normally used with diode type detectors. This circuit uses standard op-amps (741, 356, or 845's) depending on speed requirements, with up to 10 megohm feedback resistors. With a 1 megohm feedback resistor, 1 microamp signals are converted to 1 volt. There is a second stage amplifier, optionally AC coupled, using a 356 op-amp and a LH4001 buffer the same as on the standard amplifier described above. There are optional feedback capacitors for filtering. All gain resistors, feedback capacitors, and the optional AC coupling capacitor are in sockets, for easier changes.

Digital Fiber Optic Link (DFOL)

This circuit was designed by Robicon Corp. [1] for use in their power supplies. With their permission, we copied their circuit and modified the pin out to work with our backplanes. The circuit, see Figure 3, is an eight-bit transmitter/receiver.

be used to customize a backplane for non-standard uses.

The standard EURO card cage will hold 20, 100 cm × 160 cm printed circuit boards. The EURO design allows for flexibility. EURO cards come in a variety of sizes, and card cages can be assembled to accommodate different sized cards. A wide variety of EURO accessories are commercially available, including power supplies, card enclosures, prototype cards, and card extenders.

The I/O Backplane (I/OBP)

The I/O backplane is a four layer printed circuit board. This board is also 0.125" thick. It is mounted to 19" × 14" aluminum panel that fits standard equipment racks. This board is set up with 20 groups of I/O plus one section called busses. The I/OBP is connected to the EBP though ribbon cable. See Figure 1. This was done to allow the user some flexibility in mounting the I/OBP. The system was designed to be mounted in a 19" equipment rack. Most users mount the I/OBP in the back of the rack. This keeps cables out of the way. Some users have mounted the I/OBP in the front of the rack for easy access to the cabling. The ribbon cable can be either 64 wire flat or 32 twisted pair type. Both can be terminated with insulation displacement connectors (IDC) There are 21 of these 64 wire ribbon cables required to connect the EBP to the I/OBP.

There are two types of connectors on the I/OBP, Lemo connectors for analog signals and a Phoenix connector for all other signals. The Phoenix connector is a two piece connector. One piece is soldered on to the I/OBP, the other piece plugs into it. The standard I/OBP has 21 Phoenix strips soldered on it. The more expensive half of the connector, a Phoenix screw terminal block is used only where needed. These Phoenix connectors have 17 terminals. There are 16 terminals for signals plus one for ground. The Lemo connectors can be either a single pin, for coaxial cables, or two pin, for shielded, twisted pair cable. The standard backplane has a two pin Lemo for the inputs and a one pin Lemo for the outputs, but any configuration is possible.

The twenty groups of I/O consists of four input Lemo's, four output Lemo's, a Phoenix connector and a 64 pin connector for the ribbon cable. See Figure 2. The Lemo connectors are not PCB mount type. Small wires about an inch long connect the Lemo's to solder pads on the PCB where etches then bring the signals to the DIN connector. PCB mount connectors would have made assembly easier but would not allow the flexibility of choosing single or double pin Lemo connectors for the I/O. By using panel mount Lemo connectors, only the hole size changes. The one pin and two pin PCB mount Lemo's have different foot prints. In order to have a choice of the having double Lemo inputs and single Lemo outputs or single in and single out would require different layouts. By using Lemo step washers, normally used to isolate the body of the connector from ground, a two pin Lemo connector, 9mm in diameter can be replaced with a one pin Lemo connector, 7mm in diameter.

The bus section is connected to the EBP through one of the ribbon cables. It brings out the 12 common bus lines to a Phoenix connector. The other 5 pins are connected through fuses to, ± 15V, +24V, + 5, and ground. The fuses are pico fuses and are located on the front of the of I/OBP. They are mounted in sockets for easy replacement. The fuses are rated at 500 milli-Amps to protect the ribbon cable.

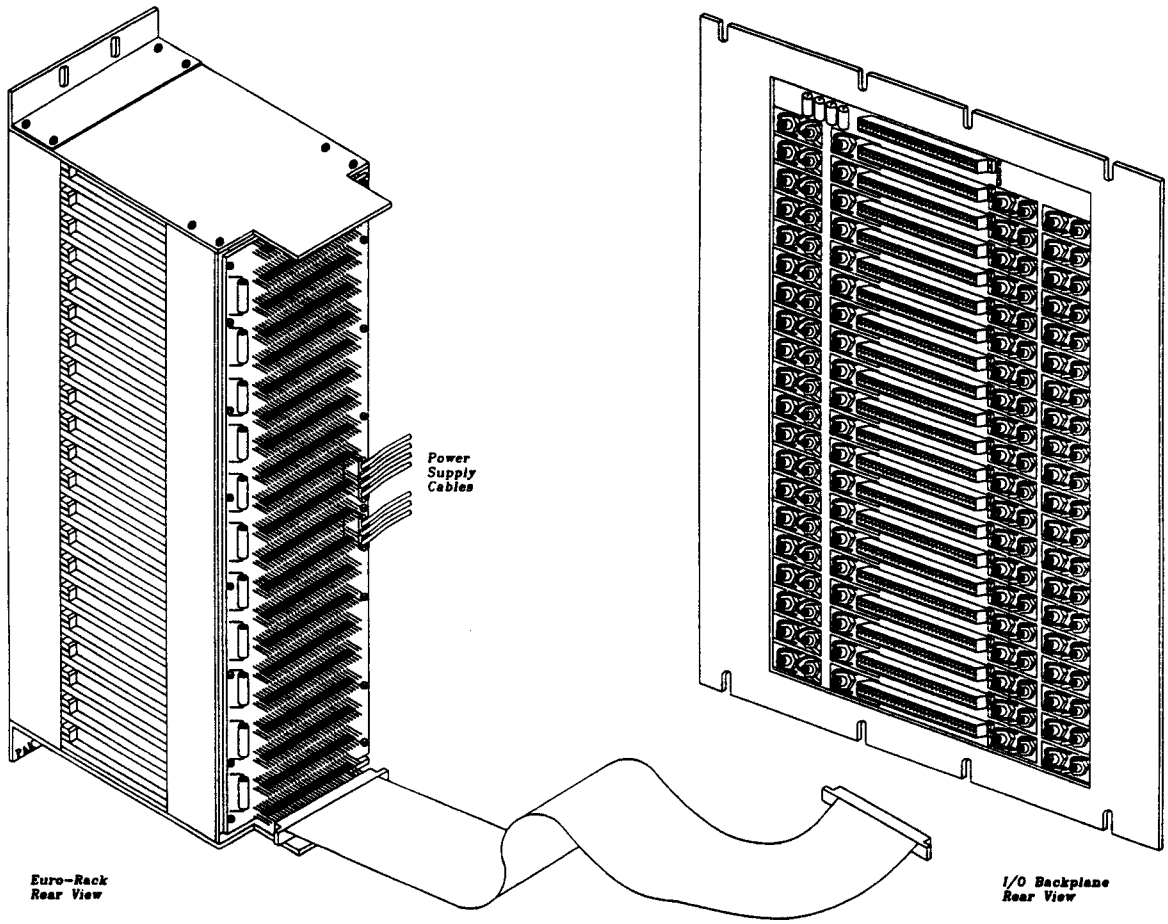

Figure 1: Euro and I/O Back Plane Assembly

The digital inputs are located on pins 1 through 8 on the Phoenix connector and the digital outputs are on pins 9 through 16. The inputs are pulled high with 2.7K ohm resistors and where designed to be driven by a PLC with 15 volt logic. The next time these boards are made the input voltage will be user selectable to 5, 15, or 24 volts. The digital, parallel data is converted to serial data with a UART (CDP1854). The serial data is then outputted to a SMA type fiber optic transmitter, Hewlett Packard HFBR-1402. The output is also available on a Lemo connector on the I/OBP for easier testing and calibration.

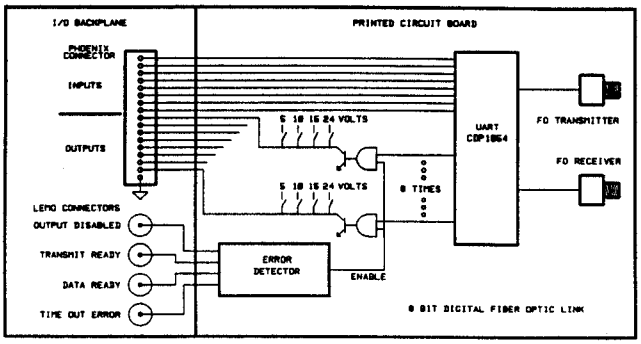

Figure 3: 8 Bit Digital Fiber Optic Link

The fiber optic input uses an HP HFBR-2402 SMA type receiver. The input can also be inputted through the I/OBP. The UART converts the data back to parallel data, and outputs it to the Phoenix connector. The digital outputs do have user selectable voltages. The voltage is jumper selectable to 5, 10, 15, or 24 volts.

These circuits are being used to send signals from potentially dangerous, high voltage areas to the C-MOD control room. There will be no copper cables running into the control room from either the power room or the cell. Over 200 fibers have been pulled from the control room to various locations.

Analog Fiber Optic Link (AFOL)

This circuit was designed by William Burke (Alcator C-MOD electronic design engineer). The AFOL circuit card has a transmitter and receiver. These are two separate circuits, unlike the DFOL. The fiber optic transmitter and receiver are the same as in the DFOL.

The transmitter input, see Figure 4, uses the Lemo connectors on the I/OBP. The input can be differential or single ended. The signal is rectified and given a 2.5 volt DC offset. The signal then goes to a voltage to frequency converter (AD654). The output of the V to F is 25 KHz to 125 KHz. The polarity of the input signal is detected, which enables one of two, one shot timers. The output of the timers is 4 micro seconds for positive voltages and 2 micro seconds for negative voltages. The output goes to the FO transmitter and to a Lemo connector on the I/OBP and is used for calibration and testing.

There is a dip switch located at the circuit input for calibration. They switch precision voltage references of ± 10 volts and ground. A frequency counter can be connected to the frequency output Lemo connector on the I/OBP and watched as one potentiometer is adjusted until the output is 125 KHz.

The receiver section, see Figure 5, of the card has two inputs, the FO receiver and a Lemo input. The signal goes to a frequency-to-voltage converter. There is one pot for adjusting

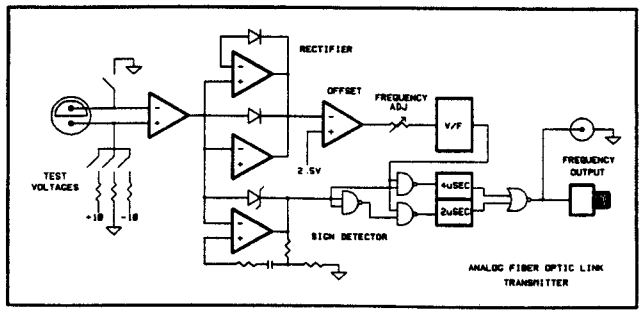

Figure 4: Analog Fiber Optic Link Transmitter

the gain of the F to V. The 2.5 volt DC offset which was added by the transmitter is then removed by adjusting one pot. This signal then goes to one of three analog switches. The signal is inverted and goes to the second analog switch. The pulse width of the input signal determines which switch is turned on. This de-rectifies the signal. The third analog switch is connected to ground. This switch is enabled when there is no input signal or a broken fiber. There is a missing or broken fiber detector circuit that outputs to a Lemo connector on the I/OBP which will be monitored by a PLC. The output of the three analog switches are wired together and go to a 2 pole 3 KHz low-pass filter and then to the output buffer.

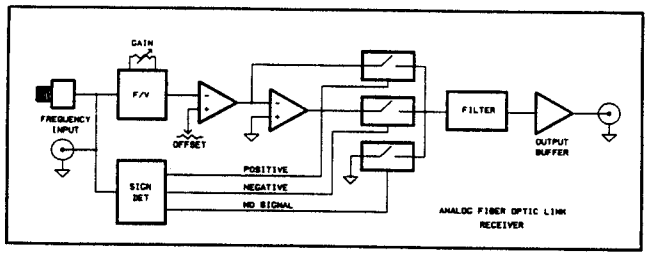

Figure 5: Analog Fiber Optic Link Receiver

Summary

As C-MOD is just starting testing, many of the circuits are now being used in systems for the first time. The system has been flexible and is being used in power systems, safety systems, data aquisition, and diagnostics.

Having a computer to do schematic capture and printed circuit board layout has made circuit fabrication, documentaiton, and Quality Assurance easier. Besides having designed the above mentioned boards, the system has been used to fabricate other, non-EURO cards. These other boards, in the past, would have been wired by hand. The computer aided design and standardizing has and will, hopefully continue to help Alcator C-MOD run, and collect data in a safe, practical and efficient way for many years to come!

References

[1] Robicon, Corp., division of High Voltage Engineering, Pittsburg, PA.

ENGINEERING DESIGN AND ANALYSIS OF THE ALCATOR C-MOD TWO-STRAP ICRF ANTENNA

Y. Takase, S. Golovato, M. Porkolab,
K. Bajwa, H. Becker, and D. Caldwell

MIT Plasma Fusion Center
167 Albany Street
Cambridge, MA 02139

Abstract: ICRF fast wave heating with up to 8 MW of rf power at 80 MHz is planned on the Alcator C-MOD tokamak ($R = 0.665\,\mathrm{m}$, $a = 0.21\,\mathrm{m}$, $\kappa \lesssim 1.8$, $B \leq 9\,\mathrm{T}$, $I \leq 3\,\mathrm{MA}$). High power heating experiments will be carried out using two sets of two-strap antennas. Engineering aspects of antenna design and results of analyses are presented. The most important consideration was mechanical integrity against very large disruption loads expected in Alcator C-Mod. Thermal analyses indicate that for a transmitted power of 2 MW the antenna can be operated without active cooling for the planned lower hybrid current driven operation of up to 10 sec duration.

Introduction

Alcator C-Mod [1] will start operation with 4 MW of ICRF heating power at 80 MHz, with future upgrade to 8 MW. During the initial start-up phase, a movable single-strap ICRF antenna [2–5] will be used in order to enable tokamak operation in a wide variety of configurations, to enable detailed coupling measurements (in particular, measurement of the antenna loading resistance as a function of plasma-antenna distance for a fixed plasma configuration), and to enable the antenna to be retracted into the port during undesirable operational conditions.

Heating experiments at the 4 MW power level are planned with two sets of phaseable two-strap antennas, which are currently being fabricated. In this paper, main design considerations and analysis results of the two-strap antenna are discussed, with emphasis on engineering aspects. Physics considerations have been presented elsewhere [6].

The two-strap antenna was designed to optimize heating while satisfying the imposed constraints. Optimization criteria include maximization of antenna power handling capability, maximization of single-pass absorption by ions, and minimization of impurity generation. Constraints include vacuum vessel geometry, mechanical and thermal loads, and compatibility with the rest of the program. Constraints imposed by space limitations, disruption loads, and thermal loads are particularly severe in compact high-field, high-current tokamaks such as Alcator C-Mod.

Antenna Design Features

The two-strap antenna is shown in Fig. 1. The spacing between the two current straps was chosen so that the radiated power is peaked at $k_\parallel \simeq \pm 10\,\mathrm{m}^{-1}$ when the two current straps are driven out of phase. This spectrum provides both good single-pass absorption by ions and high enough loading resistance. In addition, impurity release is effectively controlled by exciting the two straps out of phase. Since this spacing corresponds approximately to half the distance between ports, two of these antennas mounted on adjacent ports will act as a four-current-strap array.

Because this antenna is larger than the ports on the vacuum vessel, antenna parts must be brought into the vessel separately and assembled inside. The port size restriction also necessitated the antenna box to be made of the front half, which holds the Faraday shield rods, and the rear half, so that each part can be inserted through the port opening.

The antenna current strap is virtually identical to that of the moveable single-strap antenna. The rf currents are fed out of phase from the top and bottom ends, and grounded at the center tap. However, a more complicated feed line system was necessary because the straps must be offset from the port opening. In the present design, rf power is fed through four 4" (10 cm) O.D. feedthroughs located directly behind the antenna backplane. The diagonal feed line sections (seen in the front view with the Faraday shield removed, in Fig. 1) are symmetric to ensure out-of-phase excitation of the top and bottom halves of the current strap. These feed line sections are shielded from the plasma by the plate which connects the inner sidewalls of the left and right halves of the antenna box. The current straps are connected to external resonant loops which may be excited either in phase or out of phase to control the toroidal phasing between the two current straps.

A single-layer circular cross section (9.5 mm diameter) rod design with 27% transparency was adopted for the Faraday shield. The Faraday shield extends over a length of 42 cm along the current strap, and the areas in front of the feeders are covered. The rods are bent radially away from the plasma at each end and attach to the antenna box outer sidewall and the inner sidewall. The rods are oriented at 10° to the horizontal direction to approximately align them with the local field line over a wide range of operating conditions. Results from 2D and 3D magnetostatic codes developed by Ryan [7] were used along with engineering and fabrication considerations to determine parameters such as the antenna box depth, current strap width, the length of the bent section of the Faraday shield, and the spacing between Faraday shield rods. Optimization criterion was to maximize the launched power for a given voltage limit.

The poloidal curvature of the antenna was matched to a typical lower single-null equilibrium of elongation $\kappa = 1.7$. It is not possible to match the antenna curvature to all possible equilibria, but it is possible to generate equilibria which match the antenna curvature over a wide range of configurations including upper single-null and double-null equilibria, with elongations in the range $1.55 \lesssim \kappa \lesssim 1.80$.

The antenna box is protected by protection tiles arranged in a "picture-frame" fashion on the outer sidewalls and top and bottom front surfaces. TiC (titanium carbide) coated TZM (Molybdenum alloy) tiles will be used during the initial "all-metallic" operation period, during which Molybdenum (uncoated) divertor and limiter tiles will be used. Boronization is planned for controlling the influx of high Z impurities. The antenna protection tiles can be replaced with tiles made of a lower Z material such as graphite or boron nitride during the later "low-Z" operation period, when the divertor and limiter tiles will be replaced with lower Z material tiles. The distance

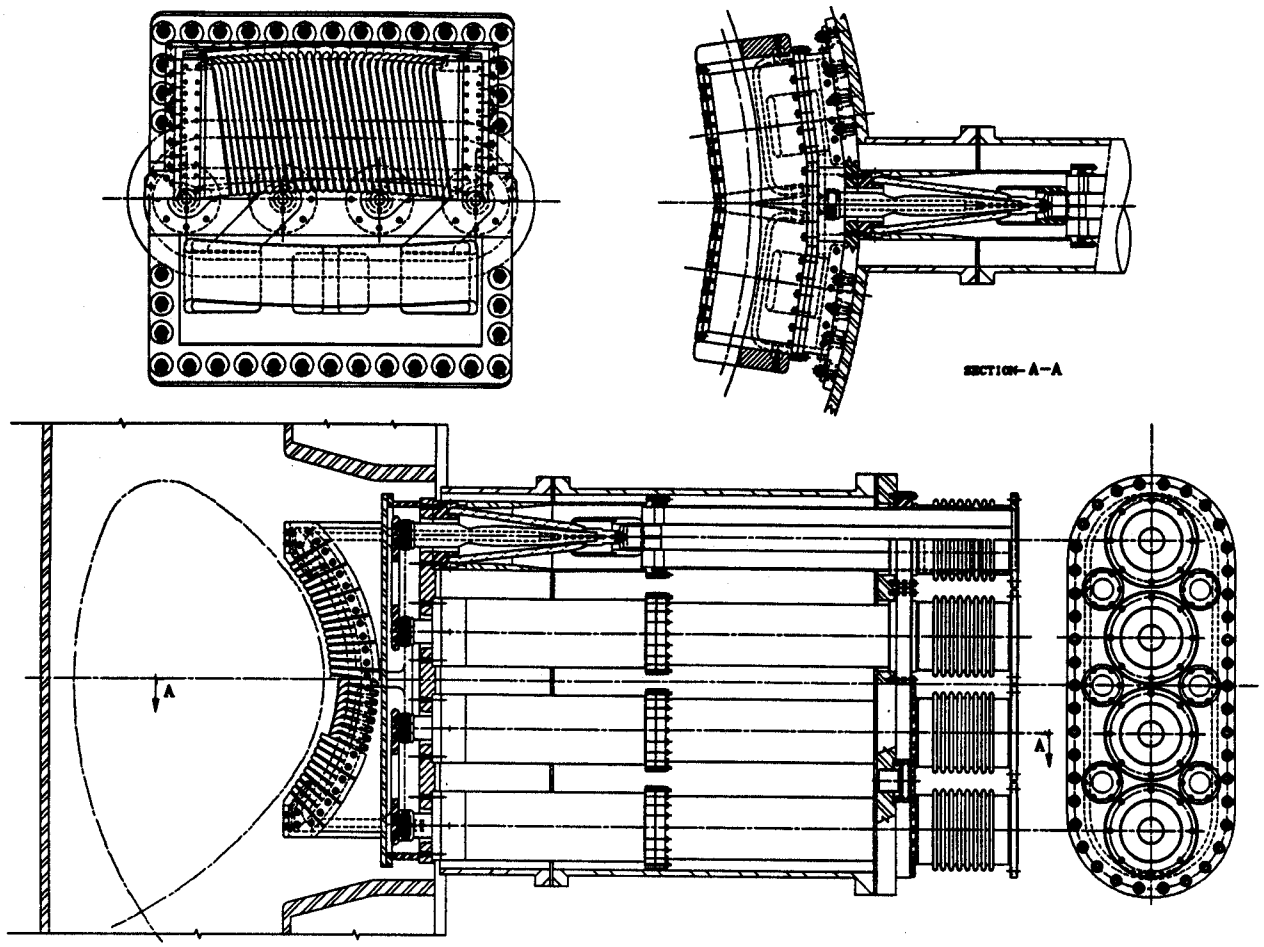

Fig. 1. The Alcator C–MOD two-strap ICRF antenna.

between the field line touching the leading edge of the tiles and the Faraday shield rod is approximately 4 mm, taking the magnetic field ripple into account.

A transmission line modeling of the antenna and matching circuit was developed and checked against measurements on a mock-up antenna [3]. For an expected voltage limit of 40 kV, a loading of 8 Ω per strap is required to radiate 2 MW into the plasma. This loading is in the range predicted by full-wave calculations [6]. The lowest loading predicted is 6 Ω for out-of-phase excitation at low density.

Disruption Analysis

The most demanding requirement in the design of the two-strap antenna was mechanical integrity against disruption-induced forces, which are much larger than for the single-strap antenna because of its larger size. Consequently, it was not possible to design a movable two-strap antenna. In the present design, the antenna backplane is attached to the 2 cm thick outer wall of the vacuum vessel to provide support for the antenna box and the current straps.

Stress analyses of the antenna were performed for plasma disruptions at 3 MA and 9 T with a thermal quench duration of 100 μs followed by a current decay phase of 3 ms (a current decay rate of 1 MA/ms). Eddy currents and resultant forces are calculated by the SPARK code, and displacements and stresses are calculated by a commercial finite element code PAFEC. Both static and dynamic analyses were performed. A vertically moving disruption gives larger forces and stresses than stationary or radially moving disruptions. Two types of vertical disruption scenarios were analyzed, one in which the vertical motion occurs on the same time scale as the current decay (3 ms), and another in which a slow vertical displacement (10 cm over 30 ms) is followed by a fast (3 ms) current decay.

It was found that during a disruption, up to 500 kA of the vacuum vessel eddy current can flow across the antenna backplane, and approximately 1 kA through a Faraday shield rod. In addition, up to 200 kA of eddy current can be induced on the antenna box, and up to 4 kA can flow through a Faraday shield rod. The stress is the highest at the joints where ends of Faraday shield rods are attached to the antenna box sidewalls. The radial arms of the Faraday shield rods must be short enough to keep the bending moments at these joints to an acceptable level. These moments are caused by the radial currents interacting with the toroidal field. In the present design with tilted Faraday shield rods, the disruption loads on the rods oppose the thermal displacement, and therefore a runaway condition will not occur.

Main components at the end of an upward-moving disruption are $M_x = 61\,\mathrm{kNm}$, $M_z = -67\,\mathrm{kNm}$, and $F_y = 59\,\mathrm{kN}$, where x, y, and z correspond to radial, transverse, and vertical directions, respectively. The studs used to hold the antenna backplane to the vacuum vessel wall must be able to withstand

these loads. The maximum deformation of the antenna box is 0.3 mm, and the internal stresses in the antenna box are well below the allowable stress.

The antenna box, Faraday shield, and current strap are made of Inconel 625 alloy for mechanical strength and for reducing the disruption-induced eddy currents. All rf current carrying surfaces are electroplated with copper. The Faraday shield rods have a further coating of TiC.

The current strap is supported at the center tap where it attaches to the antenna backplane. The displacement at the end of the diagonal feed line section, where it attaches to the center conductor of the feedthrough, can be as large as 2.5 mm during a disruption. Beryllium copper bellows are provided to mechanically isolate the feedthroughs from such displacements. The outer conductor of the coaxial transmission lines are mechanically isolated from the vacuum vessel by stainless steel bellows at the port flange to take up the differential expansion. The internal stresses in the current strap are well below the allowable stress.

Thermal Analysis

Thermal analyses were performed using a commercial finite element analysis code ANSYS. A total heating power of 6 MW (4 MW ICRF and 2 MW ohmic or lower hybrid) was assumed, 2 MW of which was assumed to be lost by radiation and 4 MW by transport loss into the scrape-off layer. A separate outboard limiter located at a different toroidal location and 1 cm radially in from the leading edge of the antenna protection tile will limit the scrape-off plasma and protect the antenna from high energy ions and runaway electrons. The corresponding power densities are 30 W/cm^2 of radiation and 1 kW/cm^2 of parallel heat flux at the leading edge of the protection tile. Assuming that the rf current is localized at the radiused edge region of the current strap, the maximum thermal loading on the current strap is estimated to be less than 4 W/cm^2 even for a conservative loading resistance of 5 Ω per strap. The radiation heat load of 30 W/cm^2 is incident on the current strap in the open regions of the Faraday shield. In addition to radiation from the plasma, 3% of the total radiated rf power was assumed to be dissipated on the Faraday shield rods. This corresponds to a maximum rf heat flux of 25 W/cm^2 each on the top and bottom sides of the Faraday shield, taking toroidal and poloidal peaking into account. The rf heat flux on Faraday shield rods is substantially lower than for the single-strap antenna (for the same transmitted power) because of its larger surface area.

The thermal analyses were performed with water cooling, with nitrogen gas cooling, and with no active cooling. Conduction cooling and radiation cooling to a 200°C background were assumed. The most heavily loaded components are the Faraday shield rods and the antenna protection tiles. A 2-D (in the horizontal plane) equivalent model was developed to represent one half of the box, and the results were compared with those obtained with a more time consuming fully 3-D model. The results were virtually identical. A cross sectional model (in the vertical plane) of the Faraday shield rod was also analyzed.

After 8 hours of 10 sec rf pulses (12 sec plasma duration) every 20 min envisioned in future rf current driven operation or long pulse ohmic operation at a reduced toroidal field of $B_T \simeq 5$ T, maximum temperature increases of 310°C (before shot) to 690°C (after shot) for the Faraday shield, and 270°C to 470°C for the protection tile, are predicted without active cooling. The temperature equilibrates within the Faraday shield rod cross section in a few seconds, but the conduction along the rod occurs on a much longer time scale of about several minutes. In contrast, equilibration time for the protection tile is less than a minute owing to its higher thermal conductivity. Fully ratcheted temperatures are attained after about 2 hours for the Faraday shield and about 4 hours for the protection tiles.

The displacements and stresses at the end of the final pulse are shown in Fig. 2. The maximum displacement is 1.8 mm at the center of the Faraday shield rod, causing it to bow out. Thermal stresses are largest at the ends of the Faraday shield rods (250 MPa), but are within allowable limits. Thermal stresses are partially relieved by the flexibility of the antenna box sidewalls. Differential thermal expansion of the antenna backplane relative to the vacuum vessel wall is negligible. These results show that no active cooling is required for the two-strap antenna for power levels and durations expected during the life of this antenna.

During a disruption, a large fraction of plasma kinetic energy and poloidal field magnetic energy may be radiated. The bulk temperature rise of the Faraday shield rod will only be 20°C, but the surface temperature rise may be as high as 600°C. The runaway electrons generated during the current decay phase of a disruption will be intercepted by the outboard limiter. The condition of the front surface of the Faraday shield will be monitored optically through a periscope, and temperatures at several critical locations will be monitored with thermocouples during the experiment.

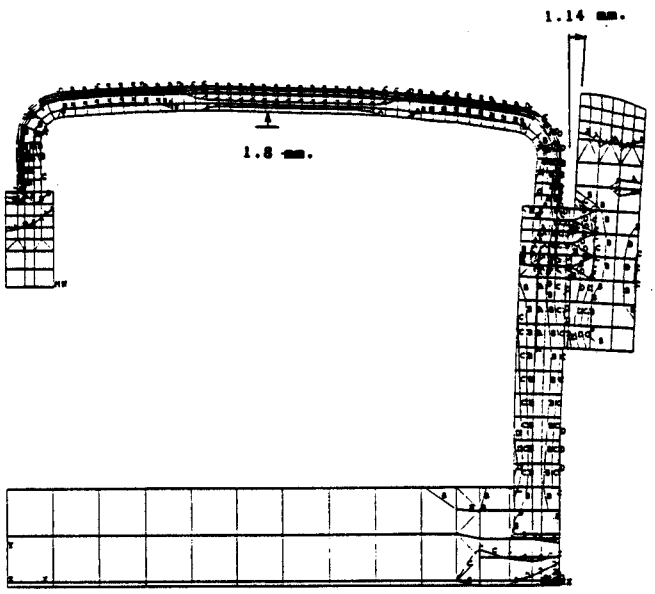

Fig. 2. Deformed shape and von Mises stress contours at the end of the final pulse.

Conclusions

Satisfactory engineering design of the two-strap antenna to be used for high power ICRF heating of Alcator C-Mod plasmas are presented, along with analysis results. The very large disruption loads expected in this device and limited space impose severe constraints on the design of such an antenna. Thermal analyses indicate that for a transmitted power of 2 MW the antenna can be operated without active cooling for the planned lower hybrid current driven operation of up to 10 sec duration.

Acknowledgments

This work was supported by U.S. DOE Contract No. DE-AC02-78ET51013.

References

[1] S. Fairfax, et al., "Alcator C-MOD," presented at the 14th IEEE/NPSS Symposium on Fusion Engineering, San Diego, CA, Sept. 30–Oct. 3, 1991.

[2] Y. Takase, et al., "Alcator C–MOD ICRF Fast Wave Antenna Design and Analysis and Expected Plasma Performance," in Proceedings of the 8th Topical Conference on Radio-Frequency Power in Plasmas, 1989 (AIP, New York 1989), pp. 346–349.

[3] S. Golovato, et al., "Alcator C–MOD ICRF Antenna and Matching Circuit," in Proceedings of the 8th Topical Conference on Radio-Frequency Power in Plasmas, 1989 (AIP, New York 1989), pp. 246–249.

[4] Y. Takase, et al., "Alcator C-Mod ICRF Antenna Design and Analysis," in Proceedings of the IEEE 13th Symposium on Fusion Engineering, 1989 (IEEE, New York, 1990), Vol. 1, pp. 211–214.

[5] S. N. Golovato, et al., "Testing and Conditioning of the First Alcator C-Mod ICRF Antenna," presented at the 9th Topical Conference on Radio Frequency Power in Plasmas, Charleston, SC, Aug. 18–21, 1991.

[6] Y. Takase, et al., "Design and Analysis of the Alcator C-Mod Two-Strap ICRF Antenna," presented at the 9th Topical Conference on Radio Frequency Power in Plasmas, Charleston, SC, Aug. 18–21, 1991.

[7] P. M. Ryan, et al., "Determination of Fields Near an ICRH Antenna Using a 3D Magnetostatic Laplace Formulation," in Proceedings of the 8th Topical Conference on Radio-Frequency Power in Plasmas, 1989 (AIP, New York, 1989), pp. 322–325.